Graph-Based Power Flow Solution Methods for Electric Power Systems

by

Ayman M. OTHMAN MOHAMED

A thesis
presented to the University of Waterloo
in fulfillment of the
thesis requirement for the degree of
Doctor of Philosophy
in
Electrical and Computer Engineering

Waterloo, Ontario, Canada, 2022

Examining Committee Membership

The following served on the Examining Committee for this thesis. The decision of the Examining Committee is by majority vote.

External Member: Medhat M. Morcos
Dept. of Electrical and Computer Engineering,
Kansas State University

Supervisor: Ramadan El-Shatshat
Dept. of Electrical and Computer Engineering,
University of Waterloo

External Member: Samir Elhedhli
Dept. of Management Sciences,
University of Waterloo

Internal Member: Kankar Bhattacharya
Dept. of Electrical and Computer Engineering,
University of Waterloo

Internal Member: Sagar Naik
Dept. of Electrical and Computer Engineering,
University of Waterloo

Author's Declaration

I hereby declare that I am the sole author of this thesis. This is a true copy of the thesis, including any required final revisions, as accepted by my examiners.

I understand that my thesis may be made electronically available to the public.

Abstract

For over half a century, Power Flow (PF) and its optimized version, Optimal Power Flow (OPF), has become one of the most important and widely used tools in power system planning, operational planning, and operation/control. The solution to the PF problem is carried out extensively for various power system activities and is essential for both off-line applications, such as planning and stability studies and online applications, including security monitoring and contingency analysis, optimal power flow, to name a few. In comparison, OPF seeks to optimize the operation and planning of electric power generation, transmission, and distribution networks subject to various system constraints and control limits. Different PF/OPF techniques have been proposed, each with its own unique formulation, solution methodology, advantages, and drawbacks. Motivated by the growing inclusion of distributed energy resources, such as highly variable renewable generating resources; and further, by the speed and convergence limitations of existing tools, this research focuses on developing simple, accurate, fast; yet, computationally efficient tools for operation and planning of electric power systems. This thesis introduces a radically new generalized direction in power system problem formulations and proposes a novel Graph Theory-based optimization algorithm for solving the PF/OPF problem, that is also suitable for transmission, distribution, and hybrid AC/DC power systems.

To start, a novel algorithm is developed for a power flow solution based on maximum-flow formulation, titled "Flow-Augmentation PF." Modeling of power system components for the proposed network-flow formulation is presented, followed by s-t flow modeling. The proposed method formulates a power flow problem as a network-flow problem and solves it by using a maximum-flow algorithm, inspired by the push-relabel max-flow technique. In contrast to previously established methods in the literature, the proposed methodology relies on transforming the power system configuration and topology into an efficient analytical form (matrices and arrays). The solution methodology of the proposed PF algorithm is discussed in detail. The methodology includes a discussion on the algorithm correctness, termination, and computational complexity. The developed Flow-Augmentation method solves the power flow problem using matrix-vector multiplication in its most abstract form,

and further, the developed method is independent of system parameters and network configuration. The proposed algorithm captures the full system model and handles any system configuration without resorting to special treatment. The presented algorithm is computationally efficient and compares favorably with current methods, in terms of execution time and accuracy.

Second, a new generalized PF/OPF framework based on the minimum-cost flow network model is introduced. The proposed formulation seeks to find the network-flow distribution that optimizes a stated objective function, such as generator costs or gas emissions, system losses, or any other indices. The solution of the PF problem is obtained by using a proposed modified version of the minimum-cost flow model, termed *MinLoss-Flow PF* algorithm. This algorithm builds upon the models developed in the above-mentioned maximum-flow-based method, in terms of system component modeling and graph formulation. The developed *MinLoss-Flow PF* focuses on finding the minimum system losses that satisfy both the technical and engineering constraints. As such, the generalized mathematical formulation, based on cost flow calculation and its properties, is developed. The *MinLoss-Flow PF* method is fully discussed and validated against well-known methods used for transmission and distribution systems.

Third, this thesis presents a sequential network-flow graph-based method for a steady-state power flow solution in hybrid AC/DC multi-terminal power systems. The proposed method is a unique and novel one, which differs from other established methods that involve the use of modified versions of classical power flow methods. The proposed method formulates the hybrid AC/DC power flow problem as a maximum network-flow problem and solves it, using a max-flow-based algorithm. The proposed flow-augmentation power flow algorithm solves the AC and DC sides sequentially while employing the detailed converter model, including the converter transformer, filter, and the converter loss parameters for converter power loss calculations. The proposed method is validated using standard hybrid 5-bus and CIGRÉ-B4-DC systems.

The performance of the novel graph-based PF/OPF tools is validated using several benchmark networks of different sizes, topologies, and parameters. Many case studies

were conducted and compared with the most commonly used techniques for transmission, distribution, and hybrid AC/DC systems. The proposed algorithm is also validated and compared with the results obtained from two commercial software packages, PSS/E and PSCAD. The proposed formulation is computationally efficient, as it is based on matrix-vector multiplication, and is also scalable, considering the formulation works as a graph-based method, which, inherently, allows for parallel computation for added computational speed. This proves to be a strong advantage for the proposed method, as a significant reduction in computational time is observed, as a result. Test results show significant computational gains of about 70% when compared with the Newton-Raphson on the IEEE 118-bus system, and a value less than 50% reduction compared with the Newton-Raphson method applied to hybrid AC/DC system. The results also show that the proposed algorithm takes less than 1.4% of the execution time required by the Backward-Forward-Sweep method on the 69-bus. The developed graph-based PF/OPF algorithms are coded in GNU OCTAVE environment and the simulation results are presented to validate the effectiveness of the proposed techniques.

Acknowledgements

All thanks and praise to Allah almighty for gifting me with the strength and abilities to succeed in completing this research. I would like to express my gratitude to my supervisor Dr. Ramadan El-Shatshat, for his insightful comments and guidance throughout this research. His enthusiasm to the research problem, comments, and advise were an invaluable driver for the completion of this research. I would like to express my thanks to Prof. Bruce Richter from Combinatorics and Optimization department at the University of Waterloo for the his patience, time, and fruitful discussions.

Moreover, I would like to thank my committee members, Prof. Medhat M. Morcos, Prof. Samir Elhedhli, Prof. Kankar Bhattacharya, and Prof. Sagar Naik for examining my thesis.

Many thanks go to the members of electrical and computer engineering department at the University of Waterloo. I would like also to thank all the research group members and graduate students community for valuable help and friendship.

I am indebted to my parents, wife and family for their endless support, patience and prayers.

Dedication

To those who inspired me the most...

Table of Contents

List of Tables

List of Figures

Nomenclature

BFS Backward Forward Sweep.

VSC Voltage source converter.

PCC Point of common coupling.

AC Alternating Current.

DC Direct Current.

KCL Kirchhoff Current Law.

KVL Kirchhoff Voltage Law.

PF Power Flow.

OPF Optimum Power Flow.

GS Gauss-Seidle.

NR Newton Raphson.

FD Fast Decoupled.

Variables

S Complex power $P + jQ$.

P_{conv} Converter side active power.

Q_{conv} Converter side reactive power.

I_{conv} Converter current.

P_{loss}^{conv} Converter power loss.

P_{dc}^{i} Converter i power on DC side.

$iter$ Iteration counter.

P Active power.

Q Reactive power.

U Voltage.

$|U|$ Voltage magnitude.

δ Voltage angel.

I Current.

Constants

Z Impedance $R + jX$.

B_f Converter low pass filter.

Z_C Converter phase reactor.

$l_{capacity}$ Branch element flow capacity.

ϵ Error tolerance.

$iterMax$ Maximum iteration counter.

N Transformer tap ratio.

τ Transformer tap ratio magnitude.

θ_{shift} Transformer tap ratio phase shifting angle.

Y Admittance.

Y_{bus} System admittance matrix.

$|U|_{min}$ Voltage magnitude lower limit.

$|U|_{max}$ Voltage magnitude upper limit.

Q_{min} Reactive power lower limit.

Q_{max} Reactive power upper limit.

a, b, c Converter quadratic loss formula parameters.

Z_{tf} Converter transformer.

Graph Theory

$G(V, E)$ Graph G with group of vertices V and edges E.

t Sink. Super-sink node.

f Flow in network edge $(j, k) \in E$.

Ψ Cost associated with flow f in edge $(j, k) \in E$.

$\mathcal{B}$ Set of buses.

$\mathcal{D}$ Set of system branches.

$\mathcal{G}$ Set of generators.

$\mathcal{L}$ Set of loads.

$\mathfrak{G}$ Impedance weighted incident matrix.

V	Graph vertices.
E	Graph edges.
n	Number of vertices in Graph $G(V, E)$.
m	Number of edges in Graph $G(V, E)$.
B	Graph vertex-edge incidence matrix.
H	Graph vertex-vertex adjacency matrix.
$\mathscr{L}$	Graph Laplacian matrix.
s	Source, Super-source node.

Chapter 1

Introduction

1.1 Preamble

The objective of power system operation and control is to ensure the quality and reliability of supply to the consumer by maintaining the load bus voltages and system frequency within permissible limits, in a manner that is most economical to the utility, from the transmission and distribution point of view. Recently, the operation and planning of electric power have undergone dramatic changes in the smart grid world. Under the deregulation and the global transformation of electric networks in the last decades, and the rapid growth in power demand, in comparison to installed supply capacity, there has been a large push for generation units to be distributed throughout the electric network. Moreover, the introduction of the hybrid AC/DC power network concept has occurred in the past decades and has only gained greater prominence in recent years, as a result of the hybrid systems' capability to transmit higher power over longer distances at higher efficiency. In addition, the hybrid AC/DC power network has the capability of connecting two or more asynchronous AC networks together. This trend has been accelerated by advances in power electronics leading to developments in inter-linking converters, and increased penetration

of renewable energy sources, in the form of solar and wind-based generation at transmission and distribution levels. This departure from classically centralized architecture and the introduction of new system typologies results in new challenges and added constraints imposed on system operation and planning. With the growing penetration of distributed energy resources, including highly variable renewable generating resources, utilities need to analyze and plan for dynamic operating conditions that can occur at any time throughout the day.

The Power Flow (PF) and its optimized version, Optimal Power Flow (OPF), are the basis of power system planning, operation, and control. For a proper and efficient operation and control of a particular power system, accurate power flow analysis results must be available. The objective of PF is to provide an operational snapshot of the system state by solving for system voltages and angles at all buses of the network, from which all other quantities can be calculated, including generation levels, branch flows, system losses, etc. A complete power flow analysis is a necessary requirement of complete electric network studies, like voltage and frequency regulation, optimum generation dispatch, demand satisfaction, fault tolerance, and more. Whereas, OPF is the optimum power flow solution that optimizes energy generation, which satisfies the PF requirements, branch thermal limits among other constraints, and most importantly, a uniquely stated objective function, e.g., minimum generation cost or minimum system losses. The PF and OPF are typically formulated as non-linear problems and solved by iterative numerical techniques and optimization methods, respectively. The following section provides an introduction and briefly reviews different PF techniques and surveys various optimization methods that have been applied to OPF.

1.2 Literature Review

This review will clearly be unable to cover every aspect of the PF and OPF problems and every proposed solution algorithm. Rather, this review will present the underlying principles and techniques of the popularly accepted approaches in the areas of PF analysis

and OPF. The PF algorithms applied to transmission networks will be discussed first, followed by those used in distribution networks. The PF methods applied to AD/DC networks will be next. At the end of this section, some critical literature review on OPF problems is presented.

1.2.1 Power Flow Algorithms

The study of electric networks, in regard to fault analysis, stability studies, and economic calculation; necessitates the simulation of the electrical flow in a power network. This simulation provides an operational snapshot of the system state by solving for system voltages, generation levels, branch flows, and system losses. The solution to the power flow problem is obtained by using numerical methods like Gauss-Seidel (GS), Newton-Raphson (NR), and Fast-Decoupled (FD) methods at the transmission level and Backward-Forward-Sweep (BFS) for distribution levels. A brief review of established PF methods, applicable to transmission and distribution networks, as well as hybrid AC/DC networks, is presented below.

Power Flow Algorithms for Transmission Systems

Many articles have addressed the problems of power flow and treated these problems in both transmission and distribution levels since the method was first introduced [1]. In the early days, power flows were conducted by ad-hoc methods and later, by an analog network analyzer [2], [3]. A new direction in power flow analysis was introduced in [4] based on the loop and track method, by modeling the electric network in the form of matrices. A shift in direction was proposed in [5] by solving an iterative nodal power flow. The added advantage of this formulation is the ease of system modification, without the need to readjust the constructed system model, with further performance improvements proposed in [6].

The Gauss iterative method and its improved version, the Gauss-Seidel method, has been adapted to solve the power flow problem [1] [5]. This method relies on the iterative

solution of the power equation, with initial solution updates, until the correction values meet a pre-specified tolerance criterion. The Gauss-Seidel is a nodal method that possesses many advantages over other network analyzers of its time. The method starts from an initial guess of the voltage profile and repeatedly updates the solution until convergence is met [7] [8]. The generator bus needs special treatment in order to maintain active power injection and voltage magnitude. However, a large disadvantage of this method involves the slow convergence rate, especially with larger systems with higher numbers of generation nodes [7].

In order to address the slow convergence rate problem of the GS method, the Newton-Raphson iterative method was introduced in the late 1960s for power flow calculations [9]. This method involves an iterative solution of complex non-linear simultaneous equations, using the Jacobean matrix, which is based on the Taylor series expansion. The Jacobean matrix facilitates the linear relationship between small changes in voltage angle and magnitude ($\delta/|U|$), and small changes in active and reactive power (P/Q), as given by [10] [8]:

$$\begin{bmatrix} \Delta P \\ \Delta Q \end{bmatrix} = \begin{bmatrix} J_{11} & J_{12} \\ J_{21} & J_{22} \end{bmatrix} \begin{bmatrix} \Delta\delta \\ \Delta|U| \end{bmatrix} \tag{1.1}$$

The solution procedure uses Gaussian elimination and back-substitution to reach convergence, once a small residual error between successive iterations is achieved. For large size networks (if the network has more than a few hundred buses), the Newton-Raphson method is employed in conjunction with sparsity programming [11] [12] [13] [14]. The method has a quadratic convergence, and for the vast majority of practical power systems, the method has been found to be very reliable. Extension of this method to the solution of three-phase systems is presented in [15]. However, the reliance on the starting point, in addition to the requirement for repeated inversion of the Jacobian matrix, which might suffer from numerical instability in some cases, are the main disadvantages of this method [7]. Further, the method is computationally expensive and does not have the speed required for

real-time applications. For this purpose, there have been developments employing various decoupled methods. Many stages of development and contributions have finally led to a fast decoupled method [16].

The Fast Decoupled method takes advantage of the loose coupling between active and reactive power flows, caused by the high branch X/R ratio. By relaxing the relationship between Q/δ and $P/|U|$, this method results in a simplified formulation and computational savings [16].Based on this, the equation 1.1 is simplified by eliminating the terms J_{12} and J_{21} to [8] [10]:

$$\begin{bmatrix} \Delta P \\ \Delta Q \end{bmatrix} = \begin{bmatrix} J_{11} & 0 \\ 0 & J_{22} \end{bmatrix} \begin{bmatrix} \Delta\delta \\ \Delta|U| \end{bmatrix} \tag{1.2}$$

However, the fast decoupled method requires significantly more iterations compared with classical Newton-Raphson (NR) methods, while every iteration is computationally less expensive [7] [17] [18]. It has been recognized for its speed and good convergence characteristics, and it may be used in real-time applications. A modified Fast Decoupled formulation was proposed in [19] for application to systems with high R/X ratio. This formulation is refereed to as BX while the standard fast decoupled formulation is refereed to as XB. Reference [20] presents an excellent review and gives the salient features and the comparative merits of different power flow solution methods applied to transmission networks.

Power Flow Algorithms for Distribution Systems

Gauss and Newton-Raphson based methods result in poor convergence of the power flow problem when applied to distribution systems, due to the natural differences found between transmission and distribution systems [21]. Backward-Forward-Sweep (BFS) method has been introduced as it lends itself easily for radial configuration of the distribution system [22]. The proposed method starts with finding net current injections, based on connected

loads, either power, current, impedance, or any combination of the above [23] [24] [25]. Treatment of weakly meshed systems is achieved through the introduction of breakpoints within any loop in the system [26] [27] [28] [29]. The prime drawback of the BFS method is the treatment of weakly meshed and meshed typologies, as BFS is designed for a purely radial system. Any loop in the system needs to be eliminated by the introduction of a break-point and a conversion of the system to a radial configuration. The introduction of any break-point in the system adds two extra conditions for every loop in the system, which were not present in the original problem conditions. The added conditions will increase the computational burden and reduce overall execution time. The effect of these added conditions would be pronounced and aggravated by the increase in the number of loops in the system, making this approach less desirable. Modeling of voltage-controlled nodes were added to the BFS formulation by [23] [25] [24]. In this formulation, the reactive power correction is related to the voltage deviation and the PV-bus to the slack bus loop impedance.

Another attempted solution, known as the Direct Solution Method (BIBC), has been introduced to address the power flow problem in distribution systems [30]. The method is a modified distribution load flow formulation, utilizing characteristic system properties. Two system unique matrices are introduced to calculate the relationship between bus injection to branch current and branch current to node voltage. Adaptation of the BIBC method to three-phase distribution systems was introduced in [31]. However, the application to a weakly meshed system requires special treatment through the introduction of breakpoints.

Inspired by the Backward-Forward-Sweep method, several graph-based methods have been introduced. These methods make use of bus-node incident matrix null space properties; however, they do not require special treatment for meshed topology [32] [33]. Formulation of generation nodes in the circuit is done in a feedback controller-like method [34] with special controller settings. Such a formulation is efficient, but lacks a clear PV node controller setting strategy.

1.2.2 Power Flow Algorithms for Hybrid AC/DC Systems

Various power flow algorithms were devised over the years to solve power flow problems in hybrid settings. Several reported techniques, such as, Newtons method [35] [36] [37] [38] [39] [40], Gauss-Seidel [41] [42], Fast-decoupled methods [43] [44] [45] [46], and Backward-Forward-Sweep methods [28] [29] [47], have been adopted to solve the AC/DC hybrid power flow problem. Article [28] proposed a method that is based on the BFS method, applicable to distribution systems. This formulation, by design, inherits all strengths and weaknesses of the BFS method and limits the application to distribution networks. Reference [29] is a follow-up article to [28] by the same authors, and employs the same method with added details of sensitivity matrix derivation and custom case studies with different R/X ratios. A modified BFS based method for hybrid AC/DC islanded micro-grid application is introduced by [47]. The paper uses two special test systems, does not describe the used converter model parameters, and is missing all details of systems data, rendering methods comparison impossible. Moreover, all used test systems are of pure radial configuration.

Converter models were incorporated with different details ranging from lossless to full detailed models [45] [48] [38]. Solutions for the AC/DC interface can be formulated in different methods, as a unified or sequential approach. The unified approach solves the hybrid AC/DC and converter equations simultaneously and updates inter-iteration variables at the same time [49] [38] [39] [40]. Such formulation would result in increased problem size. In contrast, the sequential approach solves AC/DC and converter equations in an algorithmic pre-defined sequence. Specifically, the output of one-step serves as the input to the proceeding step iteratively [36] [48][37]. Some considerations were made recently to improve the scalability of some methods in the literature, as in [50] [51] [52], where the focus is large systems scalability and reduced computational burden, by using parallel and high-performance computing. In the above-mentioned methods, the graph techniques have only been used for system partitioning in order to facilitate parallel computation, while the solution methodology makes use of the fast decoupled power flow method.

All previously mentioned methods present a compromise of some sort. First, Newton-Raphson based methods are more computationally extensive, leading to scalability issues

originating from Jacobean formulation and subsequent inversion [53]. Next, Gauss-Seidel methods are inherently slow, which would be further aggravated by bigger and more interconnected systems. Further, decoupled methods are relatively fast and do not require extensive computation, at the expense of an approximate and simplified formulation. The Backward-Forward-Sweep-based methods are limited to radial distribution networks. Treatment of non-radial systems is achieved by converting the system into radial topology by introducing loop break-points [28], while voltage-controlled nodes are treated using decoupled approach [29] and increasing the computational burden and overall runtime.

1.2.3 Optimal Power Flow

OPF is the backbone for optimizing power system activities. General OPF is formulated to optimize an objective function, that includes state and decision variables subject to equality and inequality constraints, consisting of power flow equations, branch thermal limits, bus voltages, etc. Usually, OPF models use accurate alternating current (AC) power flow equations, and in some special cases, direct current (DC) approximations are used instead, such as in contingency analysis, etc. The OPF problem is a non-convex optimization problem, and it is computationally challenging for large systems [54]. Several extensive reviews in the field of the conventional OPF problem and methods can be found in [55], [56], [57], and [58].

Many solution techniques have been developed over the years to solve OPF problems. The linearized dispatch problem was solved using a modified simplex method for online applications in [59], while the security dispatch problem was solved using a modified simplex method [60]. Mathematical programming and artificial intelligence techniques [61], [62], [63], [64], [65], [66], [67], and [68] were introduced, primarily, for cost reduction (profit optimization) and/or system loss minimization. The generalized non-linear OPF, using Lagrangian multipliers and pertaining to some similarities to the Newton-Raphson PF method, is presented in [69] to handle inequalities for economic dispatch. The gradient-based method was proposed in [70] using a combination of a penalty function and Lagrangian multipliers to incorporate steady-state security and insecurity constraints. A

significant improvement was proposed in [71], relying on the complex Hessian matrix approximation for online security-constrained optimal dispatch.

An efficient OPF solution based on the Newton-Raphson method was introduced in [72]. Initially, this solution was formulated to reduce line losses by the selection of reactive power flows and transformer tap settings. The dual problem was formulated using Karush-Kuhan-Tucker (KKT) conditions and solving on Lagrangian variables. Further computational speed improvements were gained by the implementation of sparse vector methods in power systems [73]. A similar approach was used for economic load dispatch problems by using the Jacobian matrix [74]. Security constrained dispatch formulation was introduced in [75] with linearized constraints around the operational point. Semidefinite programming (SDP) OPF formulation was introduced in [76] and its global solution is guaranteed if certain necessary conditions are met. Nevertheless, all the above-mentioned optimization technique solvers are either computationally burdensome or sensitive to initialization or do not guarantee a global optimal.

1.3 Motivation

As discussed above, the concept of PF, and its optimized version OPF, are mature subjects and have been extensively addressed in the literature. Many excellent papers have been written describing various methods for solving the PF or OPF equations. Each of these methods possesses advantages and disadvantages under certain conditions. PF calculations are performed in power system planning, operational planning, and operational control. In transmission systems, PF analysis has been used to solve very large systems, and to solve multiple cases for different purposes, such as outage security assessment; and within more complicated calculations, such as optimization and stability. In distribution systems operation and control, PF has been used to determine the settings of reactive power and voltage control devices, and to identify the system control parameters of the distributed generation output power. While in the planning phase, PF is required to determine the effects of adding and removing different components on the system performance and to

evaluate the optimal sizing of different power system components. The important properties required of a PF solution method include high computational speed, low storage requirements, reliable convergence, and versatility. The challenge presented involves the selection of the best PF solution method for a given application. The relative properties and performances of different PF methods can be influenced substantially by the types and sizes of problems to be solved, and by the precise details of implementation. The choice of a particular PF method mainly depends on the system configurations (transmission, distribution, or AC/DC hybrid), applications (offline or online), and, the accuracy of the required solution. From the previous survey, it seems that there is no available generic, efficient, fast, and robust PF method that is suitable for transmission and distribution configurations, as well as AC/DC hybrid systems, and can be employed for planning and operation/control. The efficient, optimum operation and planning of electric power systems have always occupied an important position in the electric power industry. OPF is the core for such optimal and efficient activities.

The steady increase in power system size and interconnection complexity increases the dimension of the PF and OPF formulation. All the presently used methods were developed for specific topologies and configurations, and some PF methods are applied to distribution networks that are characterized by unidirectional energy flow. Moreover, some current techniques are capable of handling the problem for off-line applications and lack the capabilities for online applications. The PF/OPF solution methodology becomes more challenging, specifically in the presence of high penetration of distributed energy resources. A fast and reliable and computationally efficient technique becomes a necessity to deal with the high level of system dynamicity that results from the presence of these distributed sources.

Motivated by the accelerated technological development in the energy sector, and by the limitations of the existing tools for solving the PF/OPF problem, this research addresses the issues highlighted above and focuses on developing modern tools for the operation and planning of electric power systems. This thesis aims to fill this gap by proposing a radically new generalized direction in power system problem formulations and proposes novel Graph Theory-based PF/OPF algorithms suitable for transmission, distribution, and

hybrid power systems. This research uses Graph Theory due to its versatility in modeling physical systems and efficient data manipulations. The proposed algorithms are simple, accurate, and fast, in addition to being computationally efficient, and scalable.

1.4 Research Contributions

The ultimate goal of this dissertation is the proposal and development of a novel generic graph-theoretic formulation and algorithms for power flow and optimal power flow solutions suitable for both transmission and distribution networks of any topology. In this context, this thesis puts forth a comprehensive toolbox for the planning, operation, and control of modern electric power networks. The proposed graph-based PF algorithm and its optimized version are comparable, in terms of speed and accuracy, to those that have been employed on transmission/distribution systems for decades. The proposed algorithms are generic, efficient, fast, and robust. The major contributions of this dissertation are:

1. Introduction of a novel graph-based power flow formulation as a maximum-flow problem and the development of a generic, fast, and efficient power flow algorithm named *Flow-Augmentation PF*. In this part of the research, the power system components models have been developed for the graph-based formulation, followed by the transformation of the power system into $s-t$ flow network. The proposed method handles any system configuration and type uniformly and makes no difference between transmission or distribution system, and is suitable for active distribution networks. The developed algorithm is formulated as matrix vector multiplication in its most abstract form, resulting in computational efficiency and scalability, allowing for parallel computation for added computational speed.

2. Extension of the proposed maximum-flow graph-based power flow formulation to multi-terminal voltage source converter-based hybrid AC/DC power systems using a sequential solution framework. The proposed method completely differs from presently known methods, which adapt classical power flow methods to hybrid AC/DC

settings. Like the *Flow-Augmentation PF*, the presented method is abstractly formulated as manipulation of algebraic structures, which proves to be a strong advantage for the developed method, resulting in a significant reduction in computational time. The solution procedure solves AC and DC parts sequentially while accounting for voltage source converter losses using a generalized full converter model.

3. Proposal of a novel generic graph-based minimum-cost flow model for PF/OPF based on the developed maximum-flow model. A special case of this model is the solution of the PF problem using the developed *MinLoss-Flow PF* algorithm. The presented method is directed by system loss minimization satisfying problem constraints. This formulation is efficient and generic for transmission and distribution systems of any configuration.

The research is novel in several respects. First, on the analytical front, this thesis presents generic graph-based techniques for solving the PF/OPF problems. The proposed method consists of novel graph-based formulations, and makes use of powerful graph techniques in solving PF/OPF problems; no other research to date presents such a generic approach and formulation. Second, on the application side, the graph-based formulation of the problem of PF/OPF for real-time application is unique. It is formulated as matrix-vector multiplication in its most abstract form, resulting in computational efficiency and scalability. Finally, this dissertation presents a new optimized solution based on a graph theory for loss minimization. The proposed formulation has great potential and can be extended to solve full-scale optimal power flow problems.

1.5 Thesis Outline

This thesis is organized into six chapters. Chapter 2 presents maximum-flow based PF solution methodology. A brief survey of the flow-based approach, components, and system modeling is presented. The *Flow-Augmentation PF* detailed discussion of algorithmic properties. Chapter 3 validates the *Flow-Augmentation PF* algorithm by simulation results on

known test cases for transmission and distribution systems of different configuration and components mix. A comparison of the proposed algorithm results against commercial software solvers is revealed. Chapter 4 proposes a generic minimum-cost flow-based solution methodology for PF/OPF, of which, a special case is the presented *MinLoss-Flow PF* method. Description of cost flow approach, modeling, and discussion and analysis of the developed algorithm are detailed. Chapter 5 adapts the *Flow-Augmentation PF* algorithm to a sequential maximum-flow-based power flow method for hybrid power systems, including a full VSC model of different topologies and control modes. Finally, Chapter 6 concludes the thesis and presents future research directions.

Chapter 2

Flow-Augmentation Power Flow Solution

2.1 Introduction

This chapter presents a graph-based solution method to the PF problem in power networks, named *Flow-Augmentation PF*. In this chapter, the PF is formulated as a graph maximum-flow problem, using the analogy between power networks and graph theory. A review of the flow-based approach is presented first, followed by electric system components modeling and transformation of power system into s-t network flow. The Maximum-Flow-based PF mathematical model and the proposed Flow-Augmentation PF solution are presented, including the algorithm correctness, termination, and computational complexity. The performance of the proposed PF method is demonstrated using a simple transmission system, which is representative of a large power system.

2.2 Network Flow Models

Flow models are one of the most researched topics in graph theory and combinatorics, with continuous improvements over the years. Among the earliest application of flow models to the commodity transportation problem was in the context of rail networks [77], which encouraged further research into the problem. The first published solution method was introduced by Ford and Fulkerson [78] and introduced the concept of minimum-cut. Various improvements of flow algorithms time complexity were made by the introduction of different concepts, like the shortest augmenting path algorithm [79] and the push-relabel algorithm [80], among other approaches.

2.2.1 Graph Theory Applications in Power Systems

Graph theory application for electric networks is a well-established area. Electric systems were, in fact, one of the motivating factors for continuing research in this field [81]. Most of the literature related to graph theory or network flow models in the context of power systems deals with specific cases, and no general method was ever proposed.

The first application of a network flow model to the power flow problem was proposed in [82]. The method relies on the selection of unique independent loops in the network, which cannot be guaranteed, and is computationally expensive and sensitive to loop-to-bus ratios. An abstract description of a network flow model was included in [83]. Minimum-cost flow model applications in power system operation were investigated in [84], including security constraints and unconstrained economic dispatch, single and multi-area load dispatch, bus observability for power system state estimation applications, and secure and economic automatic generation control, among other applications.

A power system restoration solution based on graph-theory is presented in [85], where non-normalized spectral clustering is used to determine the optimum network islanding partitions for parallel restoration. Power system studies under fault conditions were introduced in [86], where Z_{loop} is constructed using graph theory relationships without the need to formulate the loop incidence matrix, which is used to calculate branch currents

and bus voltages during fault conditions. Power routing through an electric network was presented in [87], with the proposed solution based on successive shortest path and scaling push-relabel algorithms. A recent review of electric networks and algebraic graph theory models and specific properties was introduced in [88], and a network simplex method application for AC power flow problems were investigated in [89], which has a long execution time, compared with Newton-Raphson based methods.

2.2.2 Graph Theory Notation

Graph. A graph $G = (V, E)$ is a collection of a finite number of vertices V and edges E. The cardinalities of the set of vertices is given by $n = |V|$, and of the set of arcs by $m = |E|$. Every edge E is characterized by two terminal vertices (u, v), both $u, v \in V$. A vertex u is said to be incident to an edge E if it lies at either ends of the arc. In other words, an edge E is said to be incident to a vertex if it's incoming or outgoing from a vertex V.

Directed and Undirected Graphs. An undirected graph $G = (V, E)$ is a graph where vertex $a \in E$ has no orientation, in the sense that vertex $a(u, v) \in E$ is equal to vertex $a(v, u) \in E$. In contrast, a directed graph is where every vertex in the graph has a specified orientation and $a(u, v) \in E$ is not equivalent to $a(v, u) \in E$.

Tree. A tree $T = (V, E)$ is a connected graph that contains no cycles, which can be directed or undirected. A tree should have a least two leave nodes.

Cycle. A cycle in graph $G = (V, E)$ is a set of edges that constitutes a closed path: for example $C = \{e_i, e_{i+1}, ..., e_k\}$, and can alternatively be represented using vertices as in $C = \{v_i, v_{i+1}, ..., v_k\}$.

Incidence Matrix. A directed graph G has a *0-1* matrix, $B(G)$, of size $m \times n$, with row and column indices of vertices and arcs of G, respectively. Such that, columns in B admits the value 1 if arc i is leaving vertex j and the value -1 if arc i is into vertex j and 0 otherwise.

Laplacian Matrix. Graph Laplacian matrix is direction independent representation matrix of graph. Laplacian is a square matrix of dimension n and defined as $\mathscr{L}(G) = BB^T$. Also, $\mathscr{L}(G) = B - D$, where D is a diagonal matrix of node degree.

2.3 Flow-Based Approach

Network flows deals with the problem of commodity transfer from the source node to the sink node using all network connections with restricted flow capacities. Receiving continued attention throughout the years, with frequent improvements in regard to computation speed. Likewise, the PF problem deals with supplying electric power from generation to the load buses. For this, building on this analogy is natural, but requires some modifications. Network flows require some adaptation to effectively work with electric networks, which stems from the different nature of the problems network flows are applied to. For example, network flows have a flow preservation property as a condition for the optimum solution, while electric networks require satisfaction of both Kirchhoff's laws and Ohm's law. Finally, electric networks need to be transformed to a graph equivalent by grouping the generation nodes and load nodes at different points while maintaining graph connectedness in an electric circuit like topology.

2.3.1 Electric System Modeling

Branch Model. All graph branches are modeled using a unified branch model for electric components, which is suitable for transmission lines, transformers, cables, and any shunt connected element. This model is an ideal phase-shifting transformer in series with a transmission line π model with branch admittance Y_{branch} and shunt charging susceptance b_c, as shown in figure 2.1. Transformer tab ratio changes branch input and output voltage and current, which is adjusted based on shunt elements. Shunt elements of branches connected to a common node are lumped together to further simplify calculations.

Shunt Elements Model. Shunt elements are modeled as shunt components with respect to specific nodes, with element impedance added to Y_{bus} at the load node.

Transformer Model. Transformer is modeled by adjusting branch impedance and adding branch sending and receiving shunt elements based on transformer tap ratio.

Generator Model. Generators are modeled as complex power injections at the generation buses and active power injections at voltage-controlled buses.

Load Model. Loads are modeled as constant power, constant current, or constant impedance. In either case, the load current is an important factor in the proposed algorithm's convergence. Constant power load current would be updated in each iteration based on load bus voltage, while constant impedance load is considered as a shunt element and incorporated in Y_{bus}.

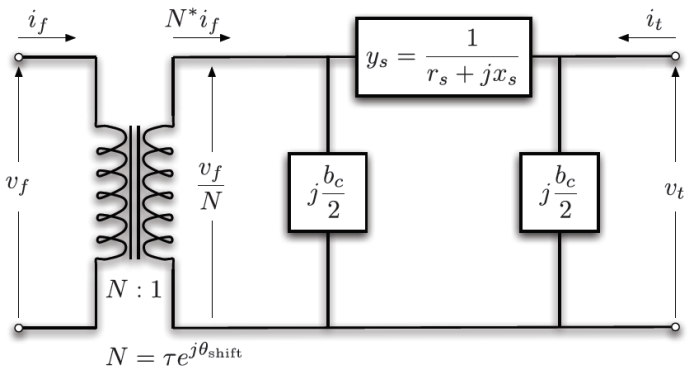

Figure 2.1: Unified branch model [92].

2.4 Power System Transformation into s-t Flow

The application of flow-based methods to electric networks requires the transformation of the power network into an *s-t* network by grouping all power sources to be connected to a *super-source* and all load points to a *super-sink*. By doing so, we can interpret the power network using graph-theoretic terminology and provide a concise mathematical description.

Take an electrical network $N_{electric} = (\mathcal{B}, \mathcal{D}, \mathcal{G}, \mathcal{L})$ consisting of a set of buses $\mathcal{B}$, a set of power lines $\mathcal{D}$, a set of generators $\mathcal{G}$, and a set of loads $\mathcal{L}$, where each line connects two buses. A bus can be connected to a generator $g \in \mathcal{G}$, a consumer or load $\ell \in \mathcal{L}$, or any other type of connection in an electric network. To transform the network $N_{electric}$ to a $s-t$ network $N_{st} = G(V, E)$, we represent every bus by a vertex, and each power line by an edge, where the power line between buses j and k corresponds to edge $(j, k) \in E$. All buses connected to generation units $\mathcal{G}$ with positive power injection are connected to an additional vertex s, called the source vertex, using lossless lines, and all load buses $\mathcal{L}$ are connected to an additional vertex t, called the sink vertex, in the same manner. The source vertex s supplies all connected load power plus network losses through generators $\mathcal{G}$, where the sum of the edge flows connecting s to generation vertices equal the sum of the total generators' power. As well, the sink vertex t sums the total system connected load. Each $(j, t) \in E$ edge is equivalent to individual load power. All connections from nodes s and t to network vertices have no electrical properties, i.e. no resistance, and thus would not affect power flow from *super-node* to subsequent nodes. Figures 2.2 shows 4-bus mesh connected system [90], figure 2.3 shows the same system in graph form, and figure 2.4 shows the system in $s-t$ form.

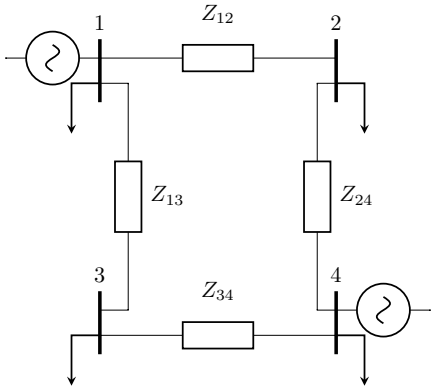

Figure 2.2: 4-bus test system one line diagram.

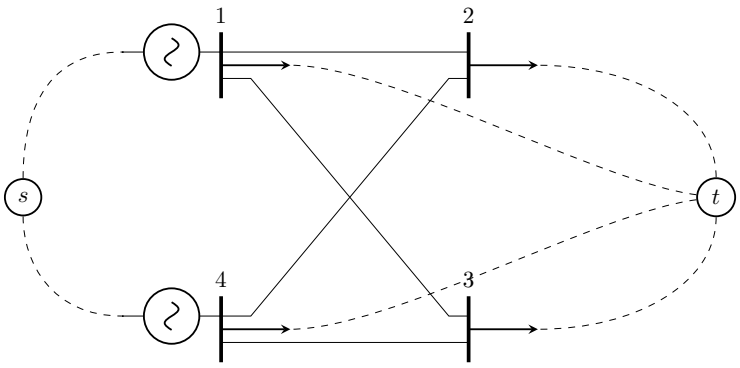

Figure 2.3: 4-bus test system in graph form.

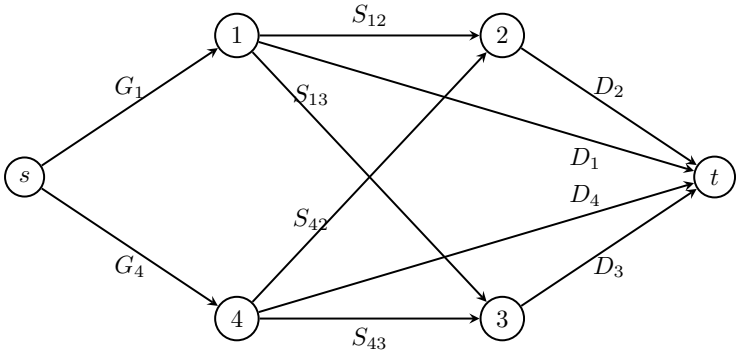

Figure 2.4: 4-bus test system in s-t form.

2.5 Maximum Flow Mathematical Model.

Considering an electric network $N_{st-electric} = (G(V, E), s, t, \mathcal{G}, \mathcal{L})$ with vertex set V, edge set E, source s, sink t, generation set $\mathcal{G}$ and load set $\mathcal{L}$. Electric power flow for the network $N_{st-electric}$ is considered feasible for the network if the feasible flow function $f : A \to \mathbb{C}$ satisfies [91]:

$$\sum_{j:(j,k)\in V} f(j,k) \quad = 0, \qquad \forall j \in V \setminus \{s,t\} \tag{2.1}$$

$$\sum_{j:(s,j)\in E} f(s,j) \quad = \textstyle\sum_{g\in\mathcal{G}} g, \qquad \forall \{s,j\} \in E \tag{2.2}$$

$$\sum_{j:(j,t)\in E} f(j,t) \quad = \textstyle\sum_{\ell\in\mathcal{L}} \ell, \qquad \forall \{j,t\} \in E \tag{2.3}$$

The flow solution satisfies load demand and voltage criteria on the generation side with the preservation of Kirchhoff's laws. Solving the power flow problem using network flow formulation would face two main challenges. First, the guarantees of preserving voltage and current laws. Secondly, the huge solution space to be explored if traditional network-flow methods are used.

2.6 Flow-Augmentation Power Flow Algorithm

The proposed algorithm solves for maximum network flow that satisfies power flow problem requirements. The flow is modeled as complex power injection at each node and branch complex power flows. The *Flow-Augmentation PF* algorithm transfers power from the generation to the demand sides with no consideration of branch capacities. It relies on the calculation of network flow augmentation that supplies demand power and maintains correct voltage magnitude at generation buses.

The goal of the solution procedure is to find the maximum complex power flow in a $s-t$ network while satisfying the fixed branch power into node t. This procedure doesn't rely on finding individual flow augmenting paths one at a time that satisfies electric systems' physics, but rather focuses on finding the total network flow that should exist to firstly satisfy demand requirements, and secondly maintain voltage magnitudes on generation buses. This goal is facilitated by formulating the solution variable as a complex power injection, exploiting the voltage and current duality relationship in electric circuits.

The network flow augmentation algorithm solves the complex power flow in the electric network by exploiting complementary slackness and tight duality gaps between node voltage and current injections. Network flow augmentation is achieved through the adjustment of network current injections on the generation side and demand side, governed by equation $S = U \cdot I^*$ after node voltage changes.

Theorem 1 (Flow-Augmentation PF Algorithm Solution Existence and Uniqueness)**.** *The solution to the power flow problem is the maximum complex power network-flow that satisfies power flow problem constraints. The solution of Flow-Augmentation PF algorithm is unique.*

Proof. The power flow solution voltage profile dictates system power injection that satisfies power flow problem conditions. In turn, results in branch current and power flow in the lossy network, satisfying Ohm's law, Kirchhoff's laws, and preservation of energy with minimum system losses. Any deviation from the unique power flow solution voltage and current vectors leads to a change in demand power injections and generation level, violating problem constraints and changing system losses. □

The solution procedure calls for network transformation to $s-t$ equivalent model first, then invoking the max-flow-based solution method. It is worth noting here that the considered network flow here is complex power S, and the resulting node voltages and node current injection dictate network current flows through network branch impedance. The max-flow-based network-flow solution converges to the power flow solution when complex power flow into sink node t satisfies demand power and network power losses. Moreover, PV bus active power injection and voltage magnitude $|U|_{pv}$ satisfies stated PV bus requirements, and reference bus $|U|_{ref}$ and δ_{ref} are met. The sum of all generation power originated from source node S equals the sum of all demand power into sink node t plus power losses dissipated throughout the network.

Generations side reactive power can be initially assigned based on the total connected load power factor. Starting with generations equals total connected load and a flat voltage profile. Bus injection currents are calculated, followed by a voltage profile update in relation

to the reference bus voltage. Demand-side current injection changes as a result of voltage level change with the preservation of demand power. This step necessitates the change of current injection at generators buses, which requires the update of the voltage profile. The resulted sum of generation bus injection power is closer to the sum of total system demand plus system losses. Allocation of real power to generation buses is straightforward, as all PV buses real power injection is defined a priori, and the difference between the total real power sum and PV node's sum is allocated to the reference bus as bus generation plus system losses.

Generation buses reactive power is adjusted based on deviations in resultant voltage magnitudes compared to specified voltage magnitudes. Initial generation reactive power is updated after the execution of every Network-flow power flow step. Since generation node's voltage magnitude is different from the required PV bus voltage magnitude, resulting in $\Delta|U|$, and the direct relation between reactive power injection and voltage magnitude, we could correct for each PV bus reactive power injection based on voltage magnitude deviation from stated voltage within generator reactive power limits, noting that $\frac{\partial Q}{\partial U}$ can be formulated in various forms. System pre-flow is generated before the iterative generation-side reactive power correction and network-flow augmentations until either error tolerance or maximum iteration counter is reached. The selected stopping criteria is the infinity norm of power injections for transmission systems, $\| S_{inj} \|_\infty$, and the infinity norm of voltage magnitude, $\| |U| \|_\infty$, for distribution systems.

The proposed flow augmentation PF procedure is presented in algorithm 1 and the flow-chart in figure 2.5. Algorithms 2, 3 and 4 presents data transformation, PF calculation and reactive power correction at generation buses.

2.6.1 Power Network Transformation

The first step is the *NetworkTransformation* step, which transforms system configuration and parameters to construct and initialize generation levels and system-wide voltages.

Algorithm 1 Flow-Augmentation PF

1: NetworkTransformation($G(V, E)$, S_{demand}, U_{ref}, Y_{branch})
2: NetworkFlowPFCalculation($G(V, E)$, S_{bus}, U_{bus}, Y_{bus})
3: iter = 0
4: **while** error $\geq \epsilon$ or iter $\leq$ maxIter **do**
5: ReactivePowerCorrection($G(V, E)$, S_{bus}, U_{bus}, Y_{bus})
6: NetworkFlowPFCalculation($G(V, E)$, S_{bus}, U_{bus}, Y_{bus})
7: iter = iter + 1
8: **end**

System topological connections are converted into directed graphs after bus renumbering. Graph incident and adjacency matrices are formulated, followed by the Y_{bus} matrix. Node voltages are initialized to a flat profile except for the voltage-controlled bus to the specified voltage magnitude $|U|_{PV}$ and angle 0. Since the initial generation starting point is equivalent to the total system connected load, $\sum S_{gen} = \sum S_{demand}$, reference bus generation is initialized to equalize the sum of system power balance with the assumption of *Zero* losses in the system. Voltage-controlled bus reactive power injection is initialized based on active power injection and total connected load power factor. Algorithm 2 presents the system transformation and variables initialization step.

2.6.2 Network-Flow PF Calculation

This procedure calculates the network power flows by correcting generators' injected complex power to maintain power flow preconditions. Generators' power is injected into node-connected arcs toward the sink node, while governed by the system physics, resulting in power losses and producing different voltage profile and current injections.

Starting with node voltages, net injected power, and Y_{bus} leads to the calculation of injected current. Calculated current injections don't satisfy the current law throughout the network. For this, reference bus current correction is required to compensate for

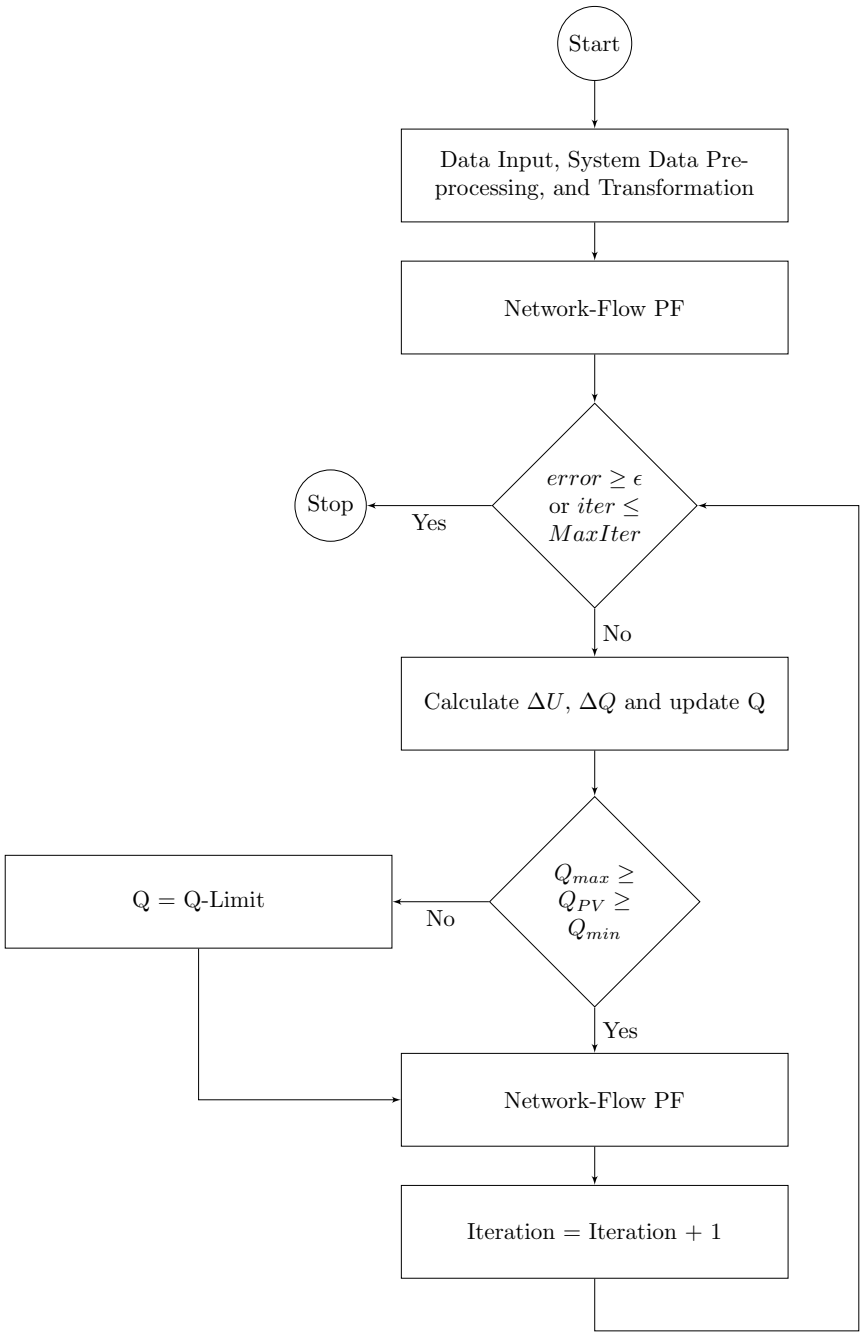

Figure 2.5: Flow-Augmentation PF algorithm flow chart.

Algorithm 2 NetworkTransformation

1: $n \leftarrow$ *number of Vertices/Nodes*
2: $m \leftarrow$ *number of Arcs/Edges*
3: $G(n, m) \leftarrow$ *Network Topology* (n, m)
4: $G(V, E) \leftarrow$ *Network Topology* $(G(n, m))$
5: $A(G) \leftarrow$ *Network Topology* $(G(n, m))$
6: $\sum S_{gen} \leftarrow \sum S_{demand}$
7: $S_{gen-pv} \leftarrow P_{bus-pv} + j(P_{bus-pv} * tan(pf_{load}))$
8: $S_{bus-ref} \leftarrow \sum S_{gen-pv} - \sum S_{demand}$
9: $U_{bus-pq} \leftarrow U_{ref}$
10: $U_{bus-pv} \leftarrow |U_{bus-pv}| \angle 0°$
11: $Y_{bus} \leftarrow A(G) * Y_{branch} * A(G)' + diag(Y_{shunt})$

initially assumed *zero* system losses. Intern, corrected calculated current, and Y_{bus} result in an updated voltage profile. Which is considered as a node voltage difference, and is used as a basis for corrected voltages in relation to the reference bus. The reference bus voltage is maintained at U_{ref} p.u. throughout the solution process. Corrected voltage and current injection adjust net injected power on the generation side of the network while maintaining demand-side power. The *NetworkFlowPFCalculation* procedure is presented in the algorithm 3.

2.6.3 Reactive Power Correction

The system power injection and voltage profile are updated after every iteration of *NetworkFlowPFCalculation* procedure. Resulting in generators voltage magnitude difference $\Delta|U_{PV}|$, which indicates the need for reactive power correction.

$$\Delta|U|_{PV} = |U|_{PV}^{specified} - |U|_{PV}^{calculated} \tag{2.4}$$

Algorithm 3 NetworkFlowPFCalculation

procedure NetworkFlowPF($G(V, E)$, S_{bus}, U_{bus}, Y_{bus})
  $S_{bus}^{inj} \leftarrow S_{bus}^{gen} - S_{bus}^{demand}$
  $I_{bus}^{inj} \leftarrow (S_{bus}^{inj}/U_{bus})^*$
  $I_{bus}^{inj-sh} \leftarrow U_{bus} \cdot Y_{shunt}$
  $I_{bus-ref}^{inj} \leftarrow -\sum I_{bus-pq}^{inj} - \sum I_{bus-pv}^{inj} - \sum I_{bus}^{inj-sh}$
  $U_{bus-diff} \leftarrow Y_{bus}^{-1} \cdot I_{bus}$
  $U_{bus} \leftarrow U_{ref} + (U_{bus-diff} - U_{bus-diff}^{ref})$
  $S_{bus}^{inj} \leftarrow U_{bus} * I_{bus}^*$
  $S_{bus}^{gen} \leftarrow S_{bus}^{inj} + S_{bus}^{demand}$
return $S_{bus}, U_{bus}, I_{inj}$

This in turn necessitates the adjustment of reactive power injection at every PV bus. Relying on the direct relationship between reactive power injection and voltage magnitude, reactive power correction for PV bus based on voltage magnitude deviation from stated voltage can be made. Reactive power correction and voltage magnitude deviation are calculated in a decoupled form as follows:

$$\Delta Q = \frac{\partial Q}{\partial |U|} \cdot \Delta |U| \tag{2.5}$$

$$\begin{bmatrix} \Delta Q_{PV} \\ \Delta Q_{PQ} \end{bmatrix} = \begin{bmatrix} \frac{\partial Q_{PV}}{\partial |U|_{PV}} & \frac{\partial Q_{PV}}{\partial |U|_{PQ}} \\ \frac{\partial Q_{PQ}}{\partial |U|_{PV}} & \frac{\partial Q_{PQ}}{\partial |U|_{PQ}} \end{bmatrix} \begin{bmatrix} \Delta |U|_{PV} \\ \Delta |U|_{PQ} \end{bmatrix} \tag{2.6}$$

Noting that $\frac{\partial Q}{\partial U}$ is a matrix of size $n \times n$, which can be formulated in different ways. The following formula was elected for this purpose [92]:

$$\frac{\partial Q}{\partial |U|} = [U] \cdot ([I_{inj}^*] + Y_{bus}^* \cdot [U^*]) \cdot [|U|^{-1}] \tag{2.7}$$

The challenge with this approach is the lack of voltage magnitude information for PQ bus, which is evident by the expansion of equation (2.7) in terms of PV and PQ terms. The effect of this missing term is pronounced with an increased ratio of PQ to PV nodes. Solving for $\Delta|U|_{PQ}$ from equation (2.6) would first require the evaluation of ΔQ_{PQ}, which is dictated by the specified reactive power from the problem statement and calculated reactive power from the system voltage profile as in the following equations:

$$\Delta Q_{PQ} = Q_{PQ}^{specified} - \Im\{[U_{PQ}] \cdot (Y_{bus_{(PQ \times n)}} \cdot U_{(n)})^*\} \tag{2.8}$$

$$\Delta|U|_{PQ} = \{\Delta Q_{PQ} - \{\frac{\partial Q_{PQ}}{\partial|U|_{PV}} \cdot \Delta|U|_{PV}\}\} \cdot \frac{\partial Q_{PQ}}{\partial|U|_{PQ}}^{-1} \tag{2.9}$$

$$\Delta Q_{PV} = \frac{\partial Q_{PV}}{\partial|U|_{PV}} \cdot \Delta|U|_{PV} + \frac{\partial Q_{PV}}{\partial|U|_{PQ}} \cdot \{\Delta Q_{PQ} - \frac{\partial Q_{PQ}}{\partial|U|_{PV}} \cdot \Delta|U|_{PV}\} \cdot \frac{\partial Q_{PQ}}{\partial|U|_{PQ}}^{-1} \tag{2.10}$$

Inclusion of Reactive Power Limits

The generators' reactive power limits are preserved after the calculation of the updated generators' reactive power injection. This preservation is achieved by fixing any violating generator reactive power to the limits, either upper or lower. Algorithm 4 demonstrates the required steps.

Algorithm 4 ReactivePowerCorrection

procedure ReactivePowerCorrection($G(V, E)$, S_{bus}, U_{bus}, Y_{bus})
    $\Delta|U|_{PV} \leftarrow |U|_{PV}^{specified} - |U|_{PV}^{calculated}$
    Enumerate sensitivity of bus reactive power injection to voltage magnitude $\frac{\partial Q}{\partial U}$ Using Equation (2.7)
    Calculate ΔQ^i Using Equation (2.10).
    $Q^{i+1} \leftarrow Q^i + (\frac{\partial Q}{\partial U} \cdot \Delta|U|_{PV})$
    $Q^{i+1} \leftarrow Q_{max}$ if $Q^{i+1} > Q_{max}$
    $Q^{i+1} \leftarrow Q_{min}$ if $Q^{i+1} < Q_{min}$
return S_{bus}

2.7 Flow-Augmentation Power Flow Algorithm Correctness and Termination

The algorithm starts with a preconditioned initialization that partially satisfies the power flow problem conditions. Demand-side power injection, generation side voltage magnitudes, and current law are initially satisfied. While, in the other hand, generation reactive power, voltage law, and overall voltage profile are not preserved. Resulting in violation of power flow conditions and lack of guarantees of minimum system losses. In every iteration, the algorithm *While* loop adjusts reactive power to correct for PV bus voltage magnitude deviation, leading to incremental improvements in voltage profile with the execution of every *NetworkFlowPFCalculation*. This continuous refined adjustment of system voltage and generators power injection leads to lower system losses compared with the preconditioned state. The Flow-Augmentation PF algorithm terminates by either achieving the pre-specified error tolerance or violating the maximum iteration counter. The iterative post-condition update of the system states drives the system closer to the final solution and eventually converges to satisfy PF constraints.

Theorem 2 (Flow-Augmentation PF Algorithm Termination)**.** *The Flow-Augmentation PF algorithm terminates with a solution of the power flow problem within the pre-specified error bounds* ϵ*.*

Proof. The solution is initialized to node power injection and voltage profile given by $S_{bus}^{int} = [s_1, s_2, ..., s_n]^T$ and $U_{bus}^{int} = [u_1, u_2, ..., u_n]^T$ respectively. Suitable power injection can be found for the slack bus to balance initial system injections with the assumption of lossless system, satisfying system power balance equation $\sum S_{generation} = \sum S_{demand} + \sum S_{loss}$. Such power injections would result in current injections $I_{bus} = [i_1, i_2, ..., i_n]^T$ given by $I_{bus}^k = \left(\frac{S_{bus}^k}{U_k}\right)^*$. The preservation of current law dictates the need of reference bus current correction, given in the form $I_{bus-ref}^{inj} = -\sum I_{bus-pq}^{inj} - \sum I_{bus-pv}^{inj} - \sum I_{bus}^{inj-sh}$. This, in turn, results in vectors U_{bus}^k and S_{bus}^k that are different from U_{bus}^{int} and S_{bus}^{int}. Any deviation of PV bus voltage magnitude, $|U|_{PV}^{specified} - |U|_{PV}^{calculated}$, dictates the correction of net reactive power injection at such bus. This correction is calculated by $\Delta Q = \frac{\partial Q}{\partial |U|} \cdot \Delta |U|$. The updated S_i^k vector results in an improved voltage profile U_{bus}^{k+1} and system power injections S_i^{k+1} that reduces the system losses. The *Flow-Augmentation* PF terminates whenever $error \leq \epsilon$ or $iter \geq iterMax$. □

2.8 Flow-Augmentation Power Flow Algorithm Computational Complexity

The Flow-Augmentation PF algorithm's complexity is dominated by steps within the *While* loop, where every iteration of the algorithm performs *RreactivePowerCorrection* step followed by *Flow-Augmentation* step till convergence criteria or maximum iteration counter is reached. The *ReactivePowerCorrection* procedure contains three computationally complex steps, steps 2, 3, and 4 in algorithm 4. Voltage magnitude difference is calculated for all PV bus in the system with a complexity of $O(n_{PV})$, where $O(.)$ is the number of the arithmetic operations and n is the number of buses in the system. Calculation of reactive power sensitivity to voltage magnitude is evaluated using equation (2.7), with all arguments in

diagonal matrix form of size $n \times n$ and the only non-diagonal argument is Y_{bus} of size $n \times n$. Since Y_{bus} is a sparse matrix, the complexity of this step $O(n^{1.2})$. The reactive power corrective step is of size $n_{PV} \times (n-1)$ times $(n-1) \times 1$ resulting in $n_{PV} \times 1$. Supplementary step complexity is $n_{PQ}^{1.4}$. The ratio of PV to PQ nodes in the system directly influences the complexity of this step, leading to $O(max\{n_{PV}, n_{PQ}^{1.4}\})$. The Flow-Augmentation PF is dominated by the solution of a linear system in the form $Y_{bus} \times U = I_{inj}$, by either multiplying Y_{bus}^{-1} of dimension $n \times n$ by current injection vector of dimension $n \times 1$, or by backward substitution of LU factored matrix with a maximum complexity of $O(n^{1.2})$ for the repeated solutions. For this, the maximum complexity of the Flow-Augmentation PF algorithm is $O(max\{n^{1.2}, n_{PQ}^{1.4}\})$, and the complexity of the special case of no PV bus in the system is $O(n^{1.2})$.

2.9 Example

This section demonstrates the proposed algorithm using the transmission level 4-bus test system discussed in section 2.4 and adopted from [90]. The system is a two-generator mesh-connected system with load demand at every bus. Figures 2.2, 2.3, and 2.4 shows the system configuration and the electric network transformation steps into an $s-t$ network respectively. Table 2.1 presents comparative results of the Flow-Augmentation PF algorithm against well-established PF methods; the comparison was in terms of injected power mismatch, $\varepsilon = 10^{-5}$, number of iterations, and overall execution time. Figure 2.6 shows the convergence error for voltage magnitude, voltage angle, generation active and reactive power injection. Figure 2.7 demonstrate PV-bus voltage magnitude deviation error of stated voltage. Figure 2.8 presents different methods convergence trend. The Table and Figures below demonstrate the fast linear convergence of the proposed method.

Table 2.1: Flow-Augmentation PF algorithm comparative results for 4-bus system.

Method	Mismatch	Iteration	Execution Time (s)
Flow-Augmentation PF	1.8356e-6	6	4.0340e-3
Newton-Raphson	1.0685e-9	3	69.0501e-3
Gauss-Seidel	5.7947e-6	18	69.3579e-3
Fast-Decoupled (BX)	6.5722e-6	4	50.7932e-3
Fast-Decoupled (XB)	5.8041e-6	4	51.0519e-3

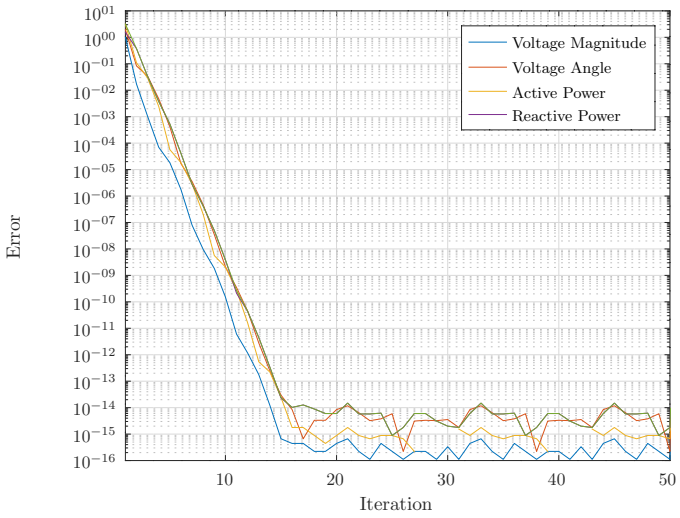

Figure 2.6: Flow-Augmentation PF convergence error for 4-bus system.

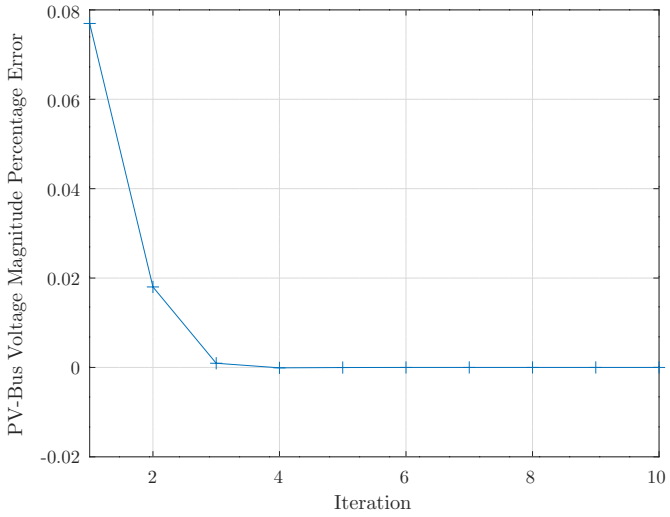

Figure 2.7: Flow-Augmentation PF PV-bus voltage magnitude error for 4-bus system.

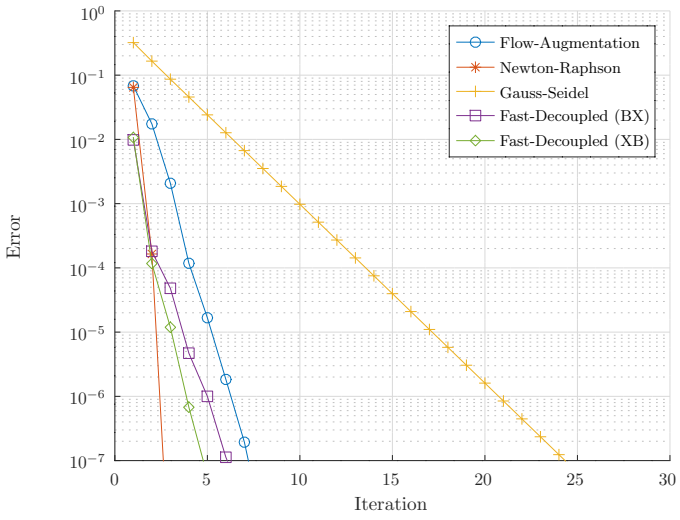

Figure 2.8: Flow-Augmentation PF algorithm comparative error convergence for 4-bus system.

2.10 Summary

In this chapter, a Flow-Augmentation PF algorithm for electric power transmission and distribution levels is presented. The developed method is generic in nature and is not affected by system topology and accommodates various branch elements. The proposed method does not require the calculation of the Jacobean matrix and subsequent inversion, as in the Newton-Raphson method, nor does it require the introduction of branch break-points and changes in system topology, as in the Backward-Forward-Sweep method. The presented method was evaluated and compared in terms of convergence and run time against well-known PF methods. The proposed method shows superior performance in comparison with those methods.

Chapter 3

Simulation Results and Analysis

3.1 Introduction

The performance of the proposed Flow-Augmentation PF solution, in terms of accuracy and convergence speed, is demonstrated using several transmission and distribution test systems and compared with Gauss-Seidel, Newton-Raphson based algorithms, and Backward-Forward-Sweep power flow method, when applicable. The performance of the algorithm is also compared with that of PSS/E and PSCAD commercial software packages. In this chapter, the Flow-Augmentation PF simulation results and the convergence characteristics, in terms of the number of iterations and algorithm accuracy, are reported.

3.2 Application to Transmission Systems

The testing and validation of the proposed algorithm using transmission test systems is presented, including WSCC 9-bus, IEEE 14-bus, IEEE 30-bus, and IEEE 118-bus systems [93] [70] [94] [95] [96] [97]. These systems contain transformers of different tap settings, shunt elements, synchronous condensers, and are operated at different voltages and loading conditions. The parameters of the test systems are given in Appendix A. Tables 3.1, 3.2,

3.3, and 3.4 present comparative convergence results, in terms of number of iterations and accuracy, of the Flow-Augmentation PF algorithm against other PF methods using different transmission systems, WSCC 9-bus, IEEE 14-bus, IEEE 30-bus, and IEEE 118-bus system respectively.

Table 3.1: Flow-Augmentation PF algorithm comparative results for WSCC 9-bus system.

Method	Mismatch	Iteration	Execution Time (s)
Flow-Augmentation PF	7.1069e-6	8	6.4061e-3
Newton-Raphson	342.1321e-9	3	69.5479e-3
Gauss-Seidel	9.6113e-6	123	141.8772e-3
Fast-Decoupled (BX)	2.3910e-6	4	78.0342e-3
Fast-Decoupled (XB)	7.5577e-6	4	53.9320e-3

Table 3.2: Flow-Augmentation PF algorithm comparative results for IEEE 14-bus system.

Method	Mismatch	Iteration	Execution Time (s)
Flow-Augmentation PF	8.6059e-6	6	5.0941e-3
Newton-Raphson	131.5780e-12	2	69.4242e-3
Gauss-Seidel	8.8967e-6	14	53.9432e-3
Fast-Decoupled (BX)	48.1103e-6	4	50.1220e-3
Fast-Decoupled (XB)	11.8822e-6	4	53.1950e-3

Table 3.3: Flow-Augmentation PF algorithm comparative results for IEEE 30-bus system.

Method	Mismatch	Iteration	Execution Time (s)
Flow-Augmentation PF	5.3752e-6	7	5.9280e-3
Newton-Raphson	956.9985e-12	3	69.8009e-3
Gauss-Seidel	9.9401e-6	373	735.4259e-3
Fast-Decoupled (BX)	13.0255e-6	5	54.0261e-3
Fast-Decoupled (XB)	11.6337e-6	7	74.1231e-3

Table 3.4: Flow-Augmentation PF algorithm comparative results for IEEE 118-bus system.

Method	Mismatch	Iteration	Execution Time (s)
Flow-Augmentation PF	6.1697e-6	22	22.7020e-3
Newton-Raphson	9.7030e-6	2	69.3870e-3
Gauss-Seidel	NC	-	-
Fast-Decoupled (BX)	52.4600e-6	4	54.0290e-3
Fast-Decoupled (XB)	6.8693e-6	4	64.5671e-3

The above tables show that the Flow-Augmentation PF has a better performance compared with that of the other well-established techniques. They also show that the overall execution time of the proposed method, when applied to transmission systems, is significantly lower than that of Newton-Raphson, Gauss-Seidel, and Fast-Decoupled methods. Its evident that the Flow-Augmentation PF algorithm requires relatively higher number of iterative steps when compared with Newton-Raphson method as demonstrated in Tables 3.1, 3.2, 3.3, 3.4 for the different test systems, while efficiently requiring lower computational time. The test results of the proposed Flow-Augmentation PF show significant computational gains, of about 70%, when compared with the Newton-Raphson on 118-bus system.

The accuracy of the Flow-Augmentation PF, using IEEE 118-bus system, is depicted in Figure 3.1. The figure shows how the variation of inter-iteration error changes as a function

of the number of iterations. Figure 3.2 displays the voltage magnitude error of the PV buses, and it shows that the error approaches zero when the algorithm converges. Figure 3.3 displays the comparative convergence characteristics (accuracy and number of iterations) of Flow-Augmentation PF method against the other PF methods. From the figure, the difference in the number of iterations stems from the linear versus quadratic convergence characteristics of the Flow-Augmentation and Newton-Raphson methods. A complete set of the algorithm performance graphs for WSCC 9-bus, IEEE 14-bus, and IEEE 30-bus test systems can be found in Appendix B. These graphs include the algorithm convergence error, PV bus voltage magnitude error, and comparative convergence characteristics with different methods.

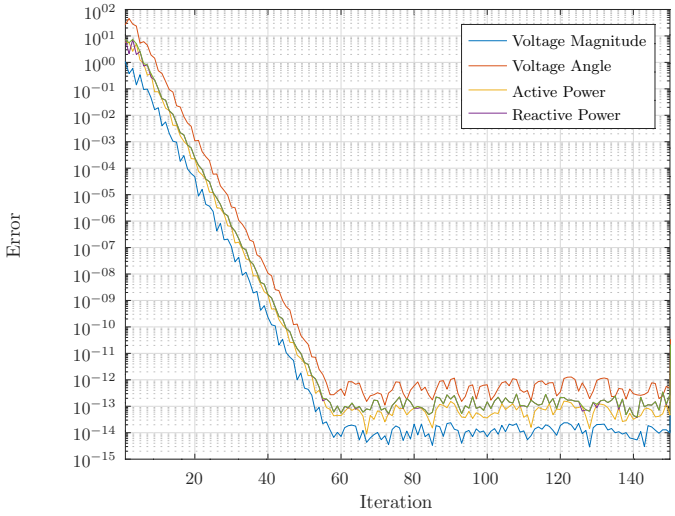

Figure 3.1: Flow-Augmentation PF algorithm convergence error for IEEE 118-bus system.

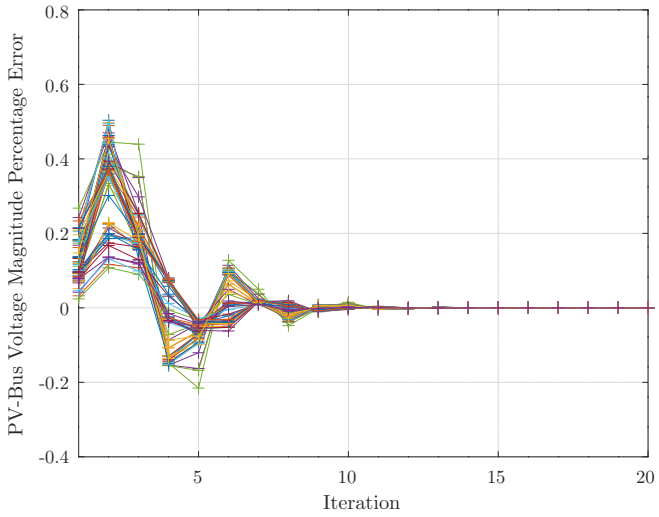

Figure 3.2: Flow-Augmentation PF algorithm PV-Bus voltage magnitude error for IEEE 118-bus system.

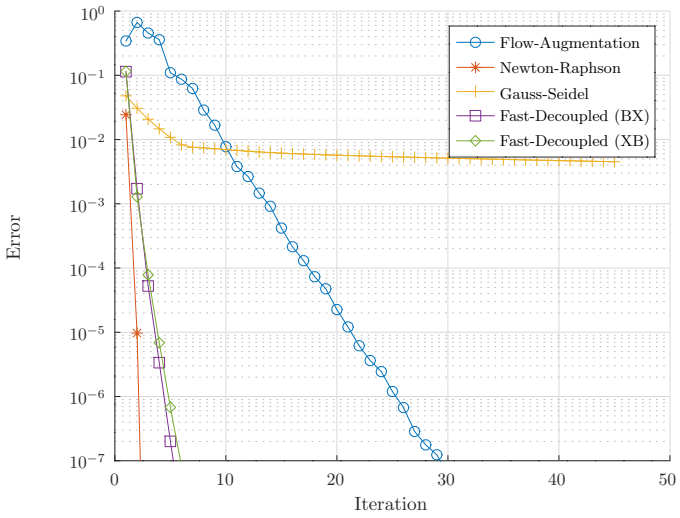

Figure 3.3: Flow-Augmentation PF algorithm comparative error convergence for IEEE 118-bus system.

3.3 Application to Distribution Systems

The verification of the developed method using distribution systems is conducted using 69-bus system under four configurations [98]. The first configuration is a pure radial topology, while the second configuration is a fully meshed topology. The mesh connection is configured by closing all tie-lines in the system between nodes 11-43, 13-21, 15-46, 50-59, and 27-65 [99]. The third and fourth configurations are made by adding distributed generations, to both the radial and the mesh configurations, in the form of voltage-controlled sources in six nodes. The distribution system configurations (Figure A.6, Figure A.7, Figure A.8) and the system and distribution generation data (Table A.13, Table A.14) are available in Appendix A. Tables 3.5, 3.6, 3.7, and 3.8 presents convergence results of the proposed Flow-Augmentation PF algorithm and other methods, applied to different configurations.

Table 3.5: Flow-Augmentation PF algorithm system comparative results for 69-bus system in radial topology.

Method	Mismatch	Iteration	Execution Time (s)
Flow-Augmentation PF	7.7523e-6	3	4.6780e-3
BFS-Current Sum	5.3351e-6	5	352.8750e-3
BFS-Power Sum	4.2967e-6	3	312.8390e-3
BFS-Impedance Sum	5.3351e-6	5	392.2720e-3
Newton-Raphson	10.4262e-9	3	73.1361e-3
Gauss-Seidel	NC	-	-
Fast-Decoupled (BX)	67.0784e-6	9	62.7921e-3
Fast-Decoupled (XB)	6.5419e-6	10	66.0350e-3

Table 3.6: Flow-Augmentation PF algorithm system comparative results for 69-bus system in meshed topology.

Method	Mismatch	Iteration	Execution Time (s)
Flow-Augmentation PF	4.1024e-6	2	4.0681e-3
BFS-Current Sum	-	-	-
BFS-Power Sum	-	-	-
BFS-Impedance Sum	-	-	-
Newton-Raphson	5.1043e-6	2	68.6810e-3
Gauss-Seidel	NC	-	-
Fast-Decoupled (BX)	47.9153e-6	7	57.9872e-3
Fast-Decoupled (XB)	1.5365e-6	7	169.2040e-3

Table 3.7: Flow-Augmentation PF algorithm system comparative results for 69-bus system in radial topology with DGs.

Method	Mismatch	Iteration	Execution Time (s)
Flow-Augmentation PF	7.9006e-6	36	39.5670e-3
BFS-Current Sum	9.4693e-6	42	417.8429e-3
BFS-Power Sum	9.8736e-6	9	348.9671e-3
BFS-Impedance Sum	9.4693e-6	42	424.0961e-3
Newton-Raphson	1.6429e-9	5	75.2490e-3
Gauss-Seidel	NC	-	-
Fast-Decoupled (BX)	NC	-	-
Fast-Decoupled (XB)	11.0546e-6	97	255.0001e-3

Table 3.8: Flow-Augmentation PF algorithm system comparative results for 69-bus system in meshed topology with DGs.

Method	Mismatch	Iteration	Execution Time (s)
Flow-Augmentation PF	8.9946e-6	24	27.6380e-3
BFS-Current Sum	-	-	-
BFS-Power Sum	-	-	-
BFS-Impedance Sum	-	-	-
Newton-Raphson	2.9838e-9	4	73.0331e-3
Gauss-Seidel	NC	-	-
Fast-Decoupled (BX)	58.2497e-6	11	67.3141e-3
Fast-Decoupled (XB)	11.5131e-6	71	202.8661e-3

The performance of the Flow-Augmentation PF algorithm for distribution systems is presented in the tables above. The tables show a significant reduction in execution time in comparison with other methods. In fact, it is evident from Table 3.5 that the Flow-Augmentation PF algorithm requires lower execution time when compared with Backward-Forward-Sweep and Newton-Raphson methods for the radial topology. The results also show that the proposed algorithm takes less than 1.5% of the execution time required by the Backward-Forward-Sweep method when applied to 69-bus. While, in the case of fully meshed topology with no DG in the system, convergence is achieved in a similar number of iterations as the Newton-Raphson method, with smaller execution time by an order of magnitude, as presented in Table 3.6. The comparison of Flow-Augmentation PF with Backward-Forward-Sweep methods is not possible in the meshed topology, as it works only with a radial configuration. The presence of generation nodes in electric power distribution networks changes the Flow-Augmentation PF algorithm convergence speed. This change originates from induced voltage magnitude mismatch at every generator node. This mismatch necessitates collective reactive power correction for generation buses. The radial configuration with PV buses is relatively slower than meshed configuration with PV buses, because in the radial configuration, there is a single path for power flow and voltage

magnitude and reactive power corrections, while in non-radial configurations, there are various power flow paths dictated by the connectivity of the system. The solution accuracy and comparative convergence of the Flow-Augmentation PF, contrary to other methods, are demonstrated in Figures 3.4, 3.5 for 69-bus system in radial topology. Comprehensive plots of the algorithm performance for the different configurations are shown in Appendix B.

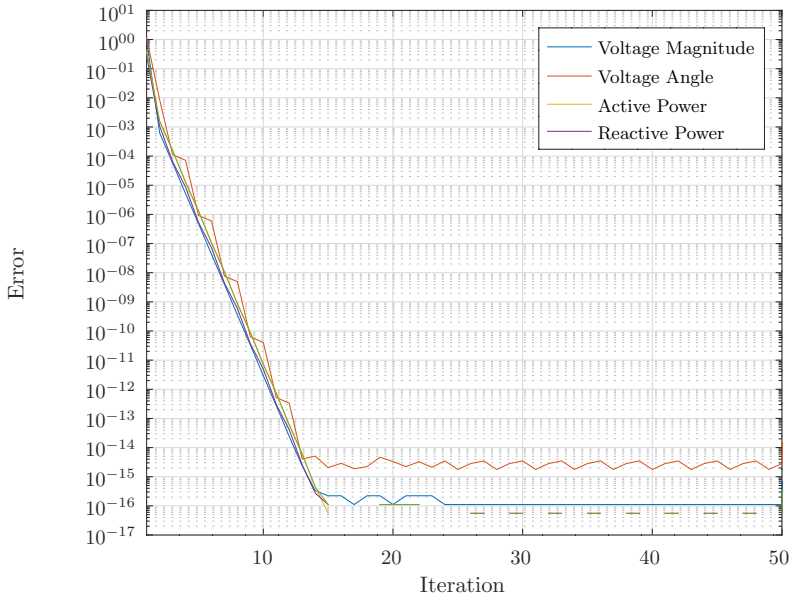

Figure 3.4: Flow-Augmentation PF algorithm convergence error for 69-bus system of radial topology.

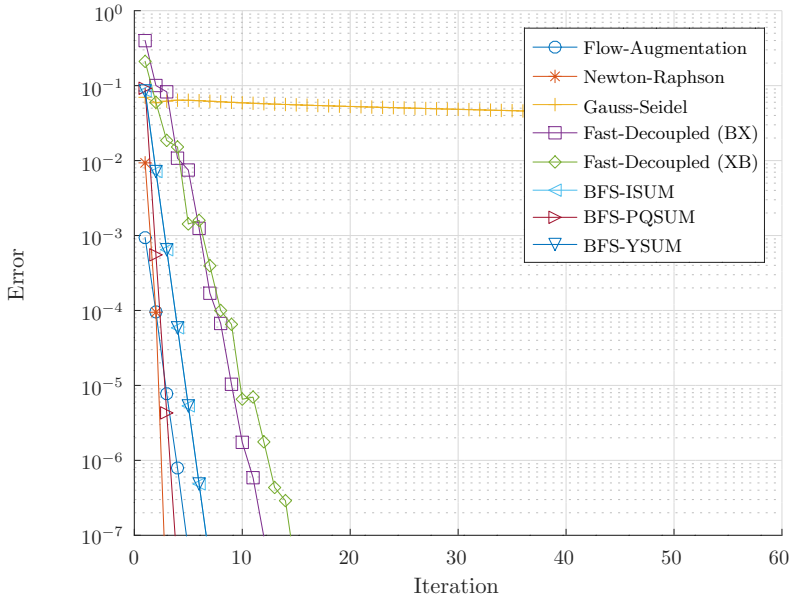

Figure 3.5: Flow-Augmentation PF algorithm comparative error convergence for 69-bus system of radial topology.

To investigate the performance of the algorithm in response to the dynamicity of the network, the above 69-bus distribution system configuration (Figure A.8) has been modified by replacing some generations with renewable sources. The distributed generations at buses 15 and 63 of the 69-bus distribution system are replaced with wind and solar-based generation resources, respectively. In the simulation, the renewable sources are operated at a constant power factor and a PQ mode. Figures 3.6 and 3.7 show the 15-minute variations of the output power of the wind and solar renewable resources. The daily load profile is presumed to follow IEEE-RTS (Institute of Electrical and Electronics Engineers Reliability Test System) hourly load model [100]. This model provides hourly peak load as a percentage of the daily peak load. A typical sample day is shown in figure 3.8.

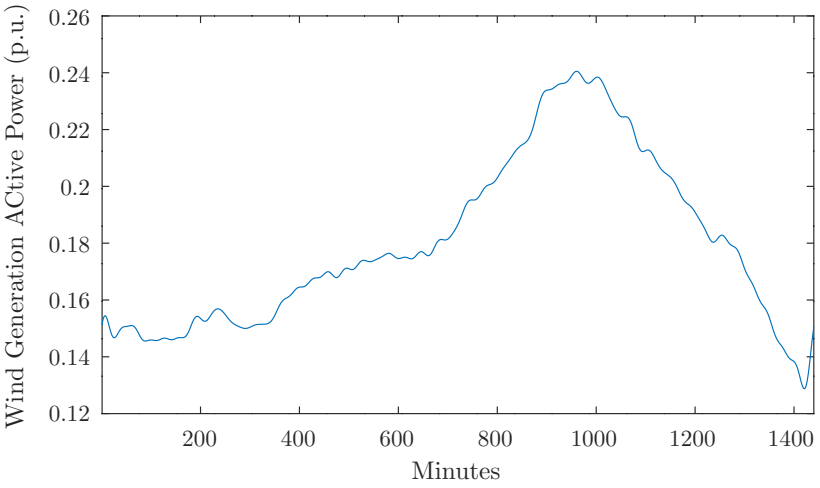

Figure 3.6: Daily wind power generation of the renewable source at bus-15 in 15-minute intervals.

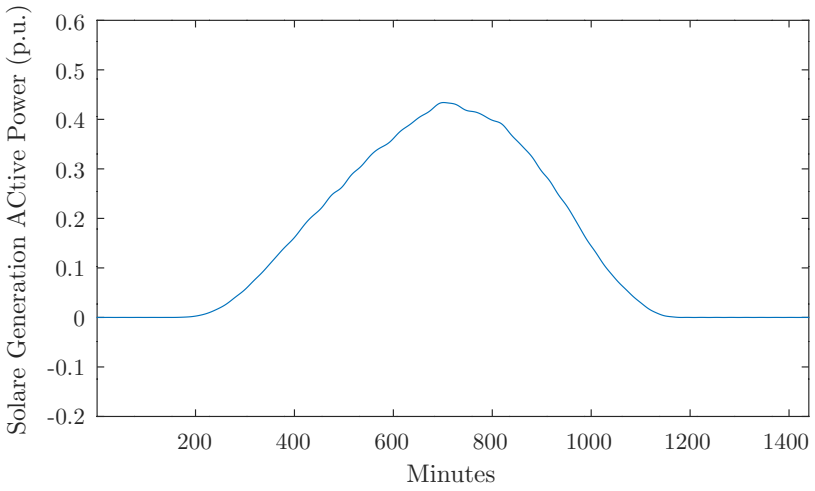

Figure 3.7: Daily solar power generation for the renewable source at bus-63 in 15-minute intervals.

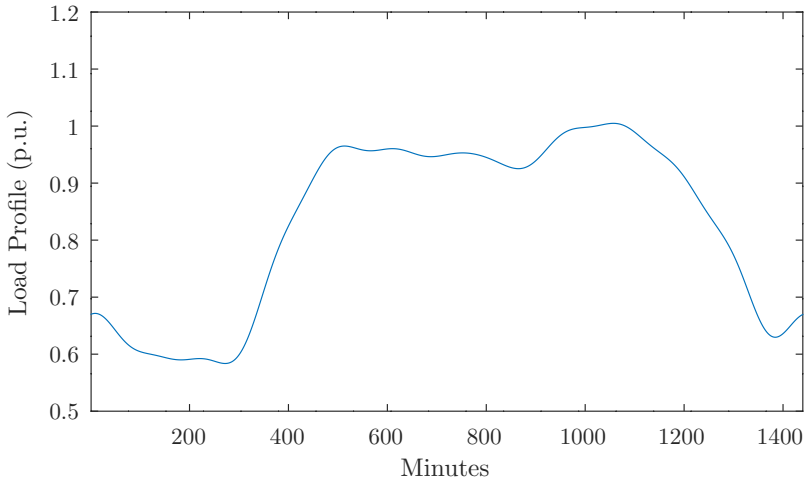

Figure 3.8: Daily load profile for the modified 69-bus system in 15-minute intervals.

To investigate the dynamic performance of the proposed methods, the above renewable generation profiles and the load are re-sampled with a sampling rate of 1-minute. Figure 3.9 shows the minute-by-minute change in the voltage profile of the renewable sources connected buses, solar and wind-generated powers, and the total load active power. The complete simulation time for the entire day (1440 minutes) is 115.56 seconds. Each snapshot takes 0.08 seconds execution time. This highlights the algorithms' capability of calculating the system variables before the changes in the system states. The overall simulation time and the time required for each time step prove the computational efficiency of the proposed algorithm in dealing with the high level of system dynamicity, which results from the presence of these renewable resources in the distribution systems. This shows the value of the developed algorithm for the analysis needed for the planning, operation, and control.

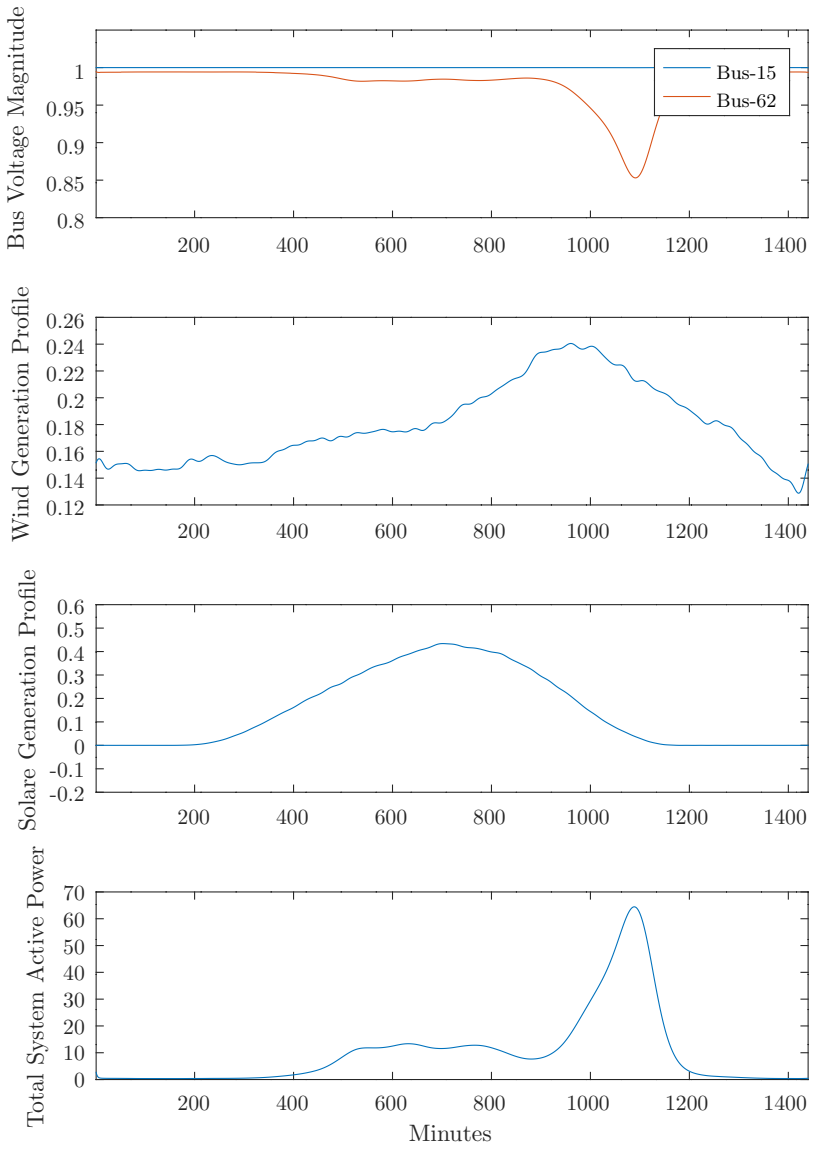

Figure 3.9: Performance of Flow-Augmentation PF algorithm with renewable sources for 69-bus system of meshed topology in 1-minute intervals.

3.4 Comparison With Commercial Software

Further validation of the proposed Flow-Augmentation PF algorithm against two commercial software packages is demonstrated in this section. The selected benchmarking software packages are PSS/E and PSCAD. PSS/E is among the leading steady-state simulation tools and currently is considered the gold standard for transmission-level planning and operational studies. PSCAD is a powerful tool for transient and dynamic studies, where it stimulates the systems by solving the underlying differential equations. For the purpose of this comparison, WSCC 9-bus, IEEE 14-bus, and IEEE 30-bus test systems are used [95]. Table 3.9 show Flow-Augmentation PF convergence mismatch, iteration counter, and execution time for a tolerance of $\epsilon = 10^{-5}$. Tables 3.10, 3.12, and 3.14 presents comparative generators level of the converged solutions, while Tables 3.11, 3.13, and 3.15 provide generators terminal voltage parameters for the three systems respectively.

Table 3.9: Flow-Augmentation PF algorithm termination results on commercial software cases.

Case System	Mismatch	Iteration	Execution Time (s)
IEEE 9-Bus	4.2226e-6	8	5.7340e-3
IEEE 14-Bus	8.6059e-6	6	4.8950e-3
IEEE 30-Bus	5.5554e-6	7	6.8829e-3

Table 3.10: Generation levels of Flow-Augmentation PF algorithm and commercial software packages in case of WSCC 9-bus system.

Bus	PSS/E [95]		PSCAD [95]		Flow-Augmentation PF	
	P	Q	P	Q	P	Q
1	0.7160	0.2790	0.7152	0.2761	0.7162	0.2774
2	1.6300	0.0490	1.6320	0.0454	1.6300	0.0385
3	0.8500	-0.1140	0.8512	-0.1170	0.8500	-0.1103

Table 3.11: Generators terminal condition of Flow-Augmentation PF algorithm and commercial software packages in case of WSCC 9-bus system.

Bus	PSCAD [95]		Flow-Augmentation PF	
	$\|U\|$	δ	$\|U\|$	δ
1	1.0400	0.0000	1.0400	0.0000
2	1.0250	9.3507	1.0250	9.2799
3	1.0250	5.1420	1.0250	4.6647

Table 3.12: Generation levels of Flow-Augmentation PF algorithm and commercial software packages in case of IEEE 14-bus system.

Bus	PSS/E [95]		PSCAD [95]		Flow-Augmentation PF	
	P	Q	P	Q	P	Q
1	2.3240	-0.1650	2.3230	-0.1548	2.3239	-0.1656
2	0.4000	0.4360	0.3995	0.4493	0.40000	0.4356
3	0.0000	0.2510	0.0007	0.2613	0.0000	0.2507
6	0.0000	0.1270	0.0020	0.1498	0.0000	0.1273
8	0.0000	0.1760	-0.0011	0.1896	0.0000	0.1762

Table 3.13: Generators terminal condition of Flow-Augmentation PF algorithm and commercial software packages in case of IEEE 14-bus system.

Bus	PSCAD [95]		Flow-Augmentation PF	
	$\|U\|$	δ	$\|U\|$	δ
1	1.0600	0.0000	1.0600	0.0000
2	1.0450	-4.9826	1.0450	-4.9826
3	1.0100	-12.7250	1.0100	-12.7250
6	1.0700	-14.2209	1.0700	-14.2210
8	1.0900	-13.3596	1.0900	-13.3600

Table 3.14: Generation levels of Flow-Augmentation PF algorithm and commercial software packages in case of IEEE 30-bus system.

Bus	PSS/E [95]		PSCAD [95]		Flow-Augmentation PF	
	P	Q	P	Q	P	Q
1	2.6090	-0.1680	2.6070	-0.1530	2.6068	-0.1430
2	0.4000	0.5000	0.3992	0.5167	0.4000	0.4990
5	0.0000	0.3690	0.0025	0.3868	0.0023	0.3575
8	0.0000	0.3710	0.0000	0.4047	0.0000	0.3625
11	0.0000	0.1620	0.0004	0.1662	0.0000	0.1605
13	0.0000	0.1060	0.0009	0.1111	0.0000	0.1046

Table 3.15: Generators terminal condition of Flow-Augmentation PF algorithm and commercial software packages in case of IEEE 30-bus system.

Bus	PSCAD [95]		Flow-Augmentation PF	
	$\|U\|$	δ	$\|U\|$	δ
1	1.0600	98.4316	1.0600	0.0000
2	1.0431	93.0798	1.0422	-5.3340
5	1.0110	84.2658	1.0076	-14.1378
8	1.0100	86.6183	1.0078	-11.7878
11	1.0820	84.3227	1.0797	-14.0995
13	1.0710	83.4883	1.0687	-14.9409

3.5 Summary

This chapter demonstrated the solution accuracy and convergence speed of the proposed Flow-Augmentation PF method for transmission and distribution systems of different configurations and components. The results showed that the proposed algorithm has superior performance, in terms of execution time and solution accuracy compared with well known methods, and leading commercial software packages.

Chapter 4

Minimum Cost Flow Based Methods

4.1 Introduction

This chapter introduces a new PF/OPF solution based on a minimum-cost flow. The chapter starts with a brief review of the cost flow approach, and then it details the generalized inverse properties and its calculation methods, as well as, its applications in cost-flow networks. Next, the formulation of a generic OPF problem as Minimum-Cost Flow model is presented, followed by the application of the algorithm *MinLoss-Flow PF* to the PF problem. The solution procedure of the proposed algorithm, its correctness, its termination, and its computational complexity are detailed. The performance of the proposed algorithm is validated using transmission and distribution networks of different topologies and compared against the well-known methods using MATPOWER toolbox. The algorithm, also, is compared with the commercial solvers, PSS/E and PSCAD.

4.2 Cost Flow Approach

The minimum cost flow problem is a general and fundamental problem in network flows, dealing with the task of optimizing network flow in regard to a specific objective and preserving a set of constraints. Minimum cost formulation encompasses a wide variety of special cases and well-known applications, like maximum flow and assignment problems. While many flow cost allocation methods may exist, the least-squares properties of the generalized inverse are uniquely descriptive of electric flows and incurred system losses [101]. In this approach, electric losses or costs are not affected by the flow path, but by source-sink locations in the network.

4.2.1 Generalized Inverse

For any $m \times n$ matrix A, there exist a unique generalized inverse A^+ that satisfies [102] [103] [104] [105] [106] where T is the matrix transpose:

$$AA^+A = A \tag{4.1}$$

$$A^+AA^+ = A^+ \tag{4.2}$$

$$(AA^+)^T = AA^+ \tag{4.3}$$

$$(A^+A)^T = A^+A \tag{4.4}$$

The generalized inverse has a least-squares property when used to solve the linear system $Ax = y$, resulting in x^* that satisfies $x^* = A^+y$ as follows:

$$\|y - Ax^*\| \text{ is minimum in all } x \in R \tag{4.5}$$

$$\|x^*\| \text{ is minimum of all } x \text{ that satisfies } \|y - Ax^*\| \tag{4.6}$$

Meaning, if there exist a solution for $Ax = y$, then $x^* = A^+y$ is a solution, and $y - Ax^* = 0$. If the system is not solvable and there are multiple solutions, x^* has the minimum norm among all existing solutions. Moreover, if there is many solutions and no unique solution, x^* produces a vector that is closest to the solution and $\|y - Ax^*\|$ is the minimum among all $x \in R$ [101] [106] [103] [104].

4.2.2 Cost Flow Networks

Let's start by examining the network in example 2.9, where the incident matrix $B(G)$ of figure 2.2 given as:

$$B = \begin{bmatrix} 1 & 1 & 0 & 0 \\ 0 & 0 & -1 & -1 \\ 0 & -1 & 0 & 1 \\ -1 & 0 & 1 & 0 \end{bmatrix} \tag{4.7}$$

Considering an interpretation of $Bx = b$, where x is vector of individual arc flows and b is vector of balancing flows at the vertices, as $x = [0.47426, 1.1774, 1.5185, 1.2012]^T$ and $b = [1.6516, 2.7197, -2.3773, -1.9906]^T$. Similarly, if $\mathfrak{G}x = a$ is considered, where $\mathfrak{G}$ is the weighted admittance incident matrix. The resulting balancing flow is amplified in relation to the arc flow, as $x = [0.47426, 1.1774, 1.5185, 1.2012]^T$ and $a = [8.1363, 12.5126, -10.7560, -9.8783]^T$. Generalized inverse $\mathfrak{G}^+$ as:

$$\mathfrak{G}^+ = \begin{bmatrix} 6.42 + 5.26i & -2.96 - 2.42i & 2.95 + 2.42i & -6.42 - 5.26i \\ 5.78 + 4.74i & -1.22 - 1.00i & -6.30 - 5.17i & 1.75 + 1.43i \\ 1.75 + 1.43i & -6.30 - 5.17i & -1.22 - 1.00i & 5.78 + 4.74i \\ 2.63 + 2.16i & -6.52 - 5.35i & 6.52 + 5.34i & -2.63 - 2.16i \end{bmatrix} \times 10^{-2} \tag{4.8}$$

Using least-squares property and scaling the incident matrix by the square root of branch impedance and using node squared injected currents, results in $x^* = \mathfrak{G}^+ a$ as the square root of branch losses [101].

$$\sqrt{x}_{loss} = \begin{bmatrix} 0.8285 + 0.6792i \\ 1.7755 + 1.4556i \\ -2.2817 - 1.8706i \\ -2.3654 - 1.9392i \end{bmatrix} \times 10^{-1} \tag{4.9}$$

$$x_{loss} = \begin{bmatrix} 0.2250 + 1.1254i \\ 1.0337 + 5.1687i \\ 1.7073 + 8.5363i \\ 1.8348 + 9.1741i \end{bmatrix} \times 10^{-2} \tag{4.10}$$

It is established from generalized inverse properties that x^* is uniquely minimizes branch losses among all flow $x^* \neq x$. Resulting in system branch losses $4.8009e-02+2.4004e-01i$ (p.u.).

4.3 OPF Mathematical Model

Network flow optimization is the selection of flow distribution functions that optimizes a stated objective function. Generalized optimum network power flow aims to find the flow that minimizes generation costs and transformer settings that preserve energy while satisfying voltage and current laws. Consider a directed electrical network $N_{st-electric} = (G = (V, E), s, t, \mathcal{G}, \mathcal{L}, l_{capacity}, \Psi)$, where $l_{capacity}$ is the line capacities and Ψ is the network-specific cost function. Ψ can be the generation cost, gas emissions, system losses, or any combination of specific network metrics. The generalized optimum power flow model can be described as:

$$minimize \quad Z(f) = \sum_{(j,k)\in E} \Psi_{(j,k)} f_{(j,k)}, \qquad \forall \{j,k\} \in E \setminus \mathcal{L} \tag{4.11a}$$

$$\text{s.t.} \quad \sum_{j:(j,k)\in V} f(j,k) = 0, \qquad \forall j \in V \setminus \{s,t\} \tag{4.11b}$$

$$\sum_{j:(s,j)\in E} f(s,j) = \sum_{g\in\mathcal{G}} g, \qquad \forall \{s,j\} \in E \tag{4.11c}$$

$$\sum_{j:(j,t)\in E} f(j,t) = \sum_{\ell\in\mathcal{L}} \ell, \qquad \forall \{j,k\} \in E \tag{4.11d}$$

$$|f_{(j,k)}| \leq |l_{capacity}|, \qquad \forall \{j,k\} \in E \tag{4.11e}$$

$$f_{(s,j)}^{min} \leq f_{(s,j)} \leq f_{(s,j)}^{max} \qquad \forall j \in E \tag{4.11f}$$

$$|U_j{}^{min}| \leq |U_j| \leq |U_j{}^{max}| \qquad \forall j \in E \tag{4.11g}$$

4.4 Application of OPF Model to PF Problem

The PF is considered a simplified OPF that uses a subset of the generalized conditions and relaxed constraints, like the generation cost, lines thermal limits, and power transformer settings. The *MinLoss-Flow PF* algorithm formulates the PF problem as a Minimum-Cost Flow problem and builds on the development of the Maximum-Flow-based PF algorithm in chapter 2. This special formulation differs from the Flow-Augmentation PF algorithm in its approach to the calculation of system losses, where the optimized cost that the proposed method minimizes is the system power losses. The proposed MinLoss-Flow PF algorithm adjusts the flow functions to minimize the system losses. A simplified model from the one presented in 4.3 is used. Consider a directed electrical network $N_{st-electric} = (G = (V,E), s, t, G, L, \Psi)$, where Ψ is the branch flow loss function.

$$
\begin{aligned}
\textit{minimize} \quad & Z(f) = \sum_{(j,k)\in E} \Psi_{(j,k)} f_{(j,k)} && \forall \{j,k\} \setminus \{s,t\} && \text{(4.12a)}\\
\text{s.t.} \quad & \sum_{j:(j,k)\in V} f(j,k) = 0, && \forall j \in V \setminus \{s,t\} && \text{(4.12b)}\\
& \sum_{j:(s,j)\in E} f(s,j) = \sum_{g\in\mathcal{G}} g, && \forall j \in E && \text{(4.12c)}\\
& \sum_{j:(j,t)\in E} f(j,t) = \sum_{\ell\in\mathcal{L}} \ell, && \forall j \in E && \text{(4.12d)}\\
& |U|_{j:PV}{}^{calculated} = |U|_{j:PV}{}^{specified}, && \forall j \in \mathcal{G} \setminus \{s\} && \text{(4.12e)}
\end{aligned}
$$

Theorem 3 (MinLoss-Flow PF Algorithm Solution Existence and Uniqueness)**.** *The solution to the power flow problem is the unique network flow associated with minimum system losses that satisfy PF problem constraints.*

Proof. The network flow associated with the minimum system losses results in a network voltage profile and node power injections that satisfy PF constraints. Deviation from this unique network flow results in a change of voltage profile throughout the system, violation of power injection constraints, and increased system losses. □

The MinLoss-Flow PF algorithm iteratively estimates and refines the total system losses associated with supplying demand power from the generation side at predetermined power injections and voltages. Once total system losses are found, network power injection is adjusted in generation buses to reflect the added demand. This increased power injection would affect the bus current injection and network voltage profile. The calculation of total network losses is achieved using a special formulation of a generalized incident matrix inverse. This iterative procedure is repeated until convergence criteria are attained. The selected criteria is $\| S_{inj} \|_\infty$ and $\| |U| \|_\infty$, for transmission and distribution systems,

respectively. Algorithm 5 and the flow-chart in figure 4.1 presents the general procedure for MinLoss-Flow PF algorithm.

Algorithm 5 MinLoss-Flow PF

1: NetworkTransformation($G(V, E)$, S_{demand}, U_{ref}, Y_{branch})
2: NetworkFlowPFCalculation($G(V, E)$, S_{bus}, U_{bus}, Y_{bus})
3: iter = 0
4: **while** error $\geq \epsilon$ or iter $\leq$ maxIter **do**
5: ReactivePowerCorrection($G(V, E)$, S_{bus}, U_{bus}, Y_{bus})
6: MinNetworkLosses
7: NetworkFlowPFCalculation($G(V, E)$, S_{bus}, U_{bus}, Y_{bus})
8: iter = iter + 1
9: **end**

4.4.1 Network Transformation

This step is based on the power network transformation procedure detailed in section 2.6.1 with the exception of the added calculation of the weighted generalized bus-branch incident matrix inverse, calculated as:

$$\mathfrak{G}^{+} = (A \cdot diag(\sqrt{Y_{brnach}}))^{+} \tag{4.13}$$

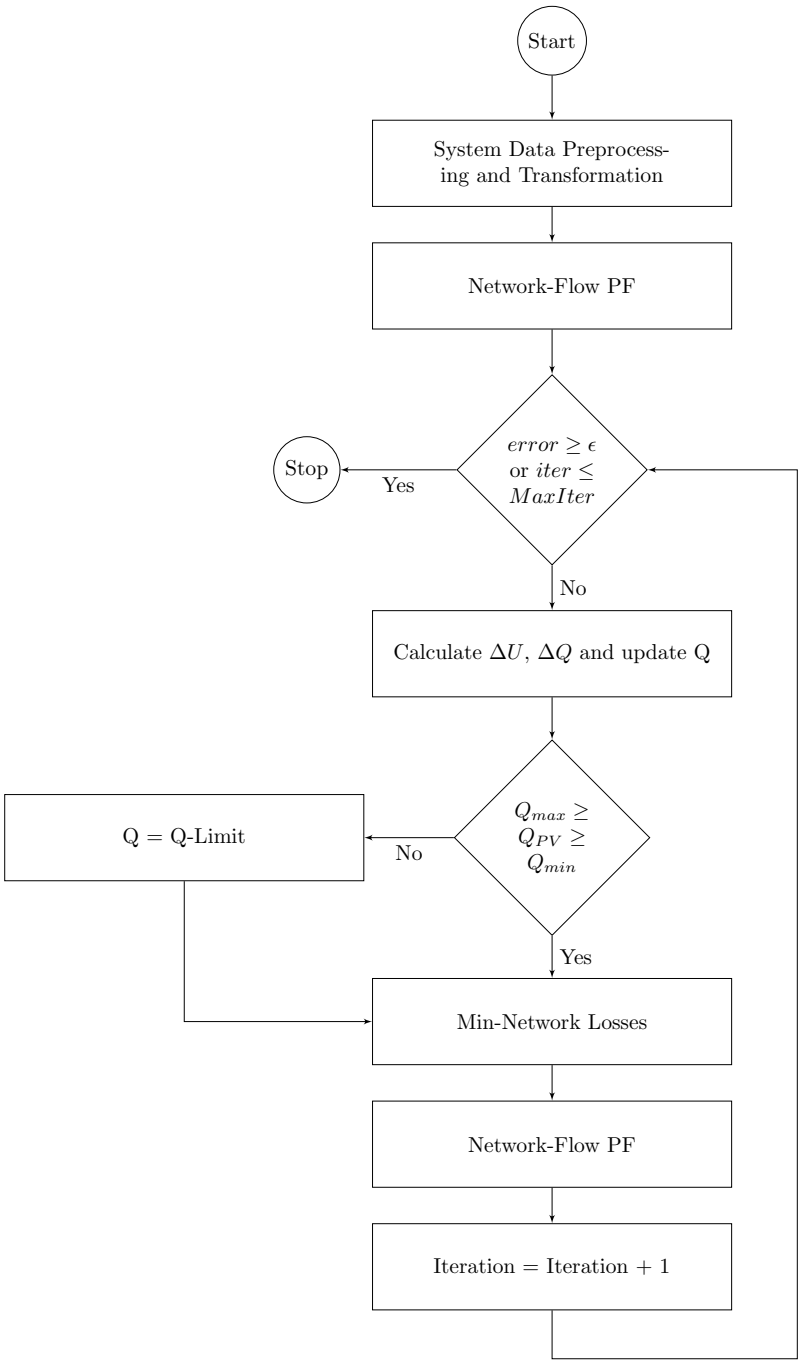

Figure 4.1: MinLoss-Flow PF algorithm flow chart.

4.4.2 Minimum Network Losses Calculation

Minimum system losses are iteratively estimated by exploiting generalized inverse minimum norm properties of the weighted incidence matrix. System losses are found by the squared sum of flows in G^+ of injected node currents. Procedure 6 presents minimum network losses calculation steps.

Algorithm 6 MinNetworkLosses

1: **procedure** MinNetworkLosses(V_{bus}, S_{bus}, G^+)
2: $\sqrt{S_{loss}} \leftarrow \mathfrak{G}^+ |I_{inj}|$
3: $S_{total-loss} \leftarrow \sum \sqrt{S_{loss}}^2$
4: **return** $S_{total-loss}$

4.5 Minimum Loss Flow Algorithm Correctness and Termination

The MinLoss-Flow PF is initialized with preserved demand-side power injection, a flat voltage profile, and a relaxed voltage law. Generation side voltage magnitude and active power injection are preserved, while slack bus power injection is relaxed, resulting in non-convergent system losses. The algorithm iteratively corrects total system losses and generators reactive power injection at all generation nodes, while preserving problem preconditions. This leads to a gradual improvement in the voltage profile and system losses with every MinLoss-Flow PF iteration. The algorithm terminates whenever the stated error tolerance is met or reaches the maximum iteration counter.

Theorem 4 (MinLoss-Flow PF Algorithm Termination)**.** *The MinLoss-Flow PF algorithm terminates with a solution of the power flow problem within the pre-specified error bounds* ϵ.

Proof. The algorithm initializes node power injection and voltage to S_{bus}^{int} and U_{bus}^{int} respectively. Slack bus power injection is considered for a lossless system satisfying supply-demand power balance. Bus current injection vector is calculated from power injection vector, leading to updated voltage profile U_{bus}^{k} and power injection S_{i}^{k}. These updated power and voltage vectors are a refined solution when compared to the initial state S_{bus}^{int} and U_{bus}^{int}. Voltage-controlled buses voltage magnitude mismatch is corrected by net reactive power injections of these buses as $\Delta Q = \frac{\partial Q}{\partial |U|} \cdot \Delta |U|$. Followed by minimum system losses update using weighted incidence matrix generalized inverse. Leading to updated power injection vector S_{i}^{k}. Resulting in an updated voltage profile U_{bus}^{k+1} and system power injections S_{i}^{k+1} that reduces the convergence error. The *MinLoss-Flow PF* terminates by reaching lower error bounds $error \leq \epsilon$ or maximum iteration number $iter \geq iterMax$. □

4.6 Minimum Loss Flow Algorithm Computational Complexity

The complexity of the MinLoss-Flow PF algorithm can be determined by examining all the steps in the *While* loop. In every iteration, MinLoss-Flow PF performs *ReactivePowerCorrection* step followed by *MinNetworkLosses* and *NetworkFlowPF* steps till convergence criteria or the maximum iteration counter is reached. The *ReactivePowerCorrection* and *Flow-Augmentation* computational complexity was evaluated in section 2.8 as $O(max\{n_{PV}+1, n_{PQ}^{1.4}\})$.

The *MinNetworkLosses* step is dominated by multiplication of the incidence matrix pseudo inverse with the current injection vector. Incident matrix pseudo inverse is a full matrix of size $m \times n$ and current vector is of size n and the resulting complexity is $O(mn)$. Complexity of the *MinLoss-Flow* algorithm is $O(max\{mn, n_{PQ}^{1.4}\})$, and for the special case of no PV bus in the system is $O(mn)$, where m is the number of branches in the system.

4.7 Example

The mechanics of the MinLoss-Flow PF algorithm are demonstrated utilizing the same test system and convergence criteria utilized in section 2.9. Table 4.1 presents the proposed algorithm termination tolerance, number of iterations, and execution time in comparison with known methods. Figure 4.2 shows the convergence error for voltage magnitude, angle, generation injection active and reactive power. Figure 4.3 demonstrates the voltage magnitude correction of generation buses, and Figure 4.4 presents the change in total system losses. Figure 4.5 shows convergence behavior of the presented method and known methods. The table and figures below facilitates the accuracy and utility of the developed algorithm.

Table 4.1: MinLoss-Flow PF algorithm comparative results for 4-bus system.

Method	Mismatch	Iteration	Execution Time (s)
MinLoss-Flow PF	4.2637e-6	6	6.1409e-3
Newton-Raphson	1.0685e-9	3	69.0501e-3
Gauss-Seidel	5.7947e-6	18	69.3579e-3
Fast-Decoupled (BX)	6.5722e-6	4	50.7932e-3
Fast-Decoupled (XB)	5.8041e-6	4	51.0519e-3

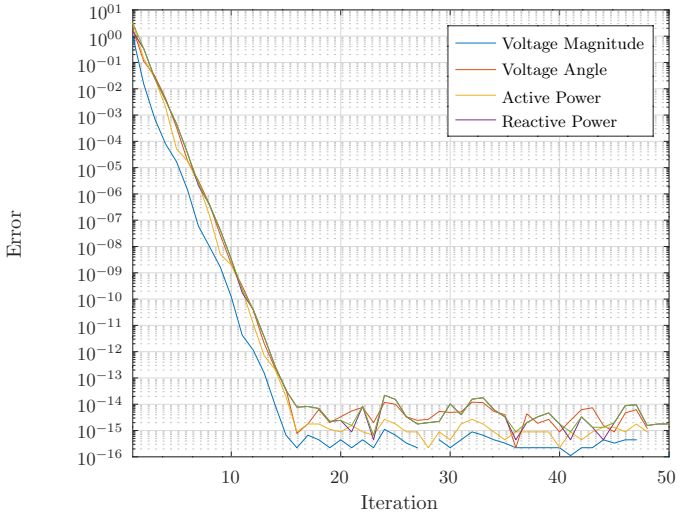

Figure 4.2: MinLoss-Flow PF algorithm error convergence for 4-bus system.

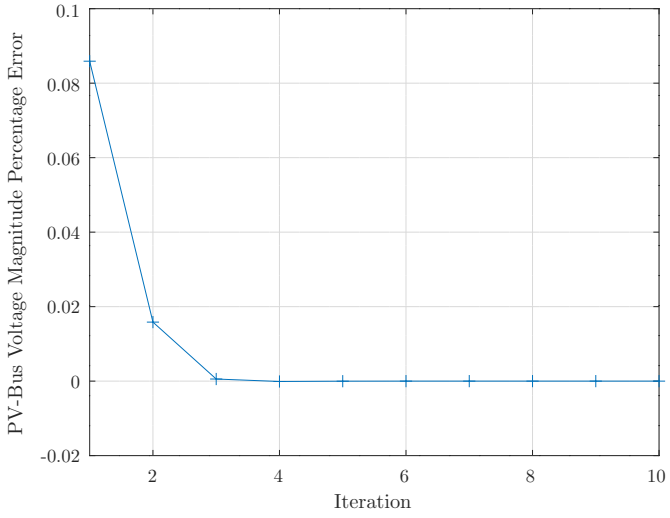

Figure 4.3: MinLoss-Flow PF algorithm PV-bus voltage magnitude error for 4-bus system.

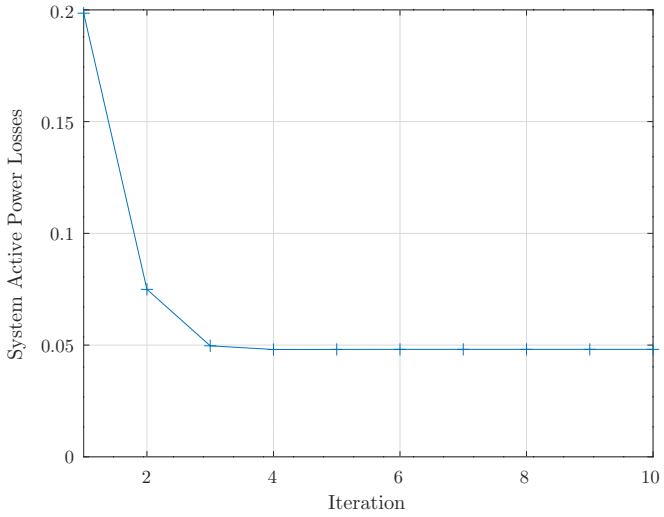

Figure 4.4: MinLoss-Flow PF algorithm system losses for 4-bus system.

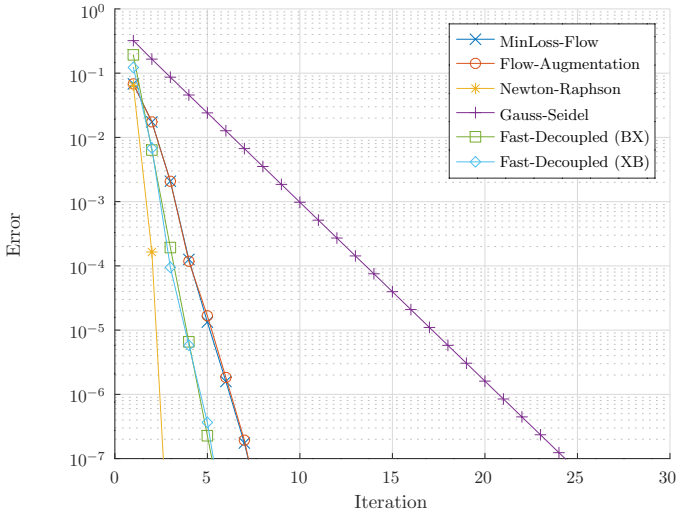

Figure 4.5: MinLoss-Flow PF algorithm comparative error convergence for 4-bus system.

4.8 Minimum Cost Flow Power Flow Simulation Results

The MinLoss-Flow PF algorithm is validated using different test systems and evaluated based on the solution convergence error, the PV bus voltage magnitude deviations, and the overall system power losses. The proposed MinLoss-Flow PF algorithm is simulated using standard test systems, shown in Sections 3.2 and 3.3. Tables 4.2, 4.3, 4.4, and 4.5 reveal convergence characteristics of the algorithm for transmission systems, while Tables 4.6, 4.7, 4.8, and 4.9 display the performance of the algorithm for the selected distribution systems.

Table 4.2: MinLoss-Flow PF algorithm comparative results for WSCC 9-bus system.

Method	Mismatch	Iteration	Execution Time (s)
MinLoss-Flow PF	5.1380e-6	8	8.1301e-3
Newton-Raphson	342.1321e-9	3	69.5479e-3
Gauss-Seidel	9.6113e-6	123	141.8772e-3
Fast-Decoupled (BX)	2.3910e-6	4	78.0342e-3
Fast-Decoupled (XB)	7.5577e-6	4	53.9320e-3

Table 4.3: MinLoss-Flow PF algorithm comparative results for IEEE 14-bus system.

Method	Mismatch	Iteration	Execution Time (s)
MinLoss-Flow PF	5.9879e-6	7	7.7119e-3
Newton-Raphson	131.5780e-12	2	69.4242e-3
Gauss-Seidel	8.8967e-6	14	53.9432e-3
Fast-Decoupled (BX)	48.1103e-6	4	50.1220e-3
Fast-Decoupled (XB)	11.8822e-6	4	53.1950e-3

Table 4.4: MinLoss-Flow PF algorithm comparative results for IEEE 30-bus system.

Method	Mismatch	Iteration	Execution Time (s)
MinLoss-Flow PF	6.0610e-6	8	9.2521e-3
Newton-Raphson	956.9985e-12	3	69.8009e-3
Gauss-Seidel	9.9401e-6	373	735.4259e-3
Fast-Decoupled (BX)	13.0255e-6	5	54.0261e-3
Fast-Decoupled (XB)	11.6337e-6	7	74.1231e-3

Table 4.5: MinLoss-Flow PF algorithm comparative results for IEEE 118-bus system.

Method	Mismatch	Iteration	Execution Time (s)
MinLoss-Flow PF	9.5847e-6	23	35.8930e-3
Newton-Raphson	9.7030e-6	2	69.3870e-3
Gauss-Seidel	NC	-	-
Fast-Decoupled (BX)	52.4600e-6	4	54.0290e-3
Fast-Decoupled (XB)	6.8693e-6	4	64.5671e-3

Table 4.6: MinLoss-Flow PF algorithm system comparative results for 69-bus system in radial topology.

Method	Mismatch	Iteration	Execution Time (s)
MinLoss-Flow PF	5.2104e-6	4	6.9852e-3
BFS-Current Sum	5.3351e-6	5	352.8750e-3
BFS-Power Sum	4.2967e-6	3	312.8390e-3
BFS-Impedance Sum	5.3351e-6	5	392.2720e-3
Newton-Raphson	10.4262e-9	3	73.1361e-3
Gauss-Seidel	NC	-	-
Fast-Decoupled (BX)	67.0784e-6	9	62.7921e-3
Fast-Decoupled (XB)	6.5419e-6	10	66.0350e-3

Table 4.7: MinLoss-Flow PF algorithm system comparative results for 69-bus system in meshed topology.

Method	Mismatch	Iteration	Execution Time (s)
MinLoss-Flow PF	0.9476e-6	3	6.2571e-3
BFS-Current Sum	-	-	-
BFS-Power Sum	-	-	-
BFS-Impedance Sum	-	-	-
Newton-Raphson	5.1043e-6	2	68.6810e-3
Gauss-Seidel	NC	-	-
Fast-Decoupled (BX)	47.9153e-6	7	57.9872e-3
Fast-Decoupled (XB)	1.5365e-6	7	169.2040e-3

Table 4.8: MinLoss-Flow PF algorithm system comparative results for 69-bus system in radial topology with DGs.

Method	Mismatch	Iteration	Execution Time (s)
MinLoss-Flow PF	0.3264e-6	82	112.7431e-3
BFS-Current Sum	9.4693e-6	42	417.8429e-3
BFS-Power Sum	9.8736e-6	9	348.9671e-3
BFS-Impedance Sum	9.4693e-6	42	424.0961e-3
Newton-Raphson	1.6429e-9	5	75.2490e-3
Gauss-Seidel	NC	-	-
Fast-Decoupled (BX)	NC	-	-
Fast-Decoupled (XB)	11.0546e-6	97	255.0001e-3

Table 4.9: MinLoss-Flow PF algorithm system comparative results for 69-bus system in meshed topology with DGs.

Method	Mismatch	Iteration	Execution Time (s)
MinLoss-Flow PF	0.1686e-6	48	66.9019e-3
BFS-Current Sum	-	-	-
BFS-Power Sum	-	-	-
BFS-Impedance Sum	-	-	-
Newton-Raphson	2.9838e-9	4	73.0331e-3
Gauss-Seidel	NC	-	-
Fast-Decoupled (BX)	58.2497e-6	11	67.3141e-3
Fast-Decoupled (XB)	11.5131e-6	71	202.8661e-3

It can be revealed from the above tables (Tables 4.2, 4.3, 4.4, and 4.5) that the MinLoss-Flow PF algorithm execution time for transmission system is lower in comparison with the results of the other methods. A reduction of around 50% in the proposed algorithm execution time compared with the Newton-Raphson method when applied to the IEEE 118-bus system. However, the number of iterative steps required to reach solution convergence is higher than that needed for the Newton-Raphson method. This is because the Network-Flow-based algorithms proposed in this thesis have a linear convergence behavior, while the Newton-Raphson method possesses a quadratic solution convergence.

The performance of MinLoss-Flow PF is demonstrated using the 69-bus distribution system, shown in Appendix C. Table 4.6, 4.7, 4.8, and 4.9 display the performance results of the proposed methods in terms of execution time and number of iterations. The results show that the execution time of the MinLoss-Flow PF is equal to 2.2% of the Backward-Forward-Sweep method running time for the radial case. Tables 4.8 and 4.9 presents algorithm execution time and convergence speed against other methods, for radial and meshed configuration in the presence of DG, respectively. A complete set of graphs detailing simulated cases convergence behavior, PV bus voltage magnitude error correction, and system active power losses are given in Appendix C. As can be seen from the tables, in

the presence of DGs, the proposed methods' execution time is higher than that of systems without DGs. The introduction of generation nodes in the distribution system with DGs reduces the convergence speed in comparison with the case without DGs. This is due to the added requirement of reactive power corrections, dictated by the deviation of generation nodes' voltage magnitude from stated values.

The discussion of test results, in this Chapter and Chapter 3, revealed that the MinLoss-Flow PF algorithm requires a relatively higher execution time when compared with the Flow-Augmentation PF algorithm. It is shown that it needs at most 67% more computational time, to reach similar convergence with other methods when used for distribution systems of different configurations, and about 57% additional time when used for transmission systems. This is due to the fact that the MinLoss-Flow PF searches for the minimum losses in the system to achieve the required accuracy. The complexity of MinLoss-Flow PF algorithm for distribution systems with no voltage-controlled nodes is $O(mn)$, while that of Flow-Augmentation PF is $O(n^{1.2})$.

The simulation of the 69-bus system with dynamically changing load and renewable generation facilitates the versatility of the developed MinLoss-Flow PF method. A similar system configuration and parameters to that used in Section 3.3 is used for this purpose. Figure 4.6 demonstrates the system response to the dynamic loads and renewable generations as presented by changes in the voltage profile. The complete simulation time for this scenario is 205.15 seconds.

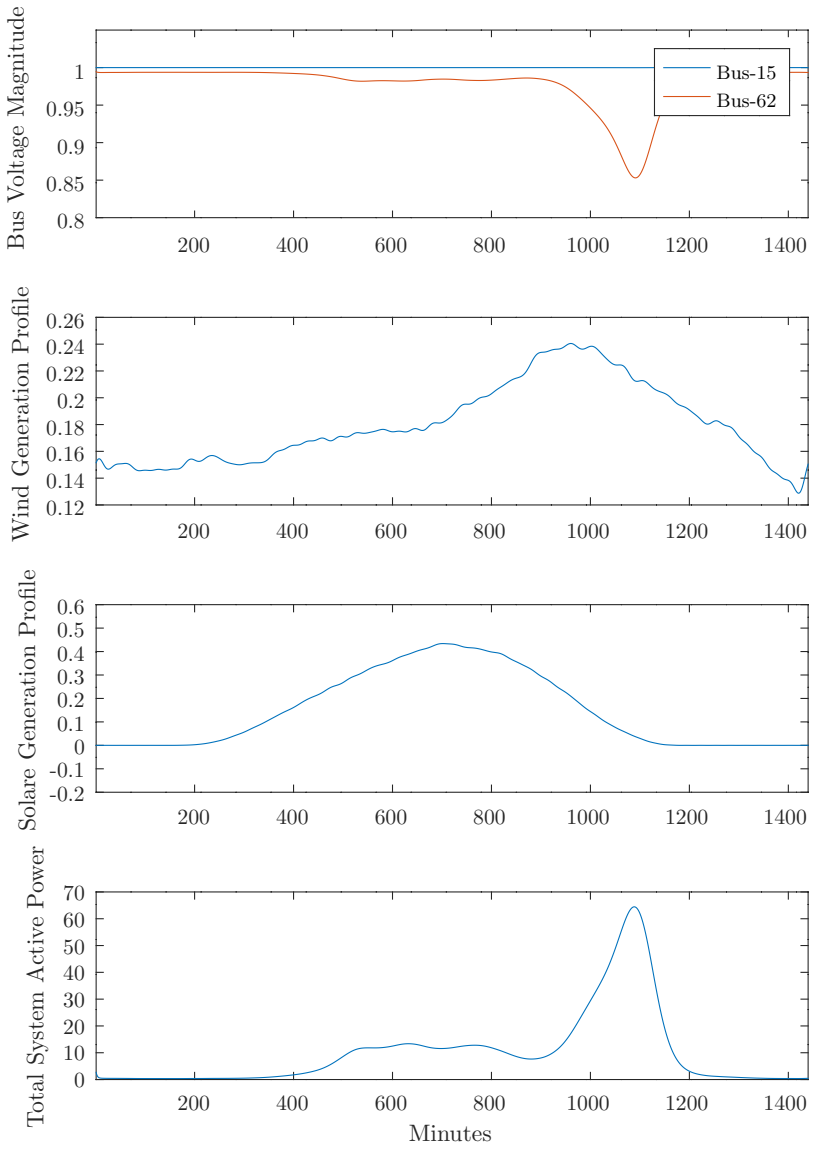

Figure 4.6: Performance of MinLoss-Flow PF algorithm with renewable sources of 69-bus system in meshed configuration.

4.9 Comparison With Commercial Software

This section provides a comparison of the proposed MinLoss-Flow PF algorithm, similar to the one presented in Chapter 3. Table 4.10 shows the results of the proposed MinLoss-Flow PF, in terms of convergence mismatch, iteration counter, and execution time when applied to the systems simulated by PSS/E and PSCAD commercial packages. Tables 4.11, 4.13, and 4.15 present the generation levels of the proposed method in comparison with that of the commercial packages. While Tables 4.12, 4.14, and 4.16 provide a comparison of the voltage parameters of generators nodes of the compared method. The results show that the generators' active power is similar to those of the commercial packages. However, the distribution of the generator's reactive power is changed as the algorithm adjusts the injected reactive power in the system to achieve a minimum system losses.

Table 4.10: MinLoss-Flow PF algorithm termination results on commercial software cases.

Case System	Mismatch	Iteration	Execution Time (s)
IEEE 9-Bus	4.6700e-6	8	7.8490e-3
IEEE 14-Bus	5.9879e-6	7	7.3361e-3
IEEE 30-Bus	1.5406e-6	8	9.3930e-3

Table 4.11: Generation levels of MinLoss-Flow PF algorithm and commercial software packages in case of WSCC 9-bus system.

Bus	PSS/E [95]		PSCAD [95]		MinLoss-Flow PF	
	P	Q	P	Q	P	Q
1	0.7160	0.2790	0.7152	0.2761	0.7163	0.2774
2	1.6300	0.0490	1.6320	0.0454	1.6300	0.0385
3	0.8500	-0.1140	0.8512	-0.1170	0.8499	-0.1102

Table 4.12: Generators terminal condition of MinLoss-Flow PF algorithm and commercial software packages in case of WSCC 9-bus system.

Bus	PSCAD [95]		MinLoss-Flow PF	
	$\|U\|$	δ	$\|U\|$	δ
1	1.0400	0.0000	1.0400	0.0000
2	1.0250	9.3507	1.0250	8.9984
3	1.0250	5.1420	1.0250	5.3161

Table 4.13: Generation levels of MinLoss-Flow PF algorithm and commercial software packages in case of IEEE 14-bus system.

Bus	PSS/E [95]		PSCAD [95]		MinLoss-Flow PF	
	P	Q	P	Q	P	Q
1	2.3240	-0.1650	2.3230	-0.1548	2.3239	-0.1654
2	0.4000	0.4360	0.3995	0.4493	0.4000	0.4355
3	0.0000	0.2510	0.0007	0.2613	0.0000	0.2507
6	0.0000	0.1270	0.0020	0.1498	0.0000	0.1273
8	0.0000	0.1760	-0.0011	0.1896	0.0000	0.1762

Table 4.14: Generators terminal condition of MinLoss-Flow PF algorithm and commercial software packages in case of IEEE 14-bus system.

Bus	PSCAD [95]		MinLoss-Flow PF	
	$\|U\|$	δ	$\|U\|$	δ
1	1.0600	0.0000	1.0600	0.0000
2	1.0450	-4.9826	1.0450	-4.9826
3	1.0100	-12.7250	1.0100	-12.7250
6	1.0700	-14.2209	1.0700	-14.2210
8	1.0900	-13.3596	1.0900	-13.3600

Table 4.15: Generation levels of MinLoss-Flow PF algorithm and commercial software packages in case of IEEE 30-bus system.

Bus	PSS/E [95]		PSCAD [95]		MinLoss-Flow PF	
	P	Q	P	Q	P	Q
1	2.6090	-0.1680	2.6070	-0.1530	2.6068	-0.1430
2	0.4000	0.5000	0.3992	0.5167	0.4000	0.4990
5	0.0000	0.3690	0.0025	0.3868	0.0023	0.3575
8	0.0000	0.3710	0.0000	0.4047	0.0000	0.3625
11	0.0000	0.1620	0.0004	0.1662	0.0000	0.1605
13	0.0000	0.1060	0.0009	0.1111	0.0000	0.1046

Table 4.16: Generators terminal condition of MinLoss-Flow PF algorithm and commercial software packages in case of IEEE 30-bus system.

Bus	PSCAD [95]		MinLoss-Flow PF	
	$\|U\|$	δ	$\|U\|$	δ
1	1.0600	98.4316	1.0600	0.0000
2	1.0431	93.0798	1.0442	-5.3340
5	1.0110	84.2658	1.0111	-14.1380
8	1.0100	86.6183	1.0125	-11.7880
11	1.0820	84.3227	1.0894	-14.0990
13	1.0710	83.4883	1.0800	-14.9410

4.10 Summary

This chapter proposed a new network-flow-based Minimum-Cost Flow model for PF/OPF in electric power systems. The developed PF method, named MinLoss-Flow PF algorithm, builds on parts of the formulation of the Flow-Augmentation PF method in Chapter 2, and estimates the system losses from the least-squares properties of the generalized inverse of the weighted incident matrix. Evaluation and comparison of the presented method were made against known PF methods, in terms of convergence and runtime. The algorithm is validated using commercial software packages, PSS/E and PSCAD, and the results show the accuracy of the presented method solution.

Chapter 5

Hybrid AC/DC Power Flow: Modeling, Formulation and Solution

5.1 Introduction

This chapter introduces a unique and novel graph-based power flow algorithm for multi-terminal voltage source converter-based hybrid AC/DC power systems using a sequential solution framework. The formulation of the power flow problem, as a maximum network-flow problem, and its solution methodology are presented. The solution procedure solves AC and DC parts sequentially, while accounting for voltage source converter losses, using a generalized converter model. The proposed method is validated using standard hybrid 5-bus and CIGRÉ-B4-DC systems.

5.2 Hybrid System Problem Formulation

Considering a hybrid electrical network $N_{electric} = (\mathcal{B}_{ac}, \mathcal{B}_{dc}, \mathcal{D}_{ac}, \mathcal{D}_{dc}, \mathcal{G}_{ac}, \mathcal{G}_{dc}, \mathcal{L}_{ac}, \mathcal{L}_{dc}, \mathcal{C}_{ACDC})$ with a set of buses $\mathcal{B}_{ac}$, a set of branches $\mathcal{D}_{ac}$, a set of generators $\mathcal{G}_{ac}$, and set of loads $\mathcal{L}_{ac}$ in the AC side, with each line connecting two buses. A bus can be connected to a generator or loads $g_{ac} \in \mathcal{G}_{ac}$ and $\ell_{ac} \in \mathcal{L}_{ac}$, respectively. Buses in the DC side can be connected to other generation $g_{dc} \in \mathcal{G}_{dc}$ or demand $\ell_{dc} \in \mathcal{L}_{dc}$ buses. While converters $\mathcal{C}_{AC-DC}$ are connecting two buses from the different grids using a specific converter control mode, either working as slack for DC-side or as a fixed power injection node or droop-based method. To transform the network $N_{electric}^{AC-DC}$ to a $s-t$ network $N_{st-electric}^{AC-DC}$ we use a similar formulation as in the generalized problem formulation, with the addition of DC network and converters connecting the two systems.

5.2.1 Hybrid System Mathematical Model

Hybrid AC-DC systems are more computationally complex than AC systems, due to the presence of a DC network and the number of converters with different control modes connecting both systems. Consider a hybrid electric network $N_{st-electric}^{AC-DC} = (G(V, E), s, t, \mathcal{G}_{ac}, \mathcal{G}_{dc}, \mathcal{L}_{ac}, \mathcal{L}_{dc}, \mathcal{C})$ with vertex set V, arc set E, source s, sink t, AC generation $\mathcal{G}_{ac}$, AC load $\mathcal{L}_{ac}$, DC generation $\mathcal{G}_{dc}$, DC loads $\mathcal{L}_{dc}$ and converters $\mathcal{C}_{AC-DC}$. A power flow for the network $N_{st-electric}^{AC-DC}$ is considered feasible for the network if the feasible flow function $f : A \to \mathbb{C}$ satisfies:

$$\sum_{(j,k)\in V_{ac}} f(j,k) \quad = 0, \qquad \forall\{j,k\} \in V_{ac} \setminus \{s,t\} \tag{5.1}$$

$$\sum_{j:(s,j)\in E_{ac}} f(s,j) \quad = \textstyle\sum_{g_{ac}\in\mathcal{G}} g_{ac}, \qquad \forall j \in E_{ac} \tag{5.2}$$

$$\sum_{j:(j,t)\in E_{ac}} f(j,t) \quad = \textstyle\sum_{\ell\in\mathcal{L}} \ell, \qquad \forall j \in E_{ac} \tag{5.3}$$

$$\sum_{(j,k)\in V_{dc}} f(j,k) \quad = 0, \quad \forall\{j,k\} \in V_{dc} \setminus \{s,t\} \tag{5.4}$$

$$\sum_{j:(s,j)\in E_{dc}} f(s,j) \quad = \textstyle\sum_{g_{dc}\in\mathcal{G}} g_{dc}, \quad \forall j \in E_{dc} \tag{5.5}$$

$$\sum_{j:(j,t)\in E_{dc}} f(j,t) \quad = \textstyle\sum_{\ell\in\mathcal{L}} \ell, \quad \forall j \in E_{dc} \tag{5.6}$$

$$\sum_{c_{ac}:(j,c)\in V_{ac}} f(j,c) \quad = \textstyle\sum_{c_{dc}:(c,k)\in V_{dc}} f(c,k) + \mathcal{C}_{losses} \tag{5.7}$$

Equations 5.1, 5.2, 5.3 models power flow on the AC side, while equations 5.4, 5.5, 5.6 models power flow on the DC side. Equation 5.7 models power flow in the power converters $\mathcal{C}_{ACDC}$. The proposed network-flow-based power flow solution algorithm sequentially solves AC and DC sides by finding flow augmentation till convergence criteria are met. The method considers detailed converter modeling [36].

5.3 Hybrid Systems Flow-Augmentation Power Flow Algorithm

Flow augmentation algorithm transfers power from generation to demand sides with no considerations of branch capacities. It relies on the calculation of network flow augmentation that supplies demand power and maintains correct voltage magnitude at generation buses. The solution procedure calls for network transformation to $s-t$ equivalent model first, then invoking max-flow-based solution method. It is worth noting here that the considered network flow here is complex power S on the AC side, and the resulting node voltages and node current injection dictates network current flows through network branch impedance. In turn, controlling converters' power flow and terminal voltages results in changes on DC side power injection and node voltages.

The solution procedure aims to find maximum complex power flow in $s-t_{ACDC}$ network satisfying the fixed branch powers into the node t, whether from AC, DC, or AC and DC sides. This procedure doesn't rely on finding individual flow augmenting paths one at a time that satisfies electric system physics, but rather, focuses on finding the total network flow that should exist to firstly, satisfy demand requirements, and secondly, maintain voltage magnitudes at generation buses while transferring power to DC-side without violating converters limits.

AC-side solution terminates when complex power flows out of source node s_{ac} into sink node t_{ac} satisfies all demand power and network power losses, as well as, PV bus active power injection and voltage magnitude $|U^{pv}|$ satisfies stated PV bus requirements, and reference bus $|U^{ref}_{ac}|$ and δ^{ref}_{ac} are met. Converters interface AC-to-DC sides and power injection and losses are considered during AC and DC-sides solutions. DC-side converges when slack node s_{dc} active power injection satisfies all demand from fixed power injection and droop controlled buses connected to the node t_{dc}, while keeping slack bus voltage at $|U^{ref}_{dc}|$. The sum of all generation power originated from source node s equals the sum of all demand power into sink node t plus power losses dissipated throughout the network. The max-flow-based network-flow solution converges to the power flow solution when AC-side, converters, and DC-side solutions converge while satisfying boundary conditions.

Network flow augmentation is achieved through the adjustment of network current injections at the generation side. Starting with generations equals total connected load and flat voltage profile for both AC and DC grids. Generations side reactive power is initially assigned based on the total connected load power factor, and converters are assumed lossless at the initialization step. Bus injection currents are calculated followed by voltage profile update in relation to reference bus voltage. Demand-side current injection changes as a result of voltage level change with the preservation of demand power. This step necessitates the change of current injection at generator buses, which requires the update of the voltage profile. The resulted sum of generation bus injection power is very close to the sum of total system demand plus system losses. Allocation of real power to generation buses is straightforward, as all PV buses real power injection is defined a priori, and differences between the total sum and PV sum is allocated to reference bus as bus generation plus

system losses. Generation buses reactive power is adjusted based on the deviations of the resulted voltage magnitudes compared to the stated PV voltage magnitude. The reference bus voltage is maintained at 1 p.u. for both AC and DC sides throughout the solution process, while initializing the remaining node voltages to the same value. Likewise, load power is fixed at stated demand values and generation power is set to the initial starting point with continuous updates in every iteration.

The computational complexity is at most $O(n^2)$, where n is the dimension of a full Y_{bus}. Further improvements can be attained by exploiting sparsity techniques for forward-backward substitution and optimal ordering [14] [11] [107]. Moreover, parallel operations could further improve scalability to bigger systems [50].

5.3.1 Hybrid Flow-Augmentation Power Flow Procedure

The Hybrid Flow-Augmentation algorithm iteratively solves the hybrid system until termination criterion or convergence is reached. Starting with AC system power flow solution, followed by reactive power correction at all PV buses. The converter's power flow and losses are calculated based on the converter's point of common coupling (PCC) voltage level, injected power, and converter control strategy. This results in finding DC grid initial injected power at all buses, except slack bus, which enables solving DC grid power flow. This, in turn, enables finding DC slack converter injected power into the AC grid at PCC. This algorithm does not dependent on power flow direction between AC and DC grids. The Hybrid Flow-Augmentation algorithm is presented in algorithm 7.

5.3.2 Flow-Augmentation Initialization Stage

System parameters are initialized as per generic network-flow initialization algorithm 2. System topology can be extracted from any system data after converting the system connections to a directed graph, in the orientation from generation to demand buses. Where bus-branch incidence matrix and bus-bus adjacency matrix are formulated, leading to Y_{bus}

Algorithm 7 Hybrid-FlowAugmentationPF

1: NetworkTransformation($G(V, E)$, S_{demand}, U_{ref}, Y_{branch})
2: **while** error $\geq \epsilon$ **do**
3: AC-NetworkFlowPFCalculation($G(V, E)$, S_{bus}, U_{bus})
4: ReactivePowerCorrection($G(V, E)$)
5: ConverterCalc
6: DC-NetworkFlowPFCalculation($G(V, E)$, S_{bus}, U_{bus})
7: SlackConverterCalc
8: **end**

formulation. Initial total generation is equated to total system demand with voltage magnitude initialized to $|U|^{ref}$ except at PV buses, where voltage magnitude is set to $|U|^{PV}$ and all voltage angles are set to 0. Generation reactive power is initialized to a value based on total load factor and bus active power injection value. Non-slack converters are initialized to a suitable power injection at PCC, while slack converter AC bus injection, from-or-to converter, is set to balance net power injection into DC grid from remaining converters.

5.3.3 AC Network Power Flow Calculation

Network-flow power flow is formulated as a maximum network flow problem, where the solution is finding the maximum flow that can be sustained in the network while preserving node flow summation without violating network limits. Adaptation of this formulation is required to successfully solve the power flow problem and accommodate problem-specific properties. This includes relaxing the limits of line flows, fixing the flow to sink node t, and introducing constraints on generation node's voltage and real power injection. The flow is a complex power injection in the network and formulated as a multiplication of voltage and current with dual properties. This algorithm uses a modified procedure of the one presented in section 2.6.2. Network-flow power flow algorithm is presented in algorithm 9.

Algorithm 8 NetworkTransformation

1: **procedure** INITIALIZE($G(V, E)$, S_{demand}, U_{ref}, Y_{branch})
2: $n \leftarrow$ number of Vertices/Nodes
3: $m \leftarrow$ number of Arcs/Edges
4: $G(n, m) \leftarrow$ Network Topology (n, m)
5: $G(V, E) \leftarrow$ *Network Topology* $(G(n, m))$
6: $A(G) \leftarrow$ *Network Topology* $(G(n, m))$
7: $H(G) \leftarrow$ *Network Topology* $(G(n, m))$
8: $\sum S_{gen} \leftarrow \sum S_{demand}$
9: pf_{load}
10: $S_{pv-gen} \leftarrow P_{pv-bus} + j(P_{pv-bus} * tan(pf_{load}))$
11: $S_{ref-bus} \leftarrow \sum S_{pv-gen} - \sum S_{demand}$
12: $U_{pq-bus} \leftarrow U_{ref}$
13: $U_{pv-bus} \leftarrow |U_{pv-bus}|\angle 0^{\circ}$
14: $Y_{bus} \leftarrow A(G) * Y_{branch} * A(G)'$
15: **return** $G(V, E), A(G), H(G), S_{gen}, S_{demand}, U_{bus}, Y_{bus}$

The algorithm pushes generation nodes' power into adjacent network arcs towards the sink node to satisfy demand power. In doing so, losses would be incurred due to network branch impedances and results in voltage difference at the end of each traversed arc, rather than at the beginning of the arc. Each intermediate node would push excess power downstream in the direction of load nodes. Resulting in the degradation of power level reaching load nodes at slightly higher voltage levels than the final power flow solution, as shown in algorithm 9 steps 2 through 6. Since load demand is fixed, the demand power is pushed in the reverse direction towards source nodes using demand-side calculated voltage values, which is considered as the reference in the $t - s$ direction, as shown in algorithm 9 steps 7 through 11. New generation side power and voltage are produced at the end of this procedure, which would be used to correct for generation reactive power assignment of PV buses using algorithm 4. Slack bus active power is found as the difference between the sum of total generation active power and total PV buses active power. A full network proce-

dure traversing in the direction source-sink-source constitutes one iteration. The step of pushing power in the $s-t$ or $t-s$ direction is achieved in a single step for all the networks.

A Hybrid AC-DC network is integrated into this procedure by including net converter complex power injection at PCC for non-slack converters, and DC grid power losses plus slack injected power and slack converter losses for the slack converter. Slack converter injected power would be refined from iteration to the next until convergence is reached.

5.3.4 Reactive Power Correction

Initial generation reactive power is updated after the execution of every AC Network-flow power flow step. Since generation nodes voltage magnitude after each iteration is different from required PV bus voltage magnitude, resulting in voltage magnitude difference ΔU. Relying on the direct relation between reactive power injection and voltage magnitude,

Algorithm 9 AC-NetworkFlowPFCalculation

procedure NetworkFlowPFCalculation($G(V, E)$, S_{bus}, U_{bus}, Y_{bus})
  $S_{bus}^{inj} \leftarrow S_{bus}^{gen} - S_{bus}^{demand}$
  $I_{bus}^{inj} \leftarrow (S_{bus}^{inj}/U_{bus})^*$
  $I_{bus}^{ref-inj} \leftarrow -\sum I_{bus}^{pq-inj} + \sum I_{bus}^{pv-inj}$
  $U_{bus-diff} \leftarrow Y_{bus}^{-1} I_{bus}$
  $U_{bus} \leftarrow U_{ref} + (U_{bus-diff} - U_{bus-diff}^{ref})$
  $I_{bus}^{inj} \leftarrow (S_{bus}^{inj}/U_{bus})^*$
  $I_{bus}^{ref-inj} \leftarrow -\sum I_{bus}^{pq-inj} + \sum I_{bus}^{pv-inj}$
  $U_{bus-diff} \leftarrow Y_{bus}^{-1} I_{bus}$
  $U_{bus} \leftarrow U_{pq} + (U_{bus-diff} - U_{bus-diff}^{pq})$
  $S_{bus}^{inj} \leftarrow U_{bus} * I_{bus}^*$
  $S_{bus}^{gen} \leftarrow S_{bus}^{inj} + S_{bus}^{demand}$
return $S_{bus}, U_{bus}, I_{inj}$

reactive power correction for PV bus based on voltage magnitude deviation from stated voltage can be made. Noting that $\frac{\partial Q}{\partial U}$ can be formulated in different ways. Algorithm 4 demonstrates the required steps.

5.3.5 Converter Power Flow

Non-slack converter's power flow, losses, and DC injected power can be calculated after estimation of converter AC bus voltage. As converter complex power injection is known in advance, that enables using simple circuit analysis to calculate converter side complex power and voltage level, which converter losses are dependent on. Converter quadratic loss parameters is used and based on [36] [48] [108] [109]. The relation between converter DC power injection, losses, and AC power injection is governed by the following equations:

$$I_{conv} = \frac{\sqrt{P_{conv}^2 + Q_{conv}^2}}{\sqrt{3}.U_c} \tag{5.8}$$

$$P_{loss}^{conv} = a + b \cdot I_{conv} + c \cdot I_{conv}^2 \tag{5.9}$$

$$P_{dc}^{i} = -P_{loss}^{i} - P_{conv}^{i} \tag{5.10}$$

Where $Pconv$, $Qconv$, Uc, and $Iconv$ are converter active power, reactive power, voltage, and current respectively. Figure 5.1 shows schematics of the generalized converter model.

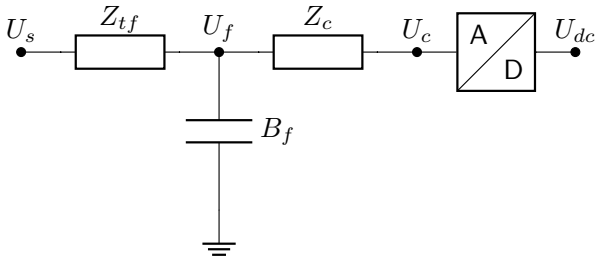

Figure 5.1: Generic VSC model.

5.3.6 DC Network Power Flow Calculation

DC grid network-flow solution is similar to AC grid network-flow solution procedure but without the presence of any PV buses. Algorithm 10 presents a required procedure for this step. Converters' power injection into DC buses is calculated from the previous step, while slack bus injection and bus voltages are directly calculated.

Algorithm 10 DC-NetworkFlowPFCalculation

procedure NetworkFlowPFCalculation($G(V, E)$, P_{bus}, U_{bus}, Y_{bus})
    $P_{bus}^{inj} \leftarrow P_{bus}^{gen} - P_{bus}^{demand}$
    $I_{bus}^{inj} \leftarrow (P_{bus}^{inj}/U_{bus})$
    $I_{bus}^{ref-inj} \leftarrow -\sum I_{bus}^{p-inj}$
    $U_{bus-diff} \leftarrow Y_{bus}^{-1} I_{bus}$
    $U_{bus} \leftarrow U_{ref} + (U_{bus-diff} - U_{bus-diff}^{ref})$
    $I_{bus}^{inj} \leftarrow (P_{bus}^{inj}/U_{bus})$
    $I_{bus}^{ref-inj} \leftarrow -\sum I_{bus}^{p-inj}$
    $U_{bus-diff} \leftarrow Y_{bus}^{-1} I_{bus}$
    $U_{bus} \leftarrow U_{pq} + (U_{bus-diff} - U_{bus-diff}^{p})$
    $P_{bus}^{inj} \leftarrow U_{bus} * I_{bus}$
    $P_{bus}^{gen} \leftarrow P_{bus}^{inj} + P_{bus}^{demand}$
return $P_{bus}, U_{bus}, I_{inj}$

5.3.7 Slack Converters Power Flow Calculation

Slack converter AC side initial power injection estimate requires continuous updates for the overall solution algorithm convergence. This requires an iterative procedure that is similar to Flow-Augmentation, but with the inclusion of a converter station, between power injection at DC side and point of common coupling on AC side.

The overall hybrid network-flow power flow algorithm is iteratively repeated until convergence criteria are reached. Starting from AC side Flow-Augmentation and subsequent reactive power correction step. Followed by AC-DC interface with DC side, through non-slack converters power injection calculation. Leading to DC power flow and updated DC grid voltage profile and slack power injection. Finally, slack converter AC side power injection is updated based on DC grid power flow, that in turn changes AC grid power flow conditions.

5.4 Example

This section demonstrates the proposed algorithm using a 5-bus test system adopted from [110]. The system is a two-generator mesh-connected system with load demand at 4 buses. Three AC-DC converters are connected to AC buses 2, 3, and 5. The converter at bus 3 is in the slack mode for the DC grid while the other converters are considered as fixed power injection. Figure 5.2 shows the hybrid AC/DC test system configuration. Figures 5.3 presents the hybrid test system in $s-t$ form highlighting power flow in generators, network and demand arcs in $s-t$ form. Table 5.1 presents converged solution for AC system voltage magnitude and angle, while Table 5.2 presents AC generator's injected power. Table 5.3 presents DC system voltages and power injections. All solutions compared with Newton-Raphson technique using MatACDC toolbox solution [48] [108]. The use of uniform criteria for the comparison of the proposed algorithm and published work is essential for objective results. The same criterion was used for loop mismatch tolerance and the maximum number of iterations for hybrid, AC, and DC stages. The used criterion is listed in Table 5.4 alongside 10-trials average execution time. The results show a high gain in computational speed, of around, 50% when compared to the hybrid AC/DC Newton-Raphson method. Figure 5.4a shows convergence error for voltage magnitude, angle, generation active, and reactive power at each iteration. Figures 5.4b shows convergence error for DC voltage and power injections.

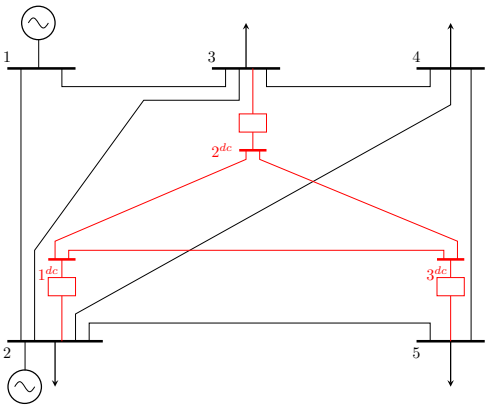

Figure 5.2: 5-bus hybrid AC/DC test system one line diagram.

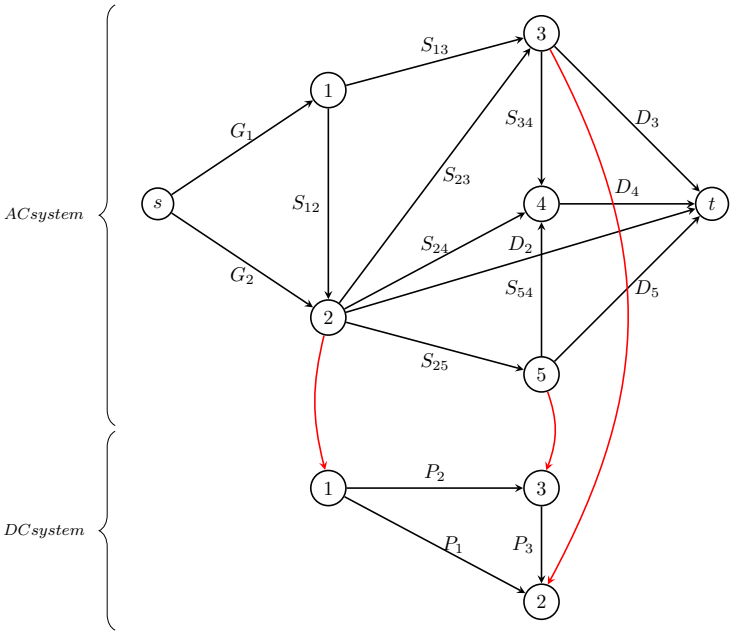

Figure 5.3: 5-bus hybrid AC/DC test system in s-t form.

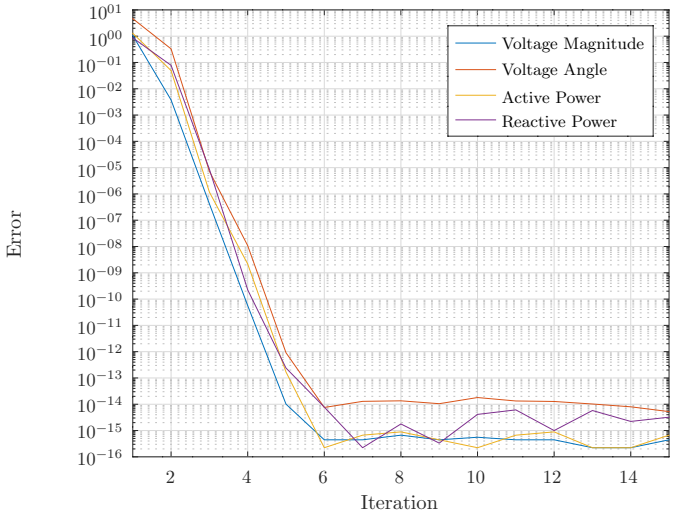

(a) AC system voltage and power error convergence.

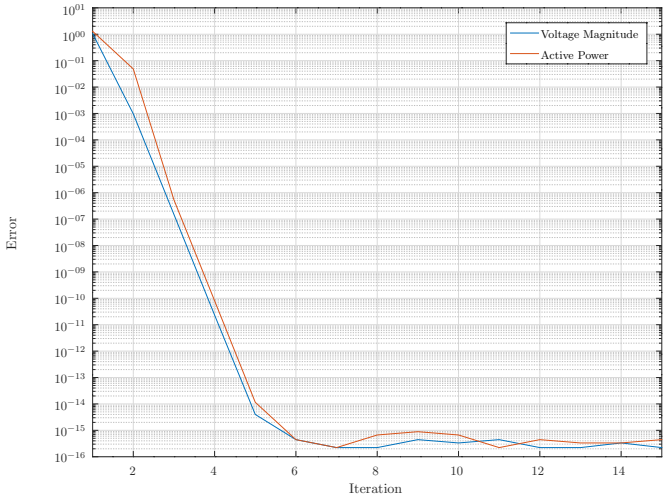

(b) DC system voltage and power error convergence.

Figure 5.4: AC and DC networks convergence error for hybrid 5-bus system.

Table 5.1: AC bus voltage comparison for hybrid 5-bus AC/DC system.

Bus Number	Newton-Raphson [48]		Network-flow PF	
	$\|U\|$	δ	$\|U\|$	δ
1	1.0600	0.0000	1.0600	0.0000
2	1.0000	-2.3954	1.0000	-2.4564
3	1.0000	-3.9249	1.0019	-3.6962
4	0.9960	-4.2875	0.9983	-3.9775
5	0.9908	-4.1662	0.9878	-4.7966

Table 5.2: AC power generation comparison for hybrid 5-bus AC/DC system.

Bus Number	Newton-Raphson [48]		Network-flow PF	
	P	Q	P	Q
1	134.1873	84.1707	134.0758	83.3121
2	40	-32.8139	40	-32.4801

Table 5.3: DC bus voltage and power injection comparison for hybrid 5-bus AC/DC system.

Bus Number	Newton-Raphson [48]		Network-flow PF	
	$\|U\|$	P	$\|U\|$	P
1	1.0156	-58.6274	1.0157	-58.6181
2	1.0000	21.3740	1.0000	21.3595
3	0.9955	36.1856	0.9955	36.1911

Table 5.4: Comparison parameters for hybrid 5-bus AC/DC system evaluation.

Criterion	Newton-Raphson [108]	Network-flow PF
AC-DC Maximum Iteration	10	10
AC-DC Tolerance (p.u.)	10^{-7}	10^{-7}
AC Maximum Iteration	10	10
AC Tolerance (p.u.)	10^{-7}	10^{-7}
DC Maximum Iteration	10	10
DC Tolerance (p.u.)	10^{-7}	10^{-7}
Execution Time (Sec)	0.146012	0.068989

5.5 Case Study

Evaluation of the proposed graph-based PF methods using hybrid benchmark system, namely CIGRÉ-B4-DC test system [111] is presented in this section. CIGRÉ B4 DC test system is a diverse system that consists of different AC and DC system topologies and voltage levels, cables and transmission lines, symmetric monopole and bi-pole converters, as well as different converters control modes. The converged solution is in close tolerance with the generalized Newton-Raphson-based method in [36].

Comparison of the proposed solution method Newton-Raphson technique using Mat-ACDC toolbox is presented in Tables 5.5, 5.6 and 5.7. Table 5.5 compares the three AC areas bus voltage magnitude and angle. Table 5.6 compares the AC grid real and reactive power injection at each bus. Table 5.7 compares DC systems bus voltage and power injection. Figure 5.6 shows AC and DC systems convergence errors. It's evident that system convergence is achieved simultaneously, even though smaller systems demonstrate higher convergence rates, like AC-3 and DCS-1 in Figure 5.6e and Figure 5.6b, due to the simpler connection and non-varying converter power injection. In contrast, AC-1 is presenting a slower convergence rate as shown in Figure 5.6a, due to the high variability in AC-side

power injection dictated by the role of acting as slack for the entire connected systems. While AC-2 is also presenting a slow rate of convergence, Figure 5.6c, as it connects DCS-2 and DCS-3.

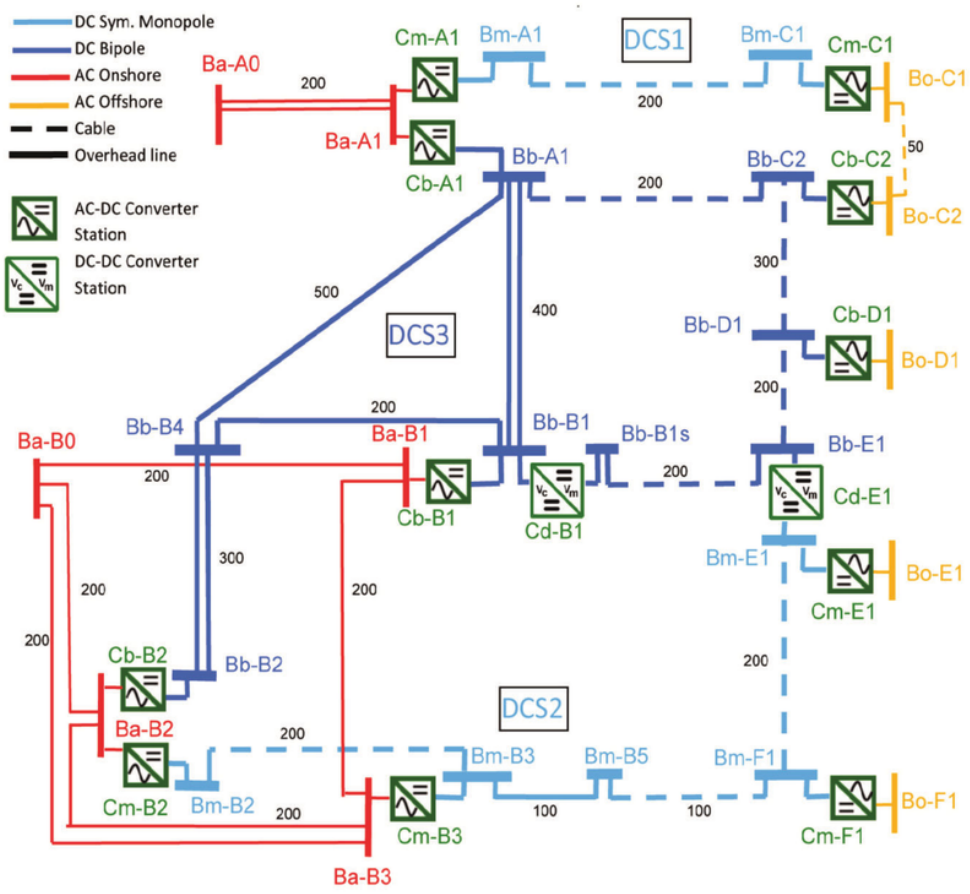

Figure 5.5: CIGRÉ B4 DC hybrid test system [111].

Table 5.5: AC bus voltage comparison for CIGRÉ B4 DC system.

System	Bus	Newton-Raphson [108]		Network-flow PF	
		$\|U\|$	δ	$\|U\|$	δ
AC-1	Ba-A0	1.0000	0.0000	1.0000	0.0000
	Ba-A1	1.0000	-6.9000	1.0000	-7.0645
AC-2	Ba-B0	1.0000	0.0000	1.0000	0.0000
	Ba-B1	1.0000	4.2000	1.0001	4.1864
	Ba-B2	1.0000	3.9000	1.0000	3.8717
	Ba-B3	1.0000	2.0000	0.9999	1.9709
AC-3	Ba-C1	1.0000	0.0000	1.0000	0.0000
	Ba-C2	1.0000	-2.4000	1.0000	-2.3535

Table 5.6: AC bus power injection comparison for CIGRÉ B4 DC system.

System	Bus	Newton-Raphson [108]		Network-flow PF	
		P	Q	P	Q
AC-1	Ba-A0	644.30	-131.80	662.32	-130.94
	Ba-A1	2000.00	0.00	2000.00	0.00
AC-2	Ba-B0	-470.20	-133.60	-467.73	-134.17
	Ba-B1	1000.00	-35.70	1000.00	-35.07
	Ba-B2	1000.00	-60.10	1000.00	-59.56
	Ba-B3	1000.00	-121.20	1000.00	-121.67
AC-3	Ba-C1	504.50	-136.90	504.46	-136.87
	Ba-C2	500.00	80.40	500.00	80.43

Table 5.7: DC bus voltage and power injection for CIGRÉ B4 DC system.

System	Bus	Newton-Raphson [108]		Network-flow PF	
		U	P	U	P
DCS-1	Bm-A1	1.0000	-393.5	1.0000	-393.50
	Bm-C1	1.0090	397.2	1.0093	397.18
DCS-2	Bm-B2	0.9900	126.0	0.9900	128.53
	Bm-B3	0.9870	-806.5	0.9869	-808.78
	Bm-B5	0.9980	-	0.9983	-
	Bm-F1	1.0070	496.1	1.0065	496.06
	Bm-E1	1.0110	-100.74	1.0112	-100.94
DCS-3	Bb-A1	1.0100	2009.7	1.0100	2021.08
	Bb-B1	0.9980	-1511.8	0.9967	-1514.46
	Bb-B2	0.9830	-1714.4	0.9802	-1718.44
	Bb-B4	0.9930	-	0.9906	-
	Bb-C2	1.0140	594.7	1.0144	597.34
	Bb-D1	1.0150	992.1	1.0152	993.34
	Bb-E1	1.0090	-301.1	1.0093	-300.86
	Bb-B1s	1.0060	-	1.0053	-

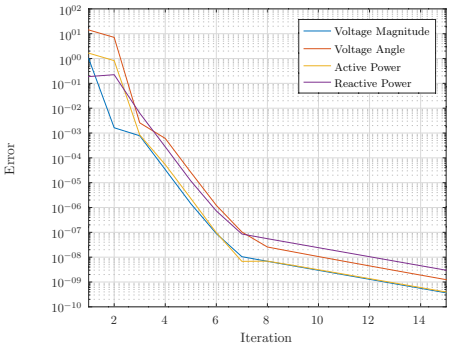

(a) AC-1 convergence error

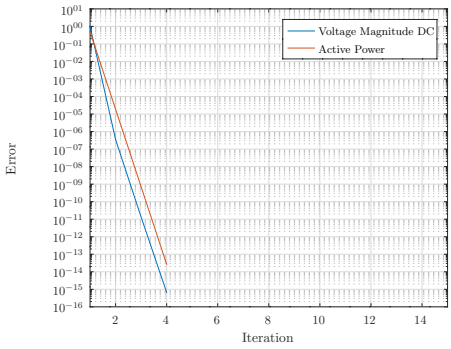

(b) DCS-1 convergence error

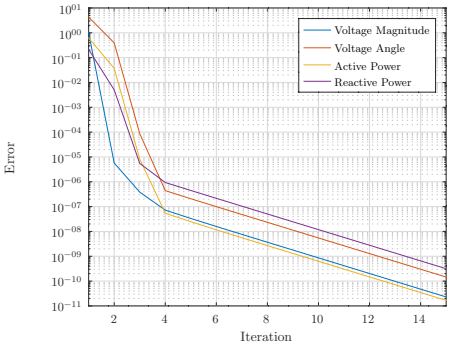

(c) AC-2 convergence error

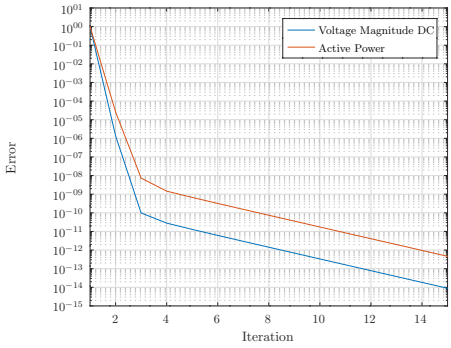

(d) DCS-2 convergence error

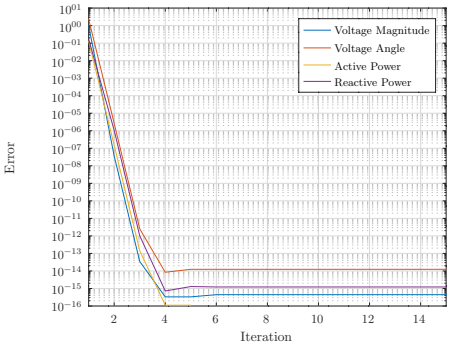

(e) AC-3 convergence error

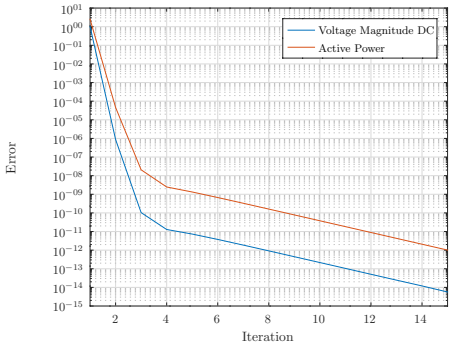

(f) DCS-3 convergence error

Figure 5.6: AC and DC networks convergence error for CIGRÉ B4 DC system.

5.6 Summary

This chapter presented a power flow solution for hybrid AC/DC systems. The proposed method formulates the hybrid AC/DC power flow problem as a maximum network-flow problem and solves it, using a max-flow-based algorithm. The method solves the AC and DC sides sequentially while employing the detailed converter model. The presented algorithm was validated and compared with the modified Newton-Raphson formulation on a hybrid 5-bus test system and CIGRÉ B4 DC system. The developed method shows considerable savings in execution time of more than 50% compared with hybrid AC/DC Newton-Raphson based method.

Chapter 6

Synopsis and Future Research

6.1 Synopsis

This thesis utilized a graph theoretic approach to the fundamental problems in electric power systems, namely power flow and optimal power flow. The conversion of the power system into a network equivalent, and the reformulation of PF/OPF as a network-flow problem, results in a generalized and efficient solution framework. The power flow problem is formulated as a graph maximum flow problem, while the optimum power flow is formulated as a graph minimum cost-flow problem. A special case of this formulation is the solution of the power flow as a sub-problem of the generic optimum power flow formulation. Application of the proposed method to the hybrid power system is also presented, to demonstrate the generality and applicability to any system type and configuration.

Chapter 2 proposes a new network-flow-based maximum-flow PF method for steady-state solution in electric power transmission and distribution levels. The proposed method is named *Flow-Augmentation PF* algorithm. The developed method is generic in nature and is not effected by system topology and accommodates various branch elements. The Flow-Augmentation PF method handles voltage-controlled nodes without the calculation of the Jacobean matrix and subsequent inversion, as in the Newton-Raphson method, nor the introduction of branch break-points and changes in system topology, as in the

Backward-Forward-Sweep method. The presented method was evaluated on standard systems and compared in terms of convergence and run time against known methods. Overall computational complexity is found to be dependent on the ratio of PV to PQ nodes. The algorithm complexity is $O(max\{n^{1.2}, n_{PQ}^{1.4}\})$ with linear convergence characteristics. Algorithm complexity is $O(n^{1.2})$ for a system consisting of no PV nodes and all PQ nodes.

Chapter 3 presents the performance of the Flow-Augmentation PF method on various transmission and distribution systems. The selected Transmission systems contain different elements from power system networks, including shunt elements, transformers with off-nominal taps, and synchronous condensers. The used distribution system was tested in radial and meshed configuration, with and without the presence of distributed generation in the system. The simulation's execution time and iteration counter are listed, alongside system voltage profile, and power injection convergence. Linear convergence behavior is presented by the Flow-Augmentation PF algorithm on the evaluated test cases. Convergence speed is also dependent on the number of generation buses, and loading conditions. This dependence is evident by the number of corrective steps needed to reduce PV bus voltage magnitude mismatch through reactive power correction, which in turn is related to the ratio of PV/PQ buses in the system. Accuracy comparison against the most recognized techniques and leading software packages, PSS/E and PSCAD, revealed favorable convergence and very low error bounds.

Chapter 4 proposes a new network-flow-based minimum-cost flow method for the power flow and optimum power flow problems in electric power systems. The proposed PF method is named *MinLoss-Flow PF* algorithm. The MinLoss-Flow PF method builds on parts of the formulation of the Flow-Augmentation PF method and differs in the evaluation of system losses. The proposed method estimates the system losses by using the least-squares properties of the generalized inverse of the weighted incident matrix. The algorithm complexity is $O(max\{mn, n_{PQ}^{1.4}\})$ with linear convergence characteristics. Algorithm complexity is $O(mn)$ for a system consisting of no PV nodes and all PQ nodes. This case can be generalized to handle network flow optimization, as in the case of optimum power flow. Simulation studies of different electric systems demonstrate convergence speed and accuracy. Further comparison with commercial software packages confirms the precision of the

solution of the presented method.

Chapter 5 proposes a steady-state hybrid multi-terminal power flow method based on sequential max-flow formulation named *Hybrid Flow-Augmentation PF*. This method is different from literature-established methods while achieving comparable accuracy and faster convergence compared to the hybrid AC/DC Newton-Raphson method when applied to benchmark systems with complete converter models. The promising generality of this method could further be extended to a hybrid optimum power flow solution method.

6.2 Future Research Directions

This thesis presents a completely new and promising research direction in algorithm design for power system applications. Network-flow-based algorithms can further be developed to benefit from acceleration in reactive power correction rate and a further reduction in computational complexity. Further extension is the generalization to include three-phase balanced and unbalanced distribution systems. The proposed MinLoss-Flow PF algorithm can be further developed into a full optimum power flow solver, by the inclusion of generation cost functions and optimum selection of transformers tap setting in the formulation. Also, the proposed hybrid AC/DC systems can be reformulated into a unified framework and further extended to hybrid optimum power flow.

References

[1] A. F. Glimn and G. W. Stagg, "Automatic Calculation of Load Flows," *Transactions of the American Institute of Electrical Engineers. Part III: Power Apparatus and Systems*, vol. 76, no. 3, pp. 817–825, 1957.

[2] D. W. C. Shen and S. Lisser, "An Analogue Computer for Automatic Determination of System Swing Curves," *Transactions of the American Institute of Electrical Engineers, Part I: Communication and Electronics*, vol. 73, pp. 475–483, Nov 1954.

[3] J. M. Henderson, "Automatic Digital Computer Solution of Load Flow Studies," *Transactions of the American Institute of Electrical Engineers. Part III: Power Apparatus and Systems*, vol. 73, Jan 1954.

[4] L. A. Dunstan, "Digital Load Flow Studies," *Transactions of the American Institute of Electrical Engineers. Part III: Power Apparatus and Systems*, vol. 73, Jan 1954.

[5] J. B. Ward and H. W. Hale, "Digital Computer Solution of Power-Flow Problems," *Transactions of the American Institute of Electrical Engineers. Part III: Power Apparatus and Systems*, vol. 75, Jan 1956.

[6] R. J. Brown and W. F. Tinney, "Digital Solutions for Large Power Networks," *Transactions of the American Institute of Electrical Engineers. Part III: Power Apparatus and Systems*, vol. 76, pp. 347–351, April 1957.

[7] P. Kundur, *Power System Stability And Control*. EPRI power system engineering series, McGraw-Hill, 1994.

[8] H. Saadat, *Power System Analysis*. McGraw-Hill Series in Electrical and Computer Engineering, WCB/McGraw-Hill, 1999.

[9] W. F. Tinney and C. E. Hart, "Power Flow Solution by Newton's Method," *IEEE Transactions on Power Apparatus and Systems*, vol. PAS-86, pp. 1449–1460, Nov 1967.

[10] F. Milano, *Power System Modelling and Scripting*. Power Systems, Springer Berlin Heidelberg, 2010.

[11] W. F. Tinney and J. W. Walker, "Direct Solutions of Sparse Network Equations by Optimally Ordered Triangular Factorization," *Proceedings of the IEEE*, vol. 55, no. 11, pp. 1801–1809, 1967.

[12] N. Sato and W. F. Tinney, "Techniques for Exploiting the Sparsity or the Network Admittance Matrix," *IEEE Transactions on Power Apparatus and Systems*, vol. 82, no. 69, pp. 944–950, 1963.

[13] E. C. Ogbuobiri, W. F. Tinney, and J. W. Walker, "Sparsity-Directed Decomposition for Gaussian Elimination on Matrices," *IEEE Transactions on Power Apparatus and Systems*, vol. PAS-89, no. 1, pp. 141–150, 1970.

[14] W. Tinney and W. Meyer, "Solution of Large Sparse Systems by Ordered Triangular Factorization," *IEEE Transactions on Automatic Control*, vol. 18, no. 4, pp. 333–346, 1973.

[15] H. Le Nguyen, "Newton-Raphson Method in Complex Form [power system load flow analysis]," *IEEE Transactions on Power Systems*, vol. 12, no. 3, pp. 1355–1359, 1997.

[16] B. Stott and O. Alsac, "Fast Decoupled Load Flow," *IEEE Transactions on Power Apparatus and Systems*, vol. PAS-93, pp. 859–869, May 1974.

[17] P. R. Bijwe, B. Abhijith, and G. K. Viswanadha Raju, "Robust Three Phase Fast Decoupled Power Flow," in *2009 IEEE/PES Power Systems Conference and Exposition*, pp. 1–5, 2009.

[18] R. K. Portelinha and O. L. Tortelli, "Three Phase Fast Decoupled Power Flow for Emerging Distribution Systems," in *2015 IEEE PES Innovative Smart Grid Technologies Latin America (ISGT LATAM)*, pp. 81–86, 2015.

[19] R. Van Amerongen, "A General-Purpose Version of The Fast Decoupled Load Flow," *IEEE Transactions on Power Systems*, vol. 4, no. 2, pp. 760–770, 1989.

[20] B. Stott, "Review of Load-Flow Calculation Methods," *Proceedings of the IEEE*, vol. 62, no. 7, pp. 916–929, 1974.

[21] W. Kersting, *Distribution System Modeling and Analysis*. CRC Press, 1st ed., 2001.

[22] D. Kersting, W.H. Mendive, *An Application of Ladder Networktheory to The Solution of Three Phase Radial Load-Flow Problem*. IEEE, 1976.

[23] D. Rajicic, R. Ackovski, and R. Taleski, "Voltage Correction Power Flow," *IEEE Transactions on Power Delivery*, vol. 9, no. 2, pp. 1056–1062, 1994.

[24] D. Rajicic and A. Dimitrovski, "A New Method for Handling PV Nodes in Backward/Forward Power Flow for Radial and Weakly Meshed Networks," in *2001 IEEE Porto Power Tech Proceedings (Cat. No.01EX502)*, vol. 3, pp. 6 pp. vol.3–, 2001.

[25] D. Rajičić and R. Taleski, "Two Novel Methods for Radial and Weakly Meshed Network Analysis," *Electric Power Systems Research*, vol. 48, no. 2, pp. 79–87, 1998.

[26] D. Shirmohammadi, H. Hong, A. Semlyen, and G. Luo, "A Compensation-Based Power Flow Method for Weakly Meshed Distribution and Transmission Networks," *IEEE Transactions on Power Systems*, vol. 3, no. 2, pp. 753–762, 1988.

[27] G. Luo and A. Semlyen, "Efficient Load Flow for Large Weakly Meshed Networks," *IEEE Transactions on Power Systems*, vol. 5, no. 4, pp. 1309–1316, 1990.

[28] K. Murari and N. Padhy, "A Network-Topology Based Approach for the Load Flow Solution of AC-DC Distribution System With Distributed Generations," *IEEE Transactions on Industrial Informatics*, vol. PP, pp. 1–1, 07 2018.

[29] K. Murari and N. Padhy, "Graph-Theoretic-Based Approach for Solving Load Flow Problem of AC-DC Radial Distribution Network with Distributed Generations," *IET Generation Transmission & Distribution*, 02 2020.

[30] J.-H. Teng, "A Direct Approach for Distribution System Load Flow Solutions," *IEEE Transactions on Power Delivery*, vol. 18, no. 3, pp. 882–887, 2003.

[31] N.-C. Yang, "Three-Phase Power Flow Calculations Using Direct Z BUS Method for Large-Scale Unbalanced Distribution Networks," *IET Generation, Transmission & Distribution*, vol. 10, no. 4, pp. 1048–1055, 2016.

[32] J. Yu, T. Shen, Y. Li, and Y. Zhang, "A Power Flow Solution for Meshed Network by Incidence Matrix," in *2017 29th Chinese Control And Decision Conference (CCDC)*, pp. 3201–3206, May 2017.

[33] T. Shen, Y. Li, and J. Xiang, "A Graph-Based Direct Approach for Distribution Systems With PV Nodes," in *2017 Eighth International Conference on Intelligent Control and Information Processing (ICICIP)*, pp. 219–224, Nov 2017.

[34] T. Shen, Y. Li, and J. Xiang, "A Graph-Based Power Flow Method for Balanced Distribution Systems," *Energies*, vol. 11, no. 3, 2018.

[35] A. Panosyan and B. R. Oswald, "Modified Newton-Raphson load flow analysis for integrated AC/DC power systems," in *39th International Universities Power Engineering Conference*, vol. 3, pp. 1223–1227 vol. 2, 2004.

[36] J. Beerten, S. Cole, and R. Belmans, "Generalized Steady-State VSC MTDC Model for Sequential AC/DC Power Flow Algorithms," *IEEE Transactions on Power Systems*, vol. 27, pp. 821–829, May 2012.

[37] A. A. Hamad, M. A. Azzouz, and E. F. El Saadany, "A Sequential Power Flow Algorithm for Islanded Hybrid AC/DC Microgrids," *IEEE Transactions on Power Systems*, vol. 31, no. 5, pp. 3961–3970, 2016.

[38] A. A. Eajal, M. A. Abdelwahed, E. F. El-Saadany, and K. Ponnambalam, "A Unified Approach to the Power Flow Analysis of AC/DC Hybrid Microgrids," *IEEE Transactions on Sustainable Energy*, vol. 7, no. 3, pp. 1145–1158, 2016.

[39] H. M. A. Ahmed, A. B. Eltantawy, and M. M. A. Salama, "A Generalized Approach to the Load Flow Analysis of AC–DC Hybrid Distribution Systems," *IEEE Transactions on Power Systems*, vol. 33, no. 2, pp. 2117–2127, 2018.

[40] E. Aprilia, K. Meng, M. Al Hosani, H. H. Zeineldin, and Z. Y. Dong, "Unified Power Flow Algorithm for Standalone AC/DC Hybrid Microgrids," *IEEE Transactions on Smart Grid*, vol. 10, no. 1, pp. 639–649, 2019.

[41] S. Messalti, S. Belkhiat, S. Saadate, and D. Flieller, "A New Approach for Load Flow Analysis of Integrated AC–DC Power Systems Using Sequential Modified Gauss–Seidel Methods," *European Transactions on Electrical Power*, vol. 22, no. 4, pp. 421–432, 2012.

[42] H. Sato and J. Arrillaga, "Improved Load-Flow Techniques for Integrated A.C.-D.C. Systems," *Proceedings of the Institution of Electrical Engineers*, vol. 116, no. 4, pp. 525–532, 1969.

[43] M. M. El-Marsafawy and R. M. Mathur, "A New, Fast Technique for Load-Flow Solution of Integrated Multi-Terminal DC/AC Systems," *IEEE Transactions on Power Apparatus and Systems*, vol. PAS-99, pp. 246–255, Jan 1980.

[44] H. Fudeh and C. M. Ong, "A Simple and Efficient AC-DC Load-Flow Method for Multiterminal DC Systems," *IEEE Transactions on Power Apparatus and Systems*, vol. PAS-100, pp. 4389–4396, Nov 1981.

[45] M. El-Hawary and S. Ibrahim, "A New Approach to AC-DC Load Flow Analysis," *Electric Power Systems Research*, vol. 33, no. 3, pp. 193–200, 1995.

[46] T. Smed, G. Andersson, G. B. Sheble, and L. L. Grigsby, "A New Approach to AC/DC Power Flow," *IEEE Transactions on Power Systems*, vol. 6, pp. 1238–1244, Aug 1991.

[47] M. E. Nassar, A. A. Hamad, M. M. A. Salama, and E. F. El-Saadany, "A novel load flow algorithm for islanded ac/dc hybrid microgrids," *IEEE Transactions on Smart Grid*, vol. 10, no. 2, pp. 1553–1566, 2019.

[48] J. Beerten, S. Cole, and R. Belmans, "A Sequential AC/DC Power Flow Algorithm for Networks Containing Multi-terminal VSC HVDC Systems," in *IEEE PES General Meeting*, pp. 1–7, July 2010.

[49] R. Chai, B. Zhang, J. Dou, Z. Hao, and T. Zheng, "Unified Power Flow Algorithm Based on the NR Method for Hybrid AC/DC Grids Incorporating VSCs," *IEEE Transactions on Power Systems*, vol. 31, pp. 4310–4318, Nov 2016.

[50] W. Feng, C. Yuan, Q. Shi, R. Dai, G. Liu, Z. Wang, and F. Li, "Graph Computing Based Distributed Parallel Power Flow for AC/DC Systems with Improved Initial Estimate," *Journal of Modern Power Systems and Clean Energy*, pp. 1–10, 2020.

[51] C. Yuan, Y. Zhou, G. Liu, R. Dai, Y. Lu, and Z. Wang, "Graph Computing-Based WLS Fast Decoupled State Estimation," *IEEE Transactions on Smart Grid*, vol. 11, no. 3, pp. 2440–2451, 2020.

[52] Q. Shi, C. Yuan, W. Feng, G. Liu, R. Dai, Z. Wang, and F. Li, "Enabling Model-Based LTI for Large-Scale Power System Security Monitoring and Enhancement With Graph-Computing-Based Power Flow Calculation," *IEEE Access*, vol. 7, pp. 167010–167018, 2019.

[53] F. L. Alvarado, "Computational Complexity in Power Systems," *IEEE Transactions on Power Apparatus and Systems*, vol. 95, no. 4, pp. 1028–1037, 1976.

[54] A. Castillo and R. P. O'Neill, "Survey of Approaches to Solving The ACOPF," tech. rep., Federal Energy Regulatory Commission, 2013.

[55] S. Frank, I. Steponavičė, and S. Rebennack, "Optimal Power Flow: A Bibliographic Survey I," *Energy Systems*, vol. 3, 09 2012.

[56] M. Huneault and F. D. Galiana, "A Survey of The Optimal Power Flow Literature," *IEEE Transactions on Power Systems*, vol. 6, pp. 762–770, May 1991.

[57] J. A. Momoh, R. Adapa, and M. E. El-Hawary, "A Review of Selected Optimal Power Flow Literature to 1993. I. Nonlinear and Quadratic Programming Approaches," *IEEE Transactions on Power Systems*, vol. 14, pp. 96–104, Feb 1999.

[58] J. Momoh, M. El-Hawary, and R. Adapa, "A Review of Selected Optimal Power Flow Literature to 1993. II. Newton, Linear Programming and Interior Point Methods," *IEEE Transactions on Power Systems*, vol. 14, no. 1, pp. 105–111, 1999.

[59] D. W. Wells, "Method for Economic Secure Loading of A Power System," *Proceedings of the Institution of Electrical Engineers*, vol. 115, pp. 1190–1194, August 1968.

[60] B. . Stott and J. L. Marinho, "Linear Programming for Power-System Network Security Applications," *IEEE Transactions on Power Apparatus and Systems*, vol. PAS-98, no. 3, pp. 837–848, 1979.

[61] S. Bruno, S. Lamonaca, G. Rotondo, U. Stecchi, and M. La Scala, "Unbalanced Three-Phase Optimal Power Flow for Smart Grids," *IEEE Transactions on Industrial Electronics*, vol. 58, no. 10, pp. 4504–4513, 2011.

[62] Z.-q. Luo, W.-k. Ma, A. M.-c. So, Y. Ye, and S. Zhang, "Semidefinite Relaxation of Quadratic Optimization Problems," *IEEE Signal Processing Magazine*, vol. 27, no. 3, pp. 20–34, 2010.

[63] B. H. Kim and R. Baldick, "Coarse-grained Distributed Optimal Power Flow," *IEEE Transactions on Power Systems*, vol. 12, no. 2, pp. 932–939, 1997.

[64] G. Hug-Glanzmann and G. Andersson, "Decentralized Optimal Power Flow Control for Overlapping Areas in Power Systems," *IEEE Transactions on Power Systems*, vol. 24, no. 1, pp. 327–336, 2009.

[65] F. Nogales, F. Prieto, and A. Conejo, "A Decomposition Methodology Applied to the Multi-Area Optimal Power Flow Problem," *Annals of Operations Research*, vol. 120, pp. 99–116, April 2003.

[66] T. Bouktir, L. Slimani, and M. Belkacemi, "A Genetic Algorithm for Solving the Optimal Power Flow Problem," *Leonardo Journal of Sciences*, vol. 3, 02 2004.

[67] J. Vlachogiannis and K. Lee, "A Comparative Study on Particle Swarm Optimization for Optimal Steady-State Performance of Power Systems," *IEEE Transactions on Power Systems*, vol. 21, no. 4, pp. 1718–1728, 2006.

[68] F.-C. L. and Y.-Y. H., "Fuzzy Dynamic Programming Approach to Reactive Power/Voltage Control in A Distribution Substation," *IEEE Transactions on Power Systems*, vol. 12, no. 2, pp. 681–688, 1997.

[69] A. H. El-Abiad and F. J. Jaimes, "A Method for Optimum Scheduling of Power and Voltage Magnitude," *IEEE Transactions on Power Apparatus and Systems*, vol. PAS-88, pp. 413–422, April 1969.

[70] O. Alsac and B. Stott, "Optimal Load Flow with Steady-State Security," *IEEE Transactions on Power Apparatus and Systems*, vol. PAS-93, pp. 745–751, May 1974.

[71] W. Barcelo, W. Lemmon, and H. Koen, "Optimization of The Real-time Dispatch With Constraints for Secure Operation of Bulk Power Systems," *IEEE Transactions on Power Apparatus and Systems*, vol. PAS-96, no. 3, pp. 741–757, 1977.

[72] J. Peschon, D. S. Piercy, W. F. Tinney, O. J. Tveit, and M. Cuenod, "Optimum Control of Reactive Power Flow," *IEEE Transactions on Power Apparatus and Systems*, vol. PAS-87, pp. 40–48, Jan 1968.

[73] W. F. Tinney, V. Brandwajn, and S. M. Chan, "Sparse Vector Methods," *IEEE Transactions on Power Apparatus and Systems*, vol. PAS-104, pp. 295–301, Feb 1985.

[74] H. H. Happ, "Optimal Power Dispatch," *IEEE Transactions on Power Apparatus and Systems*, vol. PAS-93, pp. 820–830, May 1974.

[75] C. W. Sanders and C. A. Monroe, "An Algorithm for Real-Time Security Constrained Economic Dispatch," *IEEE Transactions on Power Systems*, vol. 2, pp. 1068–1074, Nov 1987.

[76] J. Lavaei and S. H. Low, "Zero Duality Gap in Optimal Power Flow Problem," *IEEE Transactions on Power Systems*, vol. 27, pp. 92–107, Feb 2012.

[77] F. R. T.E. Harris, "Fundamentals of A Method for Evaluating Rail Net Capacities," *Research Memorandum RM-1573*, 1955.

[78] L. R. Ford and D. R. Fulkerson, "Maximal Flow Through a Network," *Canadian Journal of Mathematics*, vol. 8, p. 399–404, 1956.

[79] J. Edmonds and R. M. Karp, "Theoretical Improvements in Algorithmic Efficiency for Network Flow Problems," *J. ACM*, vol. 19, pp. 248–264, Apr. 1972.

[80] A. V. Goldberg and R. E. Tarjan, "A New Approach to the Maximum-flow Problem," *J. ACM*, vol. 35, pp. 921–940, Oct. 1988.

[81] C. Thomassen, "Resistances and currents in infinite electrical networks," *Journal of Combinatorial Theory, Series B*, vol. 49, no. 1, pp. 87 – 102, 1990.

[82] K. Takahashi, Y. Sekine, and T. Umezu, "Network-Flow Method Applied to Load-Flow Calculation," *IEEE Transactions on Power Apparatus and Systems*, vol. PAS-87, pp. 1939–1949, Nov 1968.

[83] J. Taylor, *Convex Optimization of Power Systems*. Convex Optimization of Power Systems, Cambridge University Press, 2015.

[84] J. Zhu, *Power Systems Applications of Graph Theory*. Energy science, engineering and technology series, Nova Science Publishers, 2009.

[85] J. Quirós-Tortós and V. Terzija, "A Graph Theory Based New Approach for Power System Restoration," in *2013 IEEE Grenoble Conference*, pp. 1–6, June 2013.

[86] T. S. Oepomo, "Applied Graph Theory and Topology for 3 Phase Power System Under Faulted Studies," in *Proceedings of the Seventh International Conference on Management Science and Engineering Management: Focused on Electrical and Information Technology Volume II*, pp. 1521–1540, Springer Berlin Heidelberg, 2014.

[87] P. Nguyen, W. Kling, G. Georgiadis, M. Papatriantafilou, L. Tuan, and L. Bertling, *Application of The Graph Theory in Managing Power Flows in Future Electric Networks*, pp. 251–266. InTech, 2012.

[88] F. Dörfler, J. W. Simpson-Porco, and F. Bullo, "Electrical Networks and Algebraic Graph Theory: Models, Properties, and Applications," *Proceedings of the IEEE*, Sept. 2017.

[89] J. Barras, S. Alec, C. Pasche, P. A. Chamorel, A. J. Germond, and D. de Werra, "Network Simplex Method Applied to AC Load-Flow Calculation," *IEEE Power Engineering Review*, vol. PER-7, no. 2, pp. 45–45, 1987.

[90] J. Grainger and W. Stevenson, *Power System Analysis*. McGraw-Hill Series in Electrical and Computer Engineering: Power and Energy, McGraw-Hill, 1994.

[91] R. K. Ahuja, T. L. Magnanti, and J. B. Orlin, *Network Flows: Theory, Algorithms, and Applications*. Upper Saddle River, NJ, USA: Prentice-Hall, Inc., 1993.

[92] R. D. Zimmerman, *AC Power Flows, Generalized OPF Costs and their Derivatives using Complex Matrix Notation*, 2010.

[93] J. Chow, ed., *Time-Scale Modeling of Dynamic Networks with Applications to Power Systems*, vol. 46. Springer, Berlin, Heidelberg, 1982.

[94] G. Bills et.al., "On-Line Stability Analysis Study," tech. rep., Edison Electric Institute, October 1970.

[95] "*IEEE* Benchmarks." `https://www.pscad.com/knowledge-base/topic-51/v-`. Accessed: 2021-11-23.

[96] "Power Systems Test Case Archive." `http://labs.ece.uw.edu/pstca/`. Accessed: 2021-11-23.

[97] R. D. Zimmerman and C. E. Murillo-Sánchez, MATPOWER *(Version 7.1)*, Oct 2020.

[98] M. E. Baran and F. F. Wu, "Network Reconfiguration in Distribution Systems for Loss Reduction and Load Balancing," *IEEE Transactions on Power Delivery*, vol. 4, pp. 1401–1407, April 1989.

[99] J. S. Savier and D. Das, "Impact of Network Reconfiguration on Loss Allocation of Radial Distribution Systems," *IEEE Transactions on Power Delivery*, vol. 22, no. 4, pp. 2473–2480, 2007.

[100] P. M. Subcommittee, "IEEE Reliability Test System," *IEEE Transactions on Power Apparatus and Systems*, vol. PAS-98, no. 6, pp. 2047–2054, 1979.

[101] Y. Ijiri, "Cost-Flow Networks and Generalized Inverses," in *Extremal Methods and Systems Analysis* (A. V. Fiacco and K. O. Kortanek, eds.), pp. 187–196, Springer Berlin Heidelberg, 1980.

[102] A. Ben-Israel, "The Moore of the Moore-Penrose Inverse," *ELA. The Electronic Journal of Linear Algebra [electronic only]*, vol. 9, 08 2002.

[103] A. Ben-Israel, "Generalized inverses of matrices and their applications," in *Extremal Methods and Systems Analysis* (A. V. Fiacco and K. O. Kortanek, eds.), pp. 154–186, Springer Berlin Heidelberg, 1980.

[104] A. Ben-israel and T. N. E. Greville, *Generalized Inverses: Theory and Applications*. CMS Books in Mathematics, Springer, New York, NY, 2003.

[105] Y. Ijiri, "On the Generalized Inverse of an Incidence Matrix," *Journal of the Society for Industrial and Applied Mathematics*, vol. 13, no. 3, pp. 827–836, 1965.

[106] C. R. Rao and S. K. Mitra, "Generalized Inverse of A Matrix and Its Applications." Proc. 6th Berkeley Sympos. math. Statist. Probab., Univ. Calif. 1970, 1, 601-620 (1972)., 1972.

[107] K. W. Chan, "Parallel Algorithms for Direct Solution of Large Sparse Power System Matrix Equations," *IEE Proceedings - Generation, Transmission and Distribution*, vol. 148, no. 6, pp. 615–622, 2001.

[108] J. Beerten and R. Belmans, "Development of an Open Source Power Flow Software For High Voltage Direct Current Grids and Hybrid AC/DC Systems: MATACDC," *IET Generation, Transmission & Distribution*, vol. 9, no. 10, pp. 966–974, 2015.

[109] J. Beerten and R. Belmans, "MatACDC - An Open Source Software Tool for Steady-state Analysis and Operation of HVDC Grids," in *11th IET International Conference on AC and DC Power Transmission*, pp. 1–9, Feb 2015.

[110] G. W. Stagg and A. H. El-Abiad, *Computer Methods in Power System Analysis*. McGraw-Hill New York, 1968.

[111] T. Vrana, S. Dennetiere, Y. Yang, J. Jardini, D. Jovcic, and H. Saad, "The CIGRÉ B4 DC Grid Test System," *CIGRE Electra*, vol. 270, 10 2013.

APPENDICES

Appendix A

Test Systems Data

A.1 4-Bus System

Table A.1: 4-bus test system bus data.

Bus	Type	$\|U\|$	Generation (P)	Demand (P)	Demand (Q)
1	Ref	1	-	50	30.99
2	PQ	-	-	170	105.35
3	PQ	-	-	200	123.94
4	PV	1.02	318	80	49.58

Table A.2: 4-bus test system branch data.

From	To	R	X	C	τ
1	2	0.01008	0.0504	0.1025	-
1	3	0.00744	0.0372	0.0775	-
2	4	0.00744	0.0372	0.0775	-
3	4	0.01272	0.0636	0.1275	-

A.2 WSCC 9-Bus System

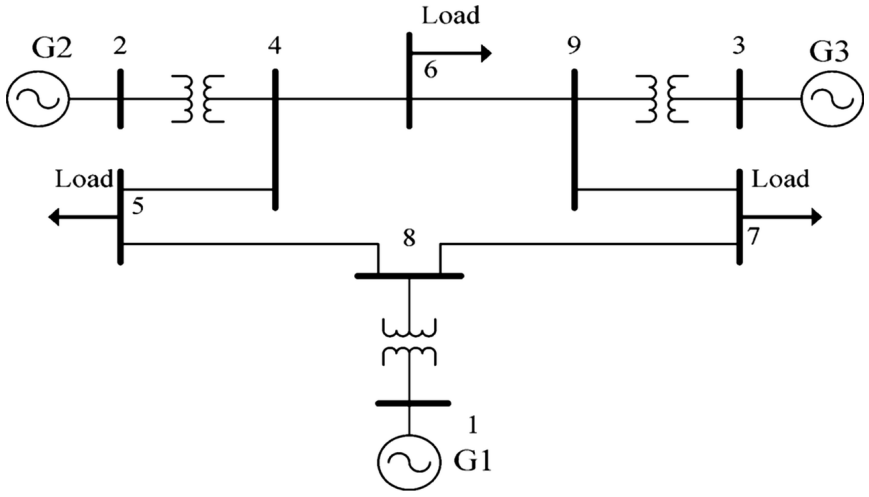

Figure A.1: WSCC 9-bus test system.

Table A.3: WSCC 9-bus test system bus data.

Bus	Type	$\|U\|$	Generation (P)	Demand (P)	Demand (Q)
1	Slack	1.040	-	-	-
2	PV	1.025	163	-	-
3	PV	1.025	85	-	-
4	PQ	-	-	-	-
5	PQ	-	-	90	30
6	PQ	-	-	-	-
7	PQ	-	-	100	35
8	PQ	-	-	-	-
9	PQ	-	-	125	50

Table A.4: WSCC 9-bus test system branch data.

From	To	R	X	C	τ
1	2	0.01008	0.0504	0.1025	-
1	3	0.00744	0.0372	0.0775	-
2	4	0.00744	0.0372	0.0775	-
3	4	0.01272	0.0636	0.1275	-
1	2	0.01008	0.0504	0.1025	-
1	3	0.00744	0.0372	0.0775	-
2	4	0.00744	0.0372	0.0775	-
3	4	0.01272	0.0636	0.1275	-
1	2	0.01008	0.0504	0.1025	-
1	3	0.00744	0.0372	0.0775	-
2	4	0.00744	0.0372	0.0775	-
3	4	0.01272	0.0636	0.1275	-

A.3 IEEE 14-Bus System

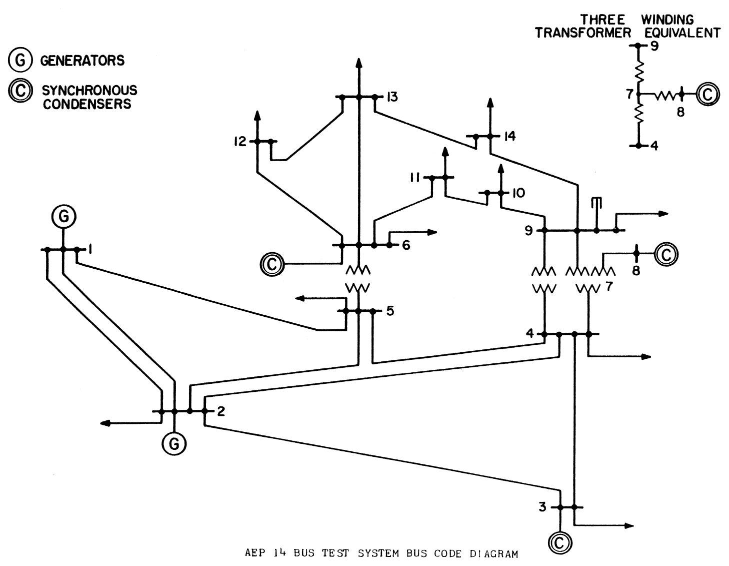

Figure A.2: IEEE 14-bus test system.

Table A.5: IEEE 14-bus test system bus data.

Bus	Type	$\|U\|$	Generation (P)	Demand (P)	Demand (Q)
1	Slack	1.060	-	-	-
2	PV	1.045	42.4	21.7	12.7
3	PV	1.010	23.4	94.2	19
4	PQ	-	-	47.8	-3.9
5	PQ	-	-	7.6	1.6
6	PV	1.070	12.2	11.2	7.5
7	PQ	-	-	-	-
8	PV	1.090	17.4	-	-
9	PQ	-	-	29.5	16.6
10	PQ	-	-	9	5.8
11	PQ	-	-	3.5	1.8
12	PQ	-	-	6.1	1.6
13	PQ	-	-	13.5	5.8
14	PQ	-	-	14.9	5

A.4 IEEE 30-Bus System

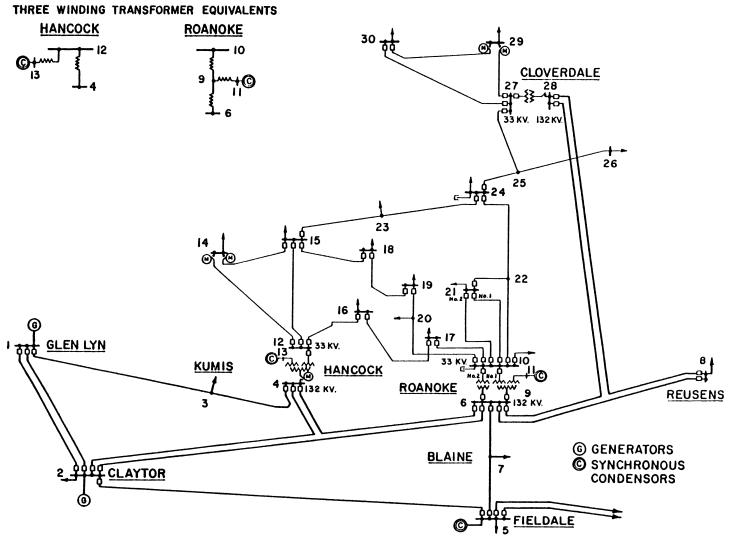

Figure A.3: IEEE 30-bus test system.

Table A.6: IEEE 14-bus test system branch data.

From	To	R	X	C	τ
1	2	0.01938	0.05917	0.0528	-
1	5	0.05403	0.22304	0.0492	-
2	3	0.04699	0.19797	0.0438	-
2	4	0.05811	0.17632	0.034	-
2	5	0.05695	0.17388	0.0346	-
3	4	0.06701	0.17103	0.0128	-
4	5	0.01335	0.04211	0	-
4	7	0	0.20912	0	0.978
4	9	0	0.55618	0	0.969
5	6	0	0.25202	0	0.932
6	11	0.09498	0.1989	0	-
6	12	0.12291	0.25581	0	-
6	13	0.06615	0.13027	0	-
7	8	0	0.17615	0	-
7	9	0	0.11001	0	-
9	10	0.03181	0.0845	0	-
9	14	0.12711	0.27038	0	-
10	11	0.08205	0.19207	0	-
12	13	0.22092	0.19988	0	-
13	14	0.17093	0.34802	0	-

Table A.7: IEEE 30-bus test system bus data.

Bus	Type	$\|U\|$	Generation (P)	Demand (P)	Demand (Q)
1	Slack	1	-	-	-
2	PV	1	60.97	21.7	12.7
3	PQ	1	-	2.4	1.2
4	PQ	-	-	7.6	1.6
5	PQ	-	-	0	0
6	PQ	-	-	0	0
7	PQ	-	-	22.8	10.9
8	PQ	-	-	30	30
9	PQ	-	-	0	0
10	PQ	-	-	5.8	2
11	PQ	-	-	0	0
12	PQ	-	-	11.2	7.5
13	PV	1	21.59	0	0

Bus	Type	$\|U\|$	Generation (P)	Demand (P)	Demand (Q)
14	PQ	-	-	6.2	1.6
15	PQ	-	-	8.2	2.5
16	PQ	-	-	3.5	1.8
17	PQ	-	-	9	5.8
18	PQ	-	-	3.2	0.9
19	PQ	-	-	9.5	3.4
20	PQ	-	-	2.2	0.7
21	PQ	-	-	17.5	11.2
22	PV	1	26.91	0	0
23	PV	1	19.20	3.2	1.6
24	PQ	-	-	8.7	6.7
25	PQ	-	-	0	0
26	PQ	-	-	3.5	2.3
27	PV	1	37	0	0
28	PQ	-	-	0	0
29	PQ	-	-	2.4	0.9
30	PQ	-	-	10.6	1.9

Table A.8: IEEE 30-bus test system branch data.

From	To	R	X	C	τ
1	2	0.02	0.06	0.03	-
1	3	0.05	0.19	0.02	-
2	4	0.06	0.17	0.02	-
3	4	0.01	0.04	0	-
2	5	0.05	0.2	0.02	-
2	6	0.06	0.18	0.02	-
4	6	0.01	0.04	0	-
5	7	0.05	0.12	0.01	-
6	7	0.03	0.08	0.01	-
6	8	0.01	0.04	0	-
6	9	0	0.21	0	-
6	10	0	0.56	0	-
9	11	0	0.21	0	-
9	10	0	0.11	0	-
4	12	0	0.26	0	-

From	To	R	X	C	τ
12	13	0	0.14	0	-
12	14	0.12	0.26	0	-
12	15	0.07	0.13	0	-
12	16	0.09	0.2	0	-
14	15	0.22	0.2	0	-
16	17	0.08	0.19	0	-
15	18	0.11	0.22	0	-
18	19	0.06	0.13	0	-
19	20	0.03	0.07	0	-
10	20	0.09	0.21	0	-
10	17	0.03	0.08	0	-
10	21	0.03	0.07	0	-
10	22	0.07	0.15	0	-
21	22	0.01	0.02	0	-
15	23	0.1	0.2	0	-
22	24	0.12	0.18	0	-
23	24	0.13	0.27	0	-
24	25	0.19	0.33	0	-
25	26	0.25	0.38	0	-
25	27	0.11	0.21	0	-
28	27	0	0.4	0	-
27	29	0.22	0.42	0	-
27	30	0.32	0.6	0	-
29	30	0.24	0.45	0	-
8	28	0.06	0.2	0.02	-
6	28	0.02	0.06	0.01	-

A.5 IEEE 118-Bus System

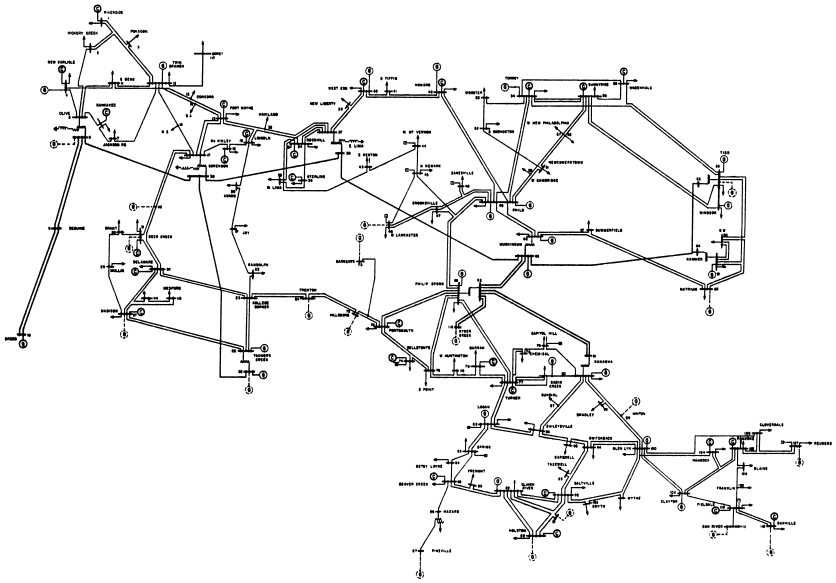

Figure A.4: IEEE 118-bus test system

Table A.9: IEEE 118-bus test system bus data.

Bus	Type	$\|U\|$	Generation (P)	Demand (P)	Demand (Q)
1	PV	0.955	-	51	27
2	PQ	-	-	20	9
3	PQ	-	-	39	10
4	PV	0.998	-	39	12
5	PQ	-	-	0	0
6	PV	0.99	-	52	22
7	PQ	-	-	19	2
8	PV	1.015	-	28	0
9	PQ	-	-	0	0
10	PV	1.05	450	0	0
11	PQ	-	-	70	23
12	PV	0.99	85	47	10
13	PQ	-	-	34	16
14	PQ	-	-	14	1

Bus	Type	$\|U\|$	Generation (P)	Demand (P)	Demand (Q)
15	PV	0.97	-	90	30
16	PQ	-	-	25	10
17	PQ	-	-	11	3
18	PV	0.973	-	60	34
19	PV	0.962	-	45	25
20	PQ	-	-	18	3
21	PQ	-	-	14	8
22	PQ	-	-	10	5
23	PQ	-	-	7	3
24	PV	0.992	-	13	0
25	PV	1.05	220	0	0
26	PV	1.015	314	0	0
27	PV	0.968	-	71	13
28	PQ	-	-	17	7
29	PQ	-	-	24	4
30	PQ	-	-	0	0
31	PV	0.967	7	43	27
32	PV	0.963	-	59	23
33	PQ	-	-	23	9
34	PV	0.984	-	59	26
35	PQ	-	-	33	9
36	PV	0.98	-	31	17
37	PQ	-	-	0	0
38	PQ	-	-	0	0
39	PQ	-	-	27	11
40	PV	0.97	-	66	23
41	PQ	-	-	37	10
42	PV	0.985	-	96	23
43	PQ	-	-	18	7
44	PQ	-	-	16	8
45	PQ	-	-	53	22
46	PV	1.005	19	28	10
47	PQ	-	-	34	0
48	PQ	-	-	20	11
49	PV	1.025	204	87	30
50	PQ	-	-	17	4
51	PQ	-	-	17	8
52	PQ	-	-	18	5
53	PQ	-	-	23	11

Bus	Type	$\|U\|$	Generation (P)	Demand (P)	Demand (Q)
54	PV	0.955	48	113	32
55	PV	0.952	-	63	22
56	PV	0.954	-	84	18
57	PQ	-	-	12	3
58	PQ	-	-	12	3
59	PV	0.985	155	277	113
60	PQ	-	-	78	3
61	PV	0.995	160	0	0
62	PV	0.998	-	77	14
63	PQ	-	-	0	0
64	PQ	-	-	0	0
65	PV	1.005	-	0	0
66	PV	1.05	392	39	18
67	PQ	-	-	28	7
68	PQ	-	-	0	0
69	Slack	1.035	-	0	0
70	PV	0.984	-	66	20
71	PQ	-	-	0	0
72	PV	0.98	-	12	0
73	PV	0.991	-	6	0
74	PV	0.958	-	68	27
75	PQ	-	-	47	11
76	PV	0.943	-	68	36
77	PV	1.006	-	61	28
78	PQ	-	-	71	26
79	PQ	-	-	39	32
80	PV	1.04	477	130	26
81	PQ	-	-	0	0
82	PQ	-	-	54	27
83	PQ	-	-	20	10
84	PQ	-	-	11	7
85	PV	0.985	-	24	15
86	PQ	-	-	21	10
87	PV	1.015	4	0	0
88	PQ	-	-	48	10
89	PV	1.005	607	0	0
90	PV	0.985	-	163	42
91	PV	0.98	-	10	0
92	PV	0.99	-	65	10

Bus	Type	$\|U\|$	Generation (P)	Demand (P)	Demand (Q)
93	PQ	-	-	12	7
94	PQ	-	-	30	16
95	PQ	-	-	42	31
96	PQ	-	-	38	15
97	PQ	-	-	15	9
98	PQ	-	-	34	8
99	PV	1.01	-	42	0
100	PV	1.017	252	37	18
101	PQ	-	-	22	15
102	PQ	-	-	5	3
103	PV	1.01	40	23	16
104	PV	0.971	-	38	25
105	PV	0.965	-	31	26
106	PQ	-	-	43	16
107	PV	0.952	-	50	12
108	PQ	-	-	2	1
109	PQ	-	-	8	3
110	PV	0.973	-	39	30
111	PV	0.98	36	0	0
112	PV	0.975	-	68	13
113	PV	0.993	-	6	0
114	PQ	-	-	8	3
115	PQ	-	-	22	7
116	PV	1.005	-	184	0
117	PQ	-	-	20	8
118	PQ	-	-	33	15

Table A.10: IEEE 118-bus test system branch data.

From	To	R	X	C	τ
1	2	0.0303	0.0999	0.0254	0
1	3	0.0129	0.0424	0.01082	0
4	5	0.00176	0.00798	0.0021	0
3	5	0.0241	0.108	0.0284	0
5	6	0.0119	0.054	0.01426	0
6	7	0.00459	0.0208	0.0055	0

From	To	R	X	C	τ
8	9	0.00244	0.0305	1.162	0
8	5	0	0.0267	0	0.985
9	10	0.00258	0.0322	1.23	0
4	11	0.0209	0.0688	0.01748	0
5	11	0.0203	0.0682	0.01738	0
11	12	0.00595	0.0196	0.00502	0
2	12	0.0187	0.0616	0.01572	0
3	12	0.0484	0.16	0.0406	0
7	12	0.00862	0.034	0.00874	0
11	13	0.02225	0.0731	0.01876	0
12	14	0.0215	0.0707	0.01816	0
13	15	0.0744	0.2444	0.06268	0
14	15	0.0595	0.195	0.0502	0
12	16	0.0212	0.0834	0.0214	0
15	17	0.0132	0.0437	0.0444	0
16	17	0.0454	0.1801	0.0466	0
17	18	0.0123	0.0505	0.01298	0
18	19	0.01119	0.0493	0.01142	0
19	20	0.0252	0.117	0.0298	0
15	19	0.012	0.0394	0.0101	0
20	21	0.0183	0.0849	0.0216	0
21	22	0.0209	0.097	0.0246	0
22	23	0.0342	0.159	0.0404	0
23	24	0.0135	0.0492	0.0498	0
23	25	0.0156	0.08	0.0864	0
26	25	0	0.0382	0	0.96
25	27	0.0318	0.163	0.1764	0
27	28	0.01913	0.0855	0.0216	0
28	29	0.0237	0.0943	0.0238	0
30	17	0	0.0388	0	0.96
8	30	0.00431	0.0504	0.514	0
26	30	0.00799	0.086	0.908	0
17	31	0.0474	0.1563	0.0399	0
29	31	0.0108	0.0331	0.0083	0
23	32	0.0317	0.1153	0.1173	0
31	32	0.0298	0.0985	0.0251	0
27	32	0.0229	0.0755	0.01926	0
15	33	0.038	0.1244	0.03194	0
19	34	0.0752	0.247	0.0632	0

From	To	R	X	C	τ
35	36	0.00224	0.0102	0.00268	0
35	37	0.011	0.0497	0.01318	0
33	37	0.0415	0.142	0.0366	0
34	36	0.00871	0.0268	0.00568	0
34	37	0.00256	0.0094	0.00984	0
38	37	0	0.0375	0	0.935
37	39	0.0321	0.106	0.027	0
37	40	0.0593	0.168	0.042	0
30	38	0.00464	0.054	0.422	0
39	40	0.0184	0.0605	0.01552	0
40	41	0.0145	0.0487	0.01222	0
40	42	0.0555	0.183	0.0466	0
41	42	0.041	0.135	0.0344	0
43	44	0.0608	0.2454	0.06068	0
34	43	0.0413	0.1681	0.04226	0
44	45	0.0224	0.0901	0.0224	0
45	46	0.04	0.1356	0.0332	0
46	47	0.038	0.127	0.0316	0
46	48	0.0601	0.189	0.0472	0
47	49	0.0191	0.0625	0.01604	0
42	49	0.0715	0.323	0.086	0
42	49	0.0715	0.323	0.086	0
45	49	0.0684	0.186	0.0444	0
48	49	0.0179	0.0505	0.01258	0
49	50	0.0267	0.0752	0.01874	0
49	51	0.0486	0.137	0.0342	0
51	52	0.0203	0.0588	0.01396	0
52	53	0.0405	0.1635	0.04058	0
53	54	0.0263	0.122	0.031	0
49	54	0.073	0.289	0.0738	0
49	54	0.0869	0.291	0.073	0
54	55	0.0169	0.0707	0.0202	0
54	56	0.00275	0.00955	0.00732	0
55	56	0.00488	0.0151	0.00374	0
56	57	0.0343	0.0966	0.0242	0
50	57	0.0474	0.134	0.0332	0
56	58	0.0343	0.0966	0.0242	0
51	58	0.0255	0.0719	0.01788	0
54	59	0.0503	0.2293	0.0598	0

From	To	R	X	C	τ
56	59	0.0825	0.251	0.0569	0
56	59	0.0803	0.239	0.0536	0
55	59	0.04739	0.2158	0.05646	0
59	60	0.0317	0.145	0.0376	0
59	61	0.0328	0.15	0.0388	0
60	61	0.00264	0.0135	0.01456	0
60	62	0.0123	0.0561	0.01468	0
61	62	0.00824	0.0376	0.0098	0
63	59	0	0.0386	0	0.96
63	64	0.00172	0.02	0.216	0
64	61	0	0.0268	0	0.985
38	65	0.00901	0.0986	1.046	0
64	65	0.00269	0.0302	0.38	0
49	66	0.018	0.0919	0.0248	0
49	66	0.018	0.0919	0.0248	0
62	66	0.0482	0.218	0.0578	0
62	67	0.0258	0.117	0.031	0
65	66	0	0.037	0	0.935
66	67	0.0224	0.1015	0.02682	0
65	68	0.00138	0.016	0.638	0
47	69	0.0844	0.2778	0.07092	0
49	69	0.0985	0.324	0.0828	0
68	69	0	0.037	0	0.935
69	70	0.03	0.127	0.122	0
24	70	0.00221	0.4115	0.10198	0
70	71	0.00882	0.0355	0.00878	0
24	72	0.0488	0.196	0.0488	0
71	72	0.0446	0.18	0.04444	0
71	73	0.00866	0.0454	0.01178	0
70	74	0.0401	0.1323	0.03368	0
70	75	0.0428	0.141	0.036	0
69	75	0.0405	0.122	0.124	0
74	75	0.0123	0.0406	0.01034	0
76	77	0.0444	0.148	0.0368	0
69	77	0.0309	0.101	0.1038	0
75	77	0.0601	0.1999	0.04978	0
77	78	0.00376	0.0124	0.01264	0
78	79	0.00546	0.0244	0.00648	0
77	80	0.017	0.0485	0.0472	0

From	To	R	X	C	τ
77	80	0.0294	0.105	0.0228	0
79	80	0.0156	0.0704	0.0187	0
68	81	0.00175	0.0202	0.808	0
81	80	0	0.037	0	0.935
77	82	0.0298	0.0853	0.08174	0
82	83	0.0112	0.03665	0.03796	0
83	84	0.0625	0.132	0.0258	0
83	85	0.043	0.148	0.0348	0
84	85	0.0302	0.0641	0.01234	0
85	86	0.035	0.123	0.0276	0
86	87	0.02828	0.2074	0.0445	0
85	88	0.02	0.102	0.0276	0
85	89	0.0239	0.173	0.047	0
88	89	0.0139	0.0712	0.01934	0
89	90	0.0518	0.188	0.0528	0
89	90	0.0238	0.0997	0.106	0
90	91	0.0254	0.0836	0.0214	0
89	92	0.0099	0.0505	0.0548	0
89	92	0.0393	0.1581	0.0414	0
91	92	0.0387	0.1272	0.03268	0
92	93	0.0258	0.0848	0.0218	0
92	94	0.0481	0.158	0.0406	0
93	94	0.0223	0.0732	0.01876	0
94	95	0.0132	0.0434	0.0111	0
80	96	0.0356	0.182	0.0494	0
82	96	0.0162	0.053	0.0544	0
94	96	0.0269	0.0869	0.023	0
80	97	0.0183	0.0934	0.0254	0
80	98	0.0238	0.108	0.0286	0
80	99	0.0454	0.206	0.0546	0
92	100	0.0648	0.295	0.0472	0
94	100	0.0178	0.058	0.0604	0
95	96	0.0171	0.0547	0.01474	0
96	97	0.0173	0.0885	0.024	0
98	100	0.0397	0.179	0.0476	0
99	100	0.018	0.0813	0.0216	0
100	101	0.0277	0.1262	0.0328	0
92	102	0.0123	0.0559	0.01464	0
101	102	0.0246	0.112	0.0294	0

From	To	R	X	C	τ
100	103	0.016	0.0525	0.0536	0
100	104	0.0451	0.204	0.0541	0
103	104	0.0466	0.1584	0.0407	0
103	105	0.0535	0.1625	0.0408	0
100	106	0.0605	0.229	0.062	0
104	105	0.00994	0.0378	0.00986	0
105	106	0.014	0.0547	0.01434	0
105	107	0.053	0.183	0.0472	0
105	108	0.0261	0.0703	0.01844	0
106	107	0.053	0.183	0.0472	0
108	109	0.0105	0.0288	0.0076	0
103	110	0.03906	0.1813	0.0461	0
109	110	0.0278	0.0762	0.0202	0
110	111	0.022	0.0755	0.02	0
110	112	0.0247	0.064	0.062	0
17	113	0.00913	0.0301	0.00768	0
32	113	0.0615	0.203	0.0518	0
32	114	0.0135	0.0612	0.01628	0
27	115	0.0164	0.0741	0.01972	0
114	115	0.0023	0.0104	0.00276	0
68	116	0.00034	0.00405	0.164	0
12	117	0.0329	0.14	0.0358	0
75	118	0.0145	0.0481	0.01198	0
76	118	0.0164	0.0544	0.01356	0

A.6 69-Bus System

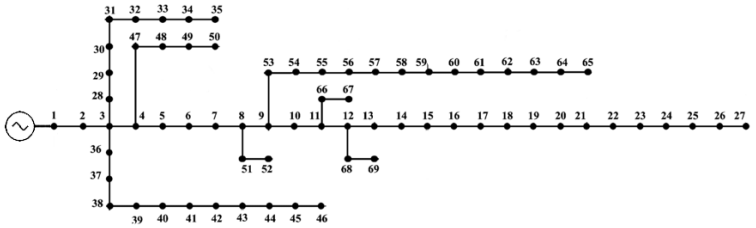

Figure A.5: 69-bus test system in radial topology.

Table A.11: 69-bus test system bus data.

Bus	Type	$\|U\|$	Generation (P)	Demand (P)	Demand (Q)
1	Slack	1	-	0	0
2	PQ	-	-	0	0
3	PQ	-	-	0	0
4	PQ	-	-	0	0
5	PQ	-	-	0	0
6	PQ	-	-	0.0026	0.0022
7	PQ	-	-	0.0404	0.03
8	PQ	-	-	0.075	0.054
9	PQ	-	-	0.03	0.022
10	PQ	-	-	0.028	0.019
11	PQ	-	-	0.145	0.104
12	PQ	-	-	0.145	0.104
13	PQ	-	-	0.008	0.0055
14	PQ	-	-	0.008	0.0055
15	PQ	-	-	0	0
16	PQ	-	-	0.0455	0.03
17	PQ	-	-	0.06	0.035
18	PQ	-	-	0.06	0.035
19	PQ	-	-	0	0
20	PQ	-	-	0.001	0.0006
21	PQ	-	-	0.114	0.081

Bus	Type	$\|U\|$	Generation (P)	Demand (P)	Demand (Q)
22	PQ	-	-	0.0053	0.0035
23	PQ	-	-	0	0
24	PQ	-	-	0.028	0.02
25	PQ	-	-	0	0
26	PQ	-	-	0.014	0.01
27	PQ	-	-	0.014	0.01
28	PQ	-	-	0.026	0.0186
29	PQ	-	-	0.026	0.0186
30	PQ	-	-	0	0
31	PQ	-	-	0	0
32	PQ	-	-	0	0
33	PQ	-	-	0.014	0.01
34	PQ	-	-	0.0195	0.014
35	PQ	-	-	0.006	0.004
36	PQ	-	-	0.026	0.0186
37	PQ	-	-	0.026	0.0186
38	PQ	-	-	0	0
39	PQ	-	-	0.024	0.017
40	PQ	-	-	0.024	0.017
41	PQ	-	-	0.0012	0.001
42	PQ	-	-	0	0
43	PQ	-	-	0.006	0.0043
44	PQ	-	-	0	0
45	PQ	-	-	0.0392	0.0263
46	PQ	-	-	0.0392	0.0263
47	PQ	-	-	0	0
48	PQ	-	-	0.079	0.0564
49	PQ	-	-	0.3847	0.2745
50	PQ	-	-	0.3847	0.2745
51	PQ	-	-	0.0405	0.0283
52	PQ	-	-	0.0036	0.0027
53	PQ	-	-	0.0043	0.0035
54	PQ	-	-	0.0264	0.019
55	PQ	-	-	0.024	0.0172
56	PQ	-	-	0	0
57	PQ	-	-	0	0
58	PQ	-	-	0	0
59	PQ	-	-	0.1	0.072
60	PQ	-	-	0	0

Bus	Type	$\|U\|$	Generation (P)	Demand (P)	Demand (Q)
61	PQ	-	-	1.244	0.888
62	PQ	-	-	0.032	0.023
63	PQ	-	-	0	0
64	PQ	-	-	0.227	0.162
65	PQ	-	-	0.059	0.042
66	PQ	-	-	0.018	0.013
67	PQ	-	-	0.018	0.013
68	PQ	-	-	0.028	0.02
69	PQ	-	-	0.028	0.02

Table A.12: 69-bus test system branch data.

From	To	R	X	C	τ
1	2	3.12e-05	7.487e-05	0	0
2	3	3.12e-05	7.487e-05	0	0
3	4	9.359e-05	0.00022461	0	0
4	5	0.00156605	0.00183434	0	0
5	6	0.0228357	0.01163	0	0
6	7	0.0237778	0.0121104	0	0
7	8	0.00575259	0.00293245	0	0
8	9	0.00307595	0.00156605	0	0
9	10	0.0510995	0.0168897	0	0
10	11	0.0116799	0.0038621	0	0
11	12	0.0443861	0.0146685	0	0
12	13	0.0642643	0.0212135	0	0
13	14	0.0651378	0.0215254	0	0
14	15	0.0660113	0.0218124	0	0
15	16	0.0122664	0.00405551	0	0
16	17	0.0233598	0.0077242	0	0
17	18	0.00029324	9.983e-05	0	0
18	19	0.0204398	0.00675711	0	0
19	20	0.0131399	0.00434252	0	0
20	21	0.0213133	0.00704412	0	0
21	22	0.0008735	0.00028701	0	0
22	23	0.00992665	0.00328185	0	0
23	24	0.0216065	0.00714394	0	0

From	To	R	X	C	τ
24	25	0.0467195	0.0154421	0	0
25	26	0.019273	0.00637028	0	0
26	27	0.0108064	0.00356885	0	0
3	28	0.00027453	0.00067384	0	0
28	29	0.00399312	0.00976443	0	0
29	30	0.0248198	0.00820462	0	0
30	31	0.00437996	0.00144751	0	0
31	32	0.0218998	0.00723753	0	0
32	33	0.0523473	0.0175697	0	0
33	34	0.106566	0.0352268	0	0
34	35	0.0919666	0.0304039	0	0
3	36	0.00027453	0.00067384	0	0
36	37	0.00399312	0.00976443	0	0
37	38	0.00656993	0.00767428	0	0
38	39	0.00189673	0.00221493	0	0
39	40	0.00011231	0.00013102	0	0
40	41	0.0454405	0.0530898	0	0
41	42	0.0193417	0.0226048	0	0
42	43	0.00255809	0.00298236	0	0
43	44	0.00057401	0.00072375	0	0
44	45	0.00679455	0.00856649	0	0
45	46	5.615e-05	7.487e-05	0	0
4	47	0.00021213	0.0005241	0	0
47	48	0.0053096	0.0129964	0	0
48	49	0.0180813	0.0442425	0	0
49	50	0.00512867	0.0125471	0	0
8	51	0.00579003	0.00295117	0	0
51	52	0.0207081	0.00695053	0	0
9	53	0.0108563	0.00552798	0	0
53	54	0.0126657	0.00645139	0	0
54	55	0.017732	0.0090282	0	0
55	56	0.017551	0.00894085	0	0
56	57	0.0992041	0.0332989	0	0
57	58	0.048897	0.0164092	0	0
58	59	0.0189798	0.00627669	0	0
59	60	0.0240898	0.0073124	0	0
60	61	0.0316642	0.0161285	0	0
61	62	0.00607703	0.00309467	0	0
62	63	0.00904692	0.00460457	0	0

From	To	R	X	C	τ
63	64	0.0443299	0.0225799	0	0
64	65	0.0649506	0.0330805	0	0
11	66	0.0125534	0.00381218	0	0
66	67	0.00029324	8.735e-05	0	0
12	68	0.046133	0.0152487	0	0
68	69	0.00029324	9.983e-05	0	0

Table A.13: 69-bus test system laterals connections branch data.

From	To	R	X	C	τ
11	43	0.0311958	0.0311958	0	0
13	21	0.0311958	0.0311958	0	0
15	46	0.0623915	0.0311958	0	0
50	59	0.1247830	0.0623915	0	0
27	65	0.0623915	0.0311958	0	0

Table A.14: 69-bus system DGs parameters.

Bus	P	$\|U\|$	Q_{MAX}	Q_{MIN}
15	0.6	1.000	0.1	-0.05
27	0.4	0.970	0.1	-0.05
33	0.4	1.000	0.1	-0.05
43	0.4	1.000	0.1	-0.05
48	0.4	1.000	0.1	-0.05
62	0.4	0.960	0.1	-0.05

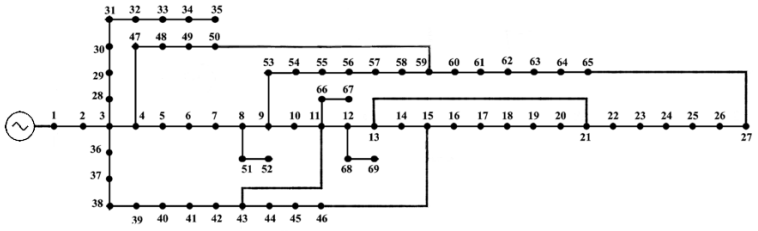

Figure A.6: 69-bus test system in meshed topology.

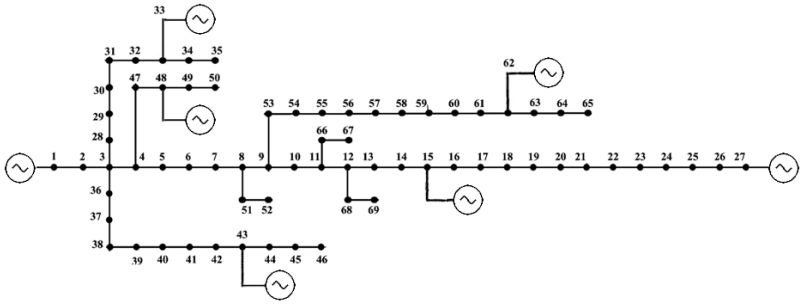

Figure A.7: 69-bus test system in radial topology with DGs.

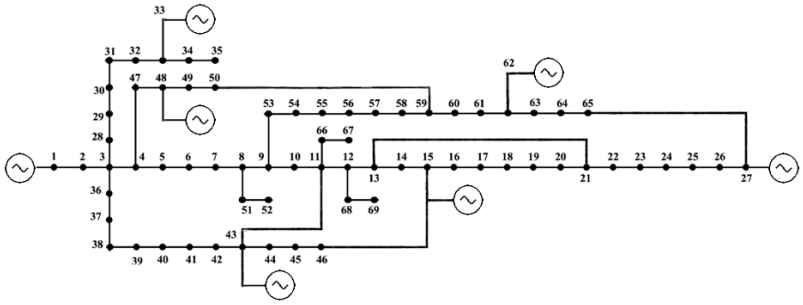

Figure A.8: 69-bus test system in meshed topology with DGs.

A.7 Hybrid 5-Bus System

Table A.15: Hybrid 5-bus test system bus data.

System	Bus		Generation		Demand	
	Number	Type	$\|U\|$	(P)	(P)	(Q)
AC	1	Slack	1.06	-	0	0
	2	PV	1.00	40	20	10
	3	PQ	-	-	45	15
	4	PQ	-	-	40	5
	5	PQ	-	-	60	10
DC	1	Slack	1.00	-	-	-
	2	P	-	-	-	-
	3	P	-	-	-	-

Table A.16: Hybrid 5-bus test system branch data.

System	Bus		Line Data		
	From	To	R	X	C
AC	1	2	0.02	0.06	0.06
	1	3	0.08	0.24	0.05
	2	3	0.06	0.18	0.04
	2	4	0.06	0.18	0.04
	2	5	0.04	0.12	0.03
	3	4	0.01	0.03	0.02
	4	5	0.08	0.24	0.05
DC	1	2	0.052	-	-
	2	3	0.052	-	-
	1	3	0.073	-	-

Table A.17: Hybrid 5-bus test system converter data.

Converter	Node		Control Mode		AC Power	Transformer		B_f	Phase Reactor	
	AC	DC	AC	DC		R_{tf}	X_{tf}		R_c	X_c
1	2	1	PQ	P	-(60,40)	0.0015	0.1121	0.0887	0.0001	0.16428
2	3	2	Slack	Slack	(0,0)	0.0015	0.1121	0.0887	0.0001	0.16428
3	5	3	PQ	P	(35,5)	0.0015	0.1121	0.0887	0.0001	0.16428

A.8 CIGRÉ B4 DC Hybrid System

Table A.18: CIGRÉ B4 DC system bus data.

System	Bus		Generation		Demand	
	Number	Type	$\|U\|$	(P)	(P)	(Q)
AC-1	Ba-A0	Slack	1.00	-	-	-
	Ba-A1	PQ	-	2000	1000	-
AC-2	Ba-B0	Slack	1.00	-	0	-
	Ba-B1	PQ	-	1000	2200	-
	Ba-B2	PQ	-	1000	2300	-
	Ba-B3	PQ	-	1000	1900	-
AC-3	Ba-C0	PQ	-	500	-	-
	Ba-C1	PQ	-	500	-	-
DCS-1	1	Slack	1.00	-	-	-
	2	P	-	-	-	-
DCS-1	1	Slack	1.00	-	-	-
	2	P	-	-	-	-
	3	P	-	-	-	-
	4	P	-	-	-	-
	5	P	-	-	-	-
DCS-1	1	Slack	1.00	-	-	-
	2	P	-	-	-	-
	3	P	-	-	-	-
	4	P	-	-	-	-
	5	P	-	-	-	-
	6	P	-	-	-	-
	7	P	-	-	-	-
	28	P	-	-	-	-

Table A.19: CIGRÉ B4 DC system branch data.

System	Bus		Line Data		
	From	To	R	X	C
AC-1	1	2	0.011080	0.14843	0.30606
AC-2	1	2	0.022161	0.29685	0.15303
	1	3	0.022161	0.29685	0.15303
	1	4	0.022161	0.29685	0.15303
	2	4	0.022161	0.29685	0.15303
	3	4	0.022161	0.29685	0.15303
AC-3	1	2	0.16038	0.15090	0.00757
DCS-1	1	2	0.038	-	-
DCS-2	1	2	0.038	-	-
	2	3	0.0266	-	-
	3	4	0.019	-	-
	4	5	0.038	-	-
DCS-3	1	2	0.012632	-	-
	1	4	0.031579	-	-
	2	4	0.012632	-	-
	3	4	0.0094737	-	-
	1	5	0.010526	-	-
	5	6	0.015789	-	-
	6	7	0.010526	-	-
	7	8	0.010526	-	-

Appendix B

Flow-Augmentation PF Systems Response

B.1 Application to Transmission Systems

B.1.1 WSCC-9 Bus Test System

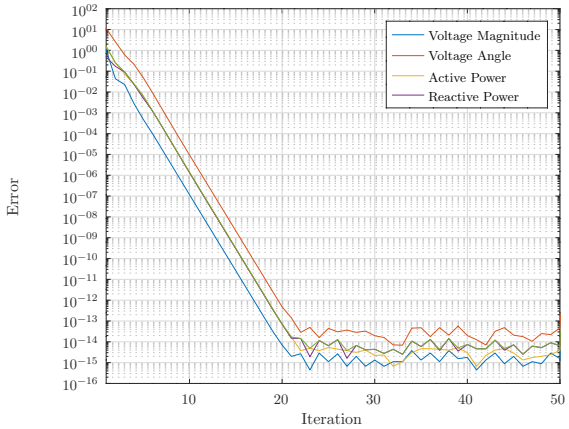

Figure B.1: Flow-Augmentation PF algorithm convergence error for WSCC 9-bus system.

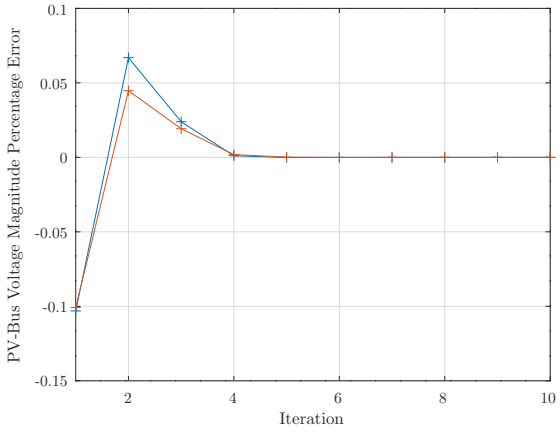

Figure B.2: Flow-Augmentation PF algorithm PV-Bus voltage magnitude error for WSCC 9-bus system.

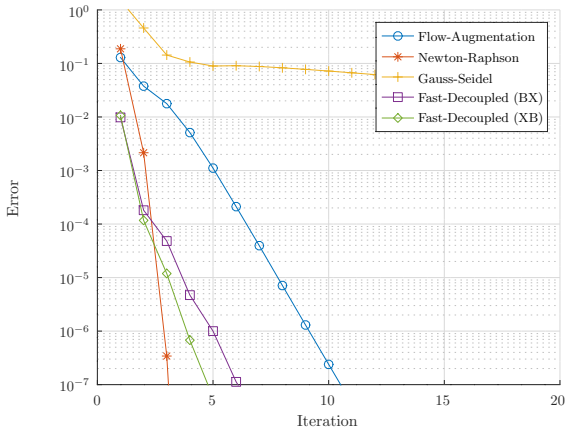

Figure B.3: Flow-Augmentation PF algorithm comparative error convergence WSCC 9-bus system.

B.1.2 IEEE-14 Bus Test System

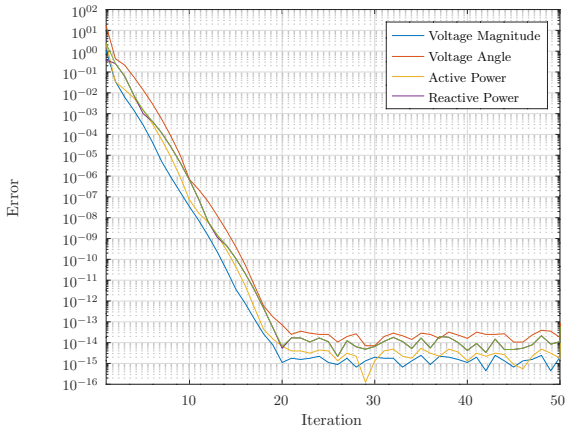

Figure B.4: Flow-Augmentation PF algorithm convergence error for IEEE 14-bus system.

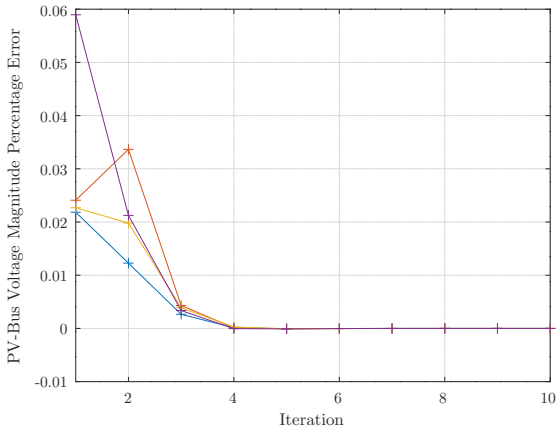

Figure B.5: Flow-Augmentation PF algorithm PV-Bus voltage magnitude error for IEEE 14-bus system.

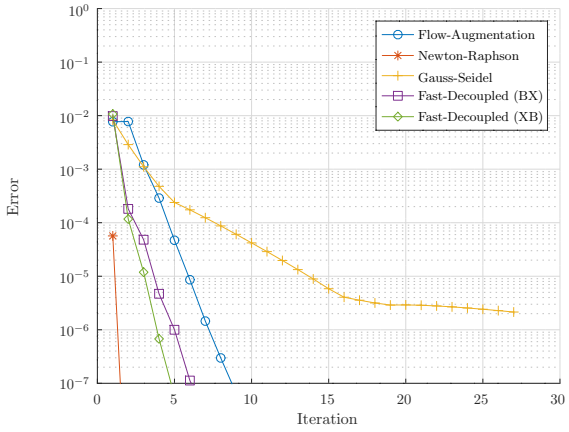

Figure B.6: Flow-Augmentation PF algorithm comparative error convergence for IEEE 14-bus system.

B.1.3 IEEE-30 Bus Test System

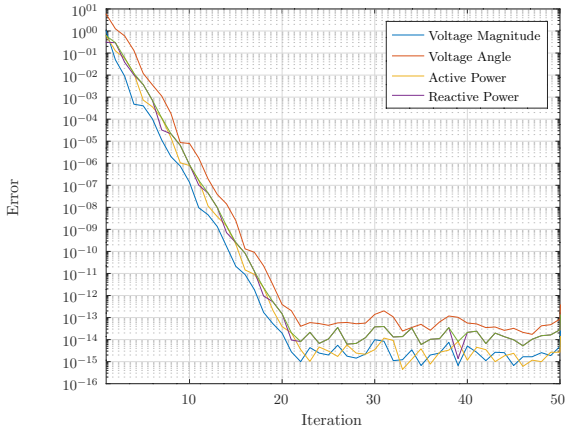

Figure B.7: Flow-Augmentation PF algorithm convergence error for IEEE 30-bus system.

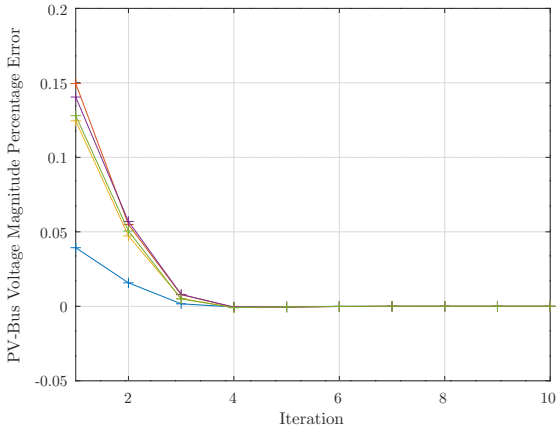

Figure B.8: Flow-Augmentation PF algorithm PV-Bus voltage magnitude error for IEEE 30-bus system.

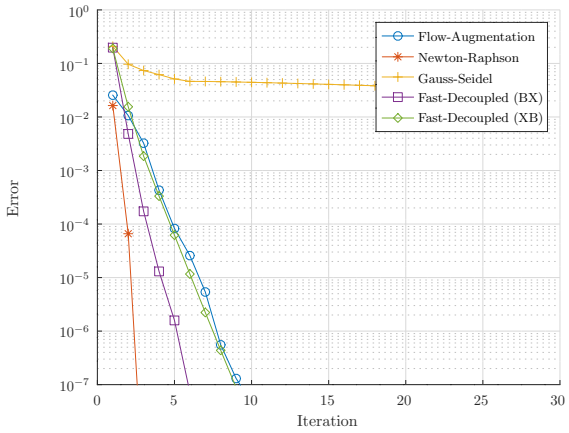

Figure B.9: Flow-Augmentation PF algorithm comparative error convergence for IEEE 30-bus system.

B.2 Application to Distribution Systems

B.2.1 Case-2 Meshed Configuration

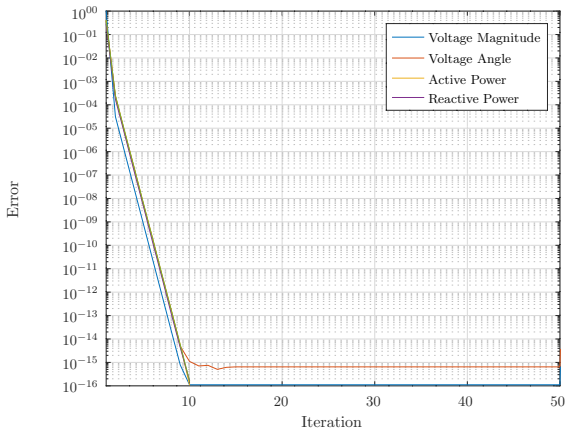

Figure B.10: Flow-Augmentation PF algorithm convergence error for 69-bus system in meshed topology.

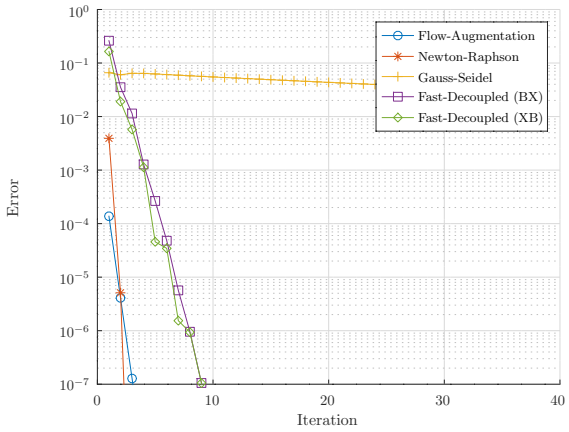

Figure B.11: Flow-Augmentation PF algorithm comparative error convergence for 69-bus system in meshed topology.

B.2.2 Case-3 Radial Configuration with DG

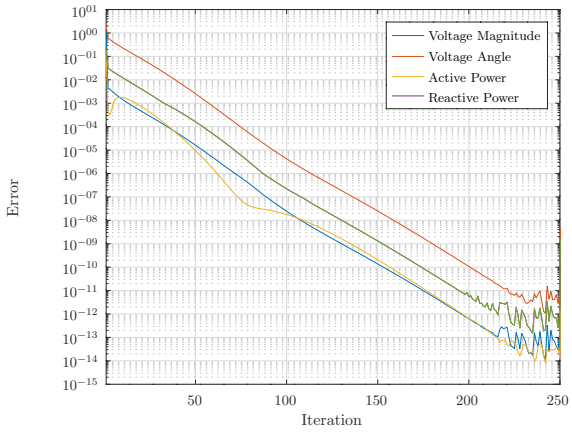

Figure B.12: Flow-Augmentation PF algorithm convergence error for 69-bus system in radial topology with DG.

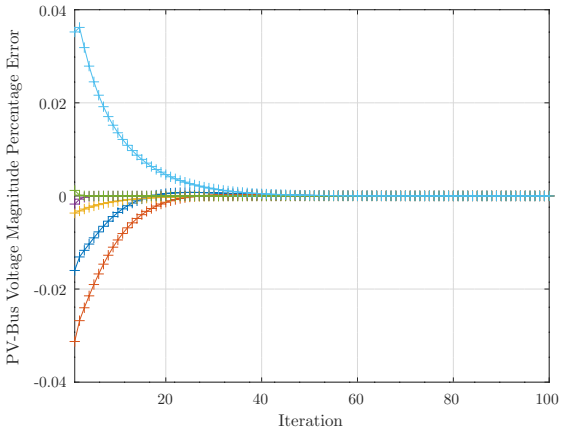

Figure B.13: Flow-Augmentation PF algorithm PV-bus voltage magnitude for 69-bus system in radial topology with DG.

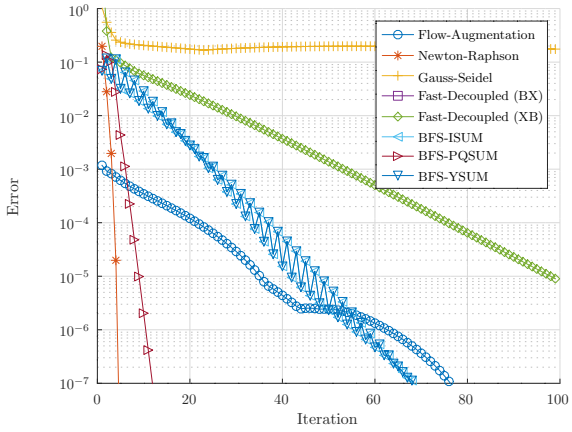

Figure B.14: Flow-Augmentation PF algorithm comparative error convergence for 69-bus system in radial topology with DG.

B.2.3 Case-4 Meshed Configuration with DG

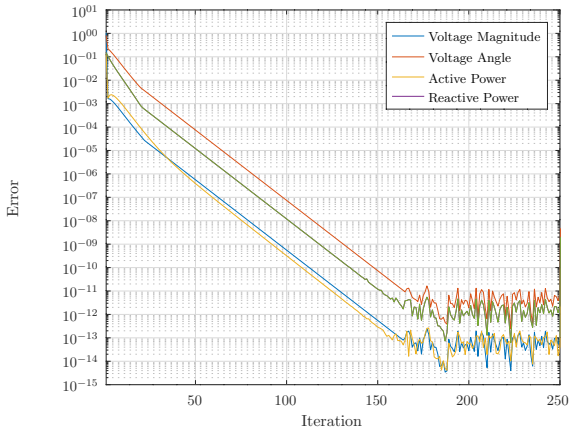

Figure B.15: Flow-Augmentation PF algorithm convergence error for 69-bus system in meshed topology with DG.

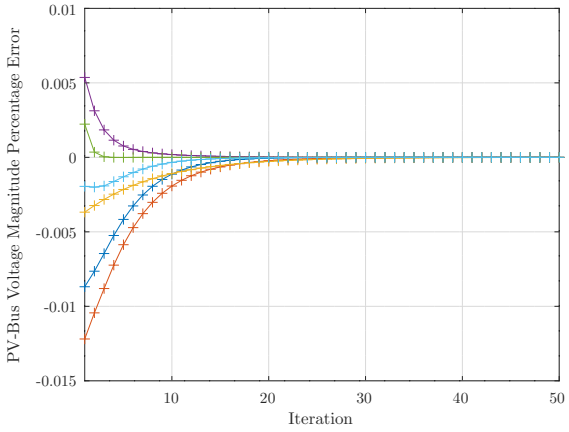

Figure B.16: Flow-Augmentation PF algorithm PV-bus voltage magnitude for 69-bus system in meshed topology with DG.

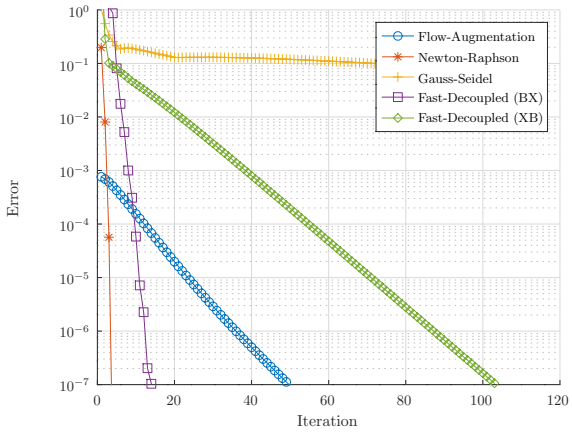

Figure B.17: Flow-Augmentation PF algorithm comparative error convergence for 69-bus system in meshed topology with DG.

Appendix C

MinLoss-Flow PF Systems Response

C.1 Application to Transmission Systems

C.1.1 WSCC-9 Bus Test System

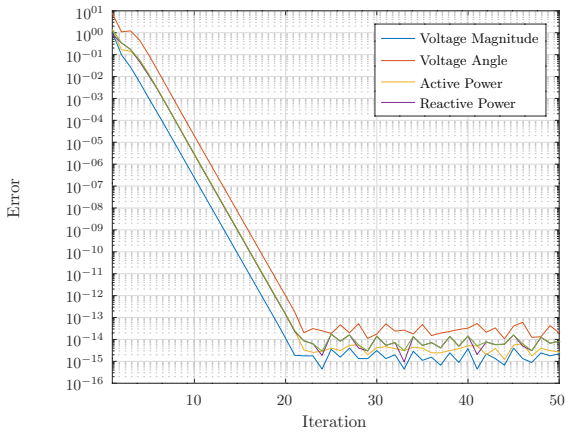

Figure C.1: MinLoss-Flow PF algorithm convergence error for WSCC 9-bus system.

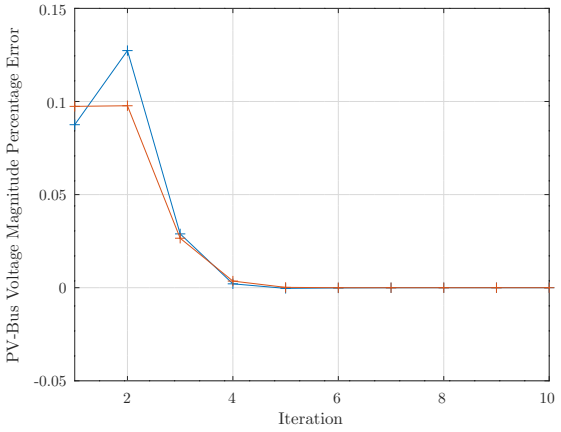

Figure C.2: MinLoss-Flow PF algorithm PV-Bus voltage magnitude error for WSCC 9-bus system.

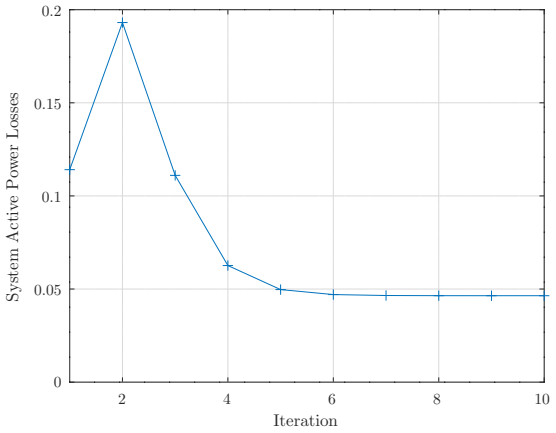

Figure C.3: MinLoss-Flow PF algorithm system losses for WSCC 9-bus system.

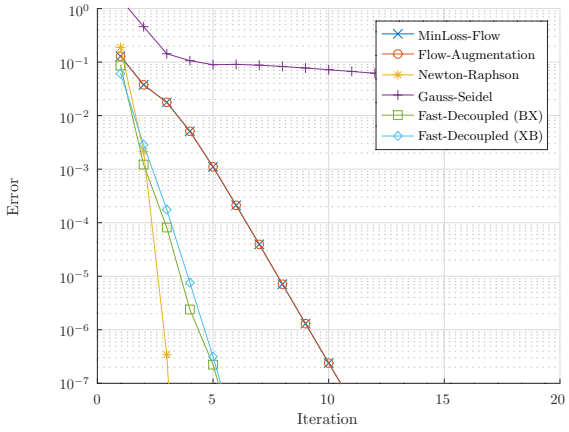

Figure C.4: MinLoss-Flow PF algorithm comparative error convergence for WSCC 9-bus system.

C.1.2 IEEE-14 Bus Test System

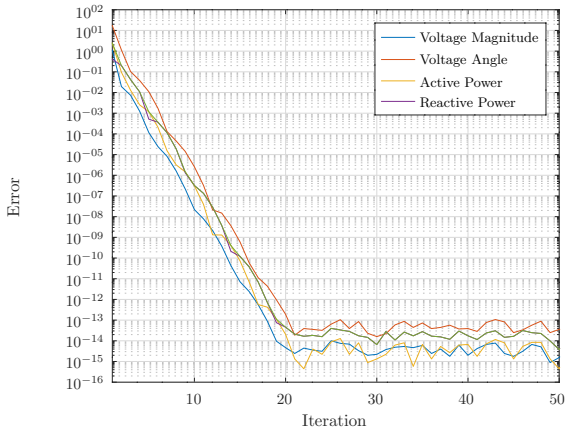

Figure C.5: MinLoss-Flow PF algorithm convergence error for IEEE 14-bus system.

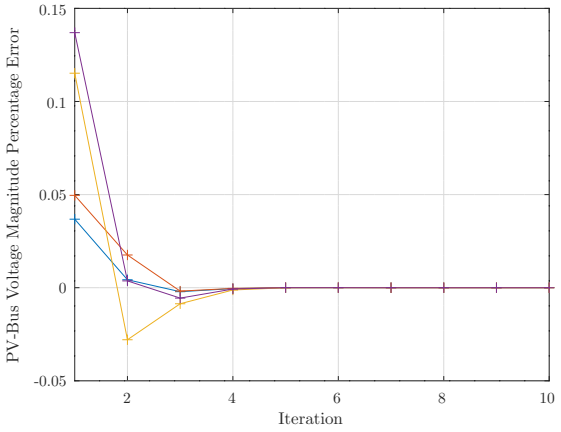

Figure C.6: MinLoss-Flow PF algorithm PV-Bus voltage magnitude error for IEEE 14-bus system.

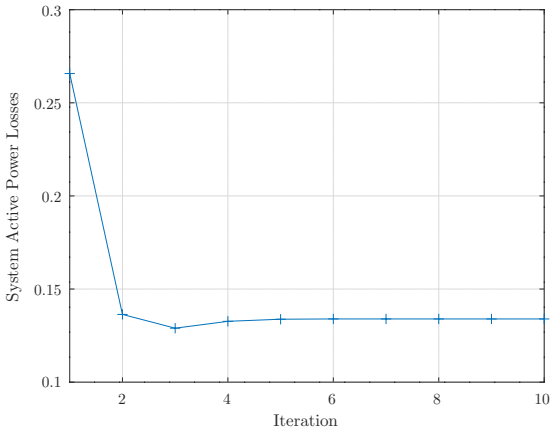

Figure C.7: MinLoss-Flow PF algorithm system losses for IEEE 14-bus system.

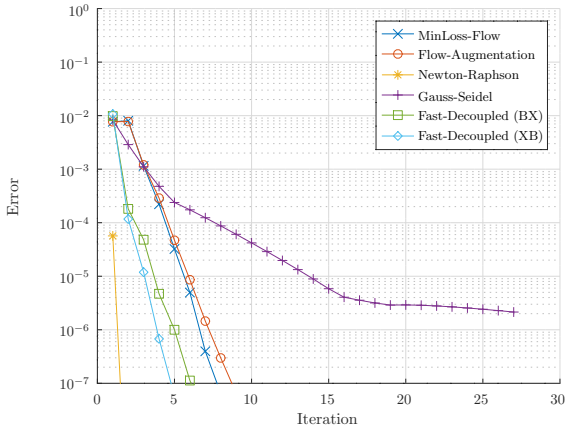

Figure C.8: MinLoss-Flow PF algorithm comparative error convergence for IEEE 14-bus system.

C.1.3 IEEE-30 Bus Test System

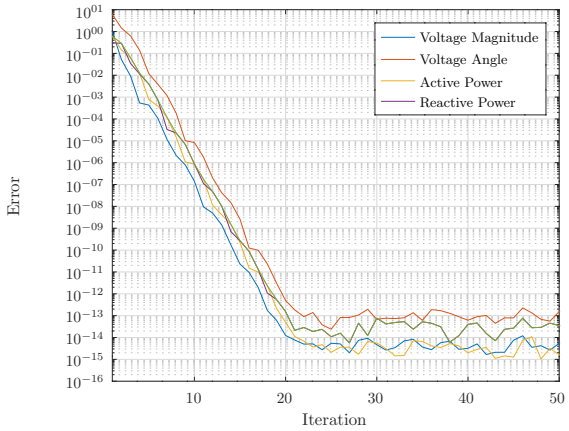

Figure C.9: MinLoss-Flow PF algorithm convergence error for IEEE 30-bus system.

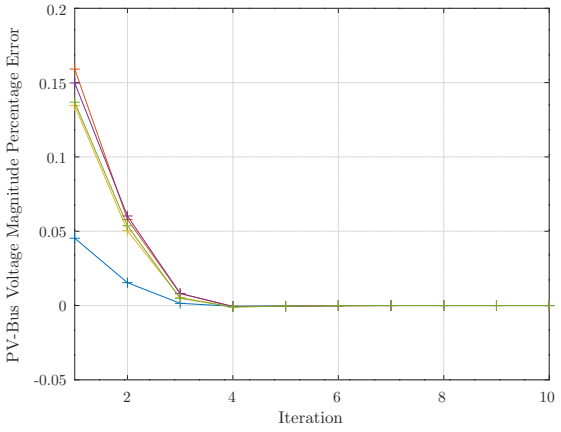

Figure C.10: MinLoss-Flow PF algorithm PV-Bus voltage magnitude error for IEEE 30-bus system.

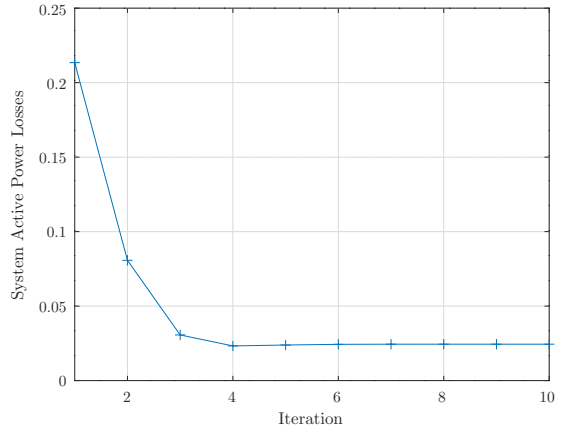

Figure C.11: MinLoss-Flow PF algorithm system losses for IEEE 30-bus system.

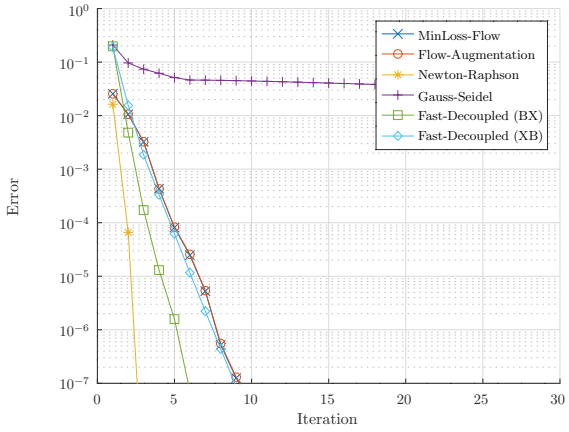

Figure C.12: MinLoss-Flow PF algorithm comparative error convergence for IEEE 30-bus system.

C.1.4 IEEE-118 Bus Test System

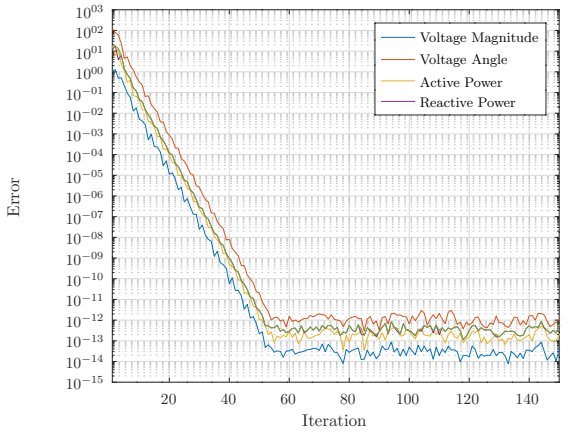

Figure C.13: MinLoss-Flow PF algorithm convergence error for IEEE 118-bus system.

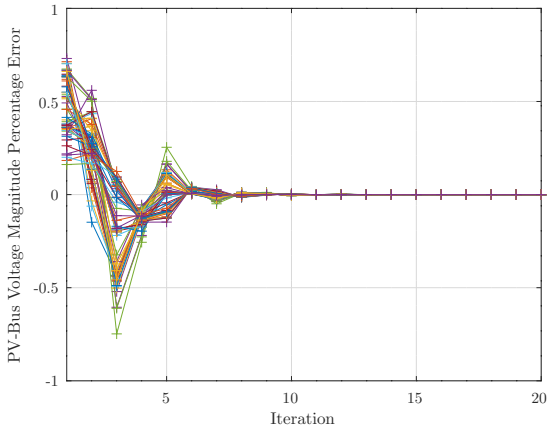

Figure C.14: MinLoss-Flow PF algorithm PV-Bus voltage magnitude error for IEEE 118-bus system.

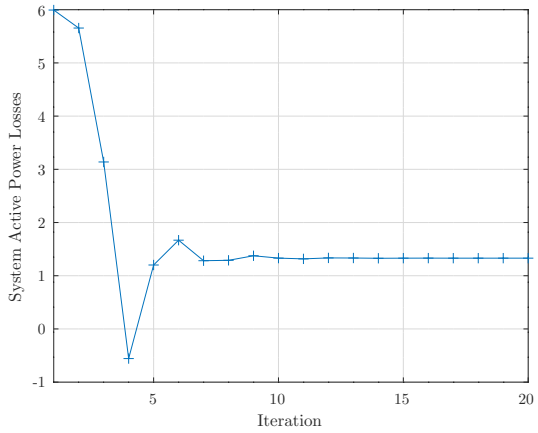

Figure C.15: MinLoss-Flow PF algorithm system losses for IEEE 118-bus system.

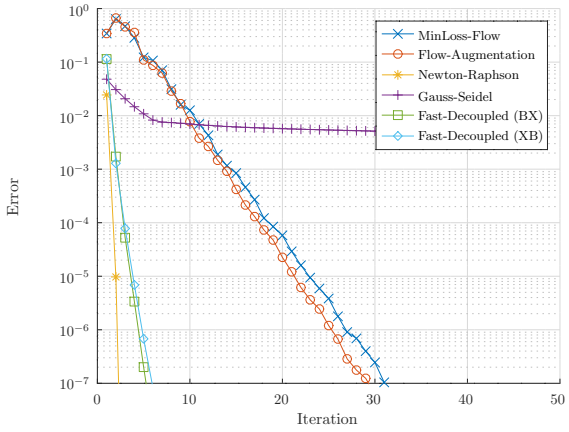

Figure C.16: MinLoss-Flow PF algorithm comparative error convergence for IEEE 118-bus system.

C.2 Application to Distribution Systems

C.2.1 Case-1 Radial Configuration

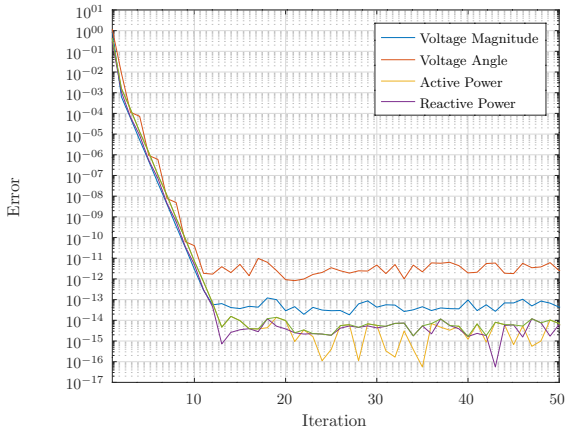

Figure C.17: MinLoss-Flow PF algorithm convergence error for 69-bus system in radial topology.

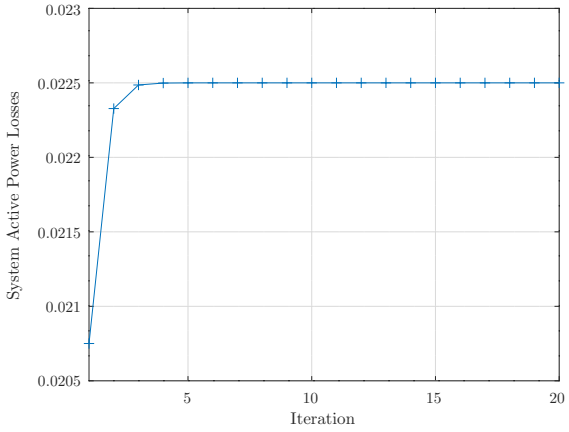

Figure C.18: MinLoss-Flow PF algorithm system losses for 69-bus system in radial topology.

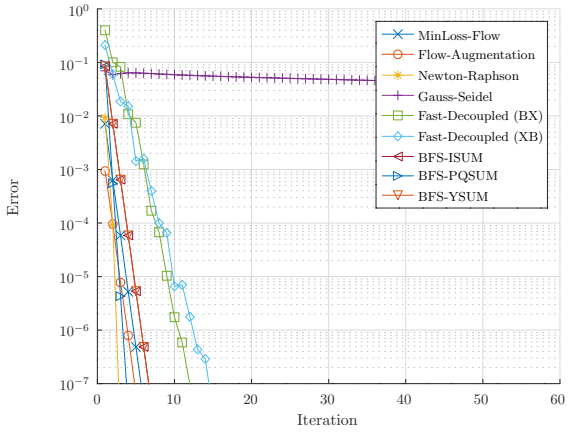

Figure C.19: MinLoss-Flow PF algorithm comparative error convergence for 69-bus system in radial topology.

C.2.2 Case-2 Meshed Configuration

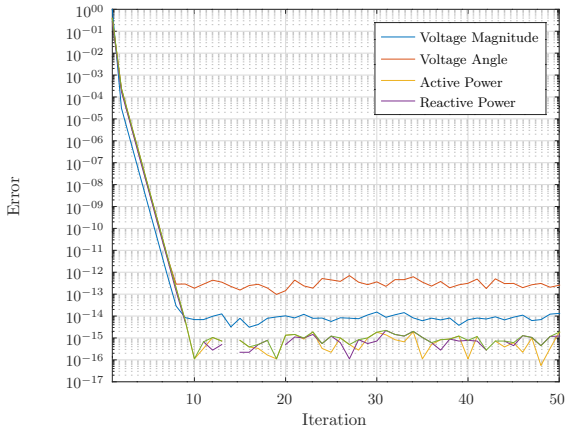

Figure C.20: MinLoss-Flow PF algorithm convergence error for 69-bus system in meshed topology.

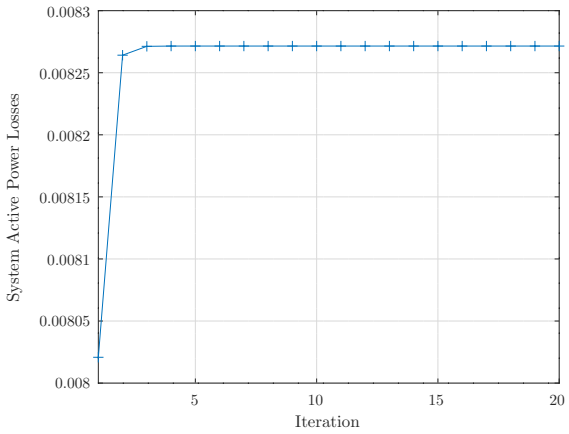

Figure C.21: MinLoss-Flow PF algorithm system losses for 69-bus system in meshed topology.

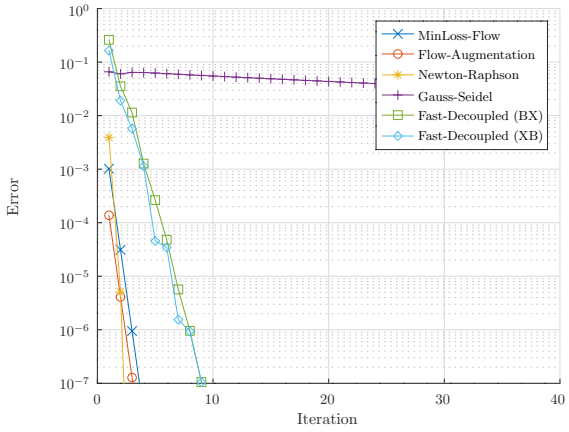

Figure C.22: MinLoss-Flow PF algorithm comparative error convergence for 69-bus system in meshed topology.

C.2.3 Case-3 Radial Configuration with DG

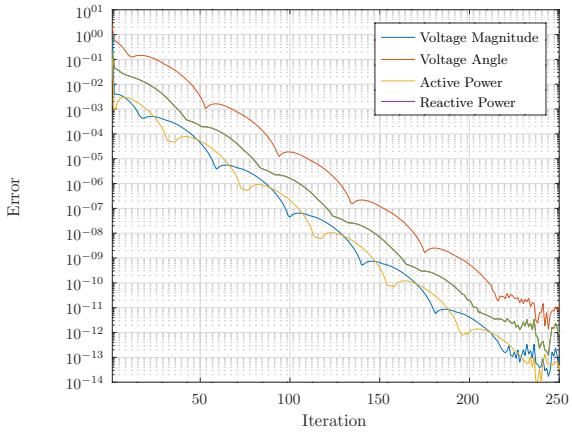

Figure C.23: MinLoss-Flow PF algorithm convergence error for 69-bus system in radial topology with DG.

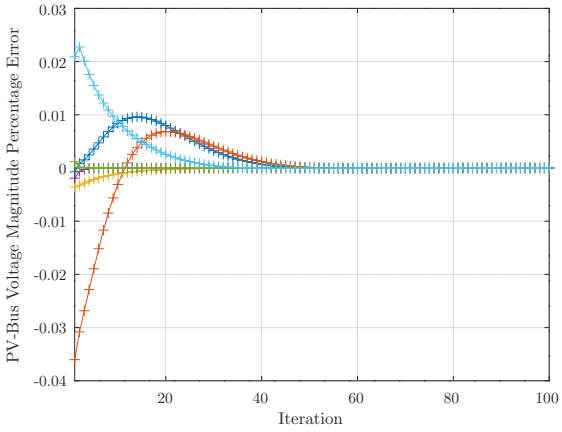

Figure C.24: MinLoss-Flow PF algorithm voltage magnitude for 69-bus system in radial topology with DG.

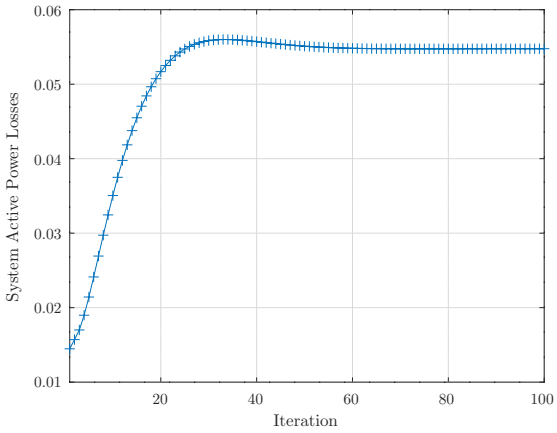

Figure C.25: MinLoss-Flow PF algorithm system losses for 69-bus system in radial topology with DG.

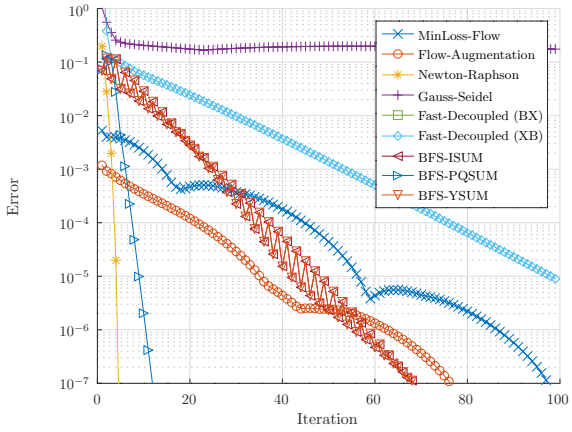

Figure C.26: MinLoss-Flow PF algorithm comparative error convergence for 69-bus system in radial topology with DG.

C.2.4 Case-4 Meshed Configuration with DG

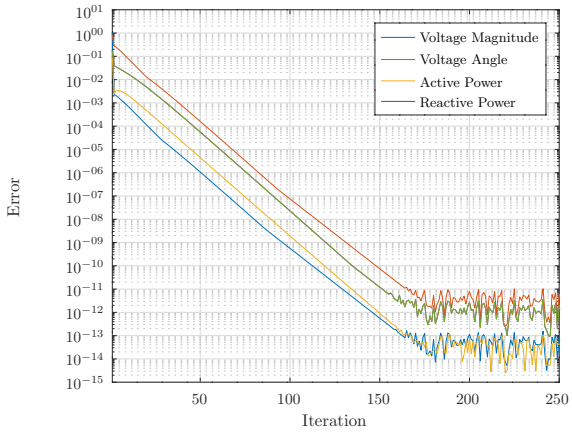

Figure C.27: MinLoss-Flow PF algorithm convergence error for 69-bus system in meshed topology with DG.

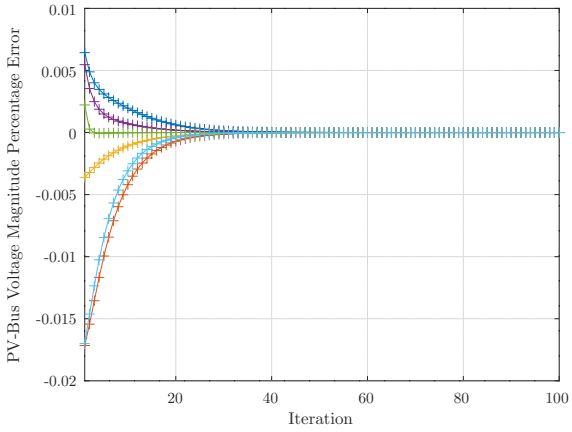

Figure C.28: MinLoss-Flow PF algorithm voltage magnitude for 69-bus system in meshed topology with DG.

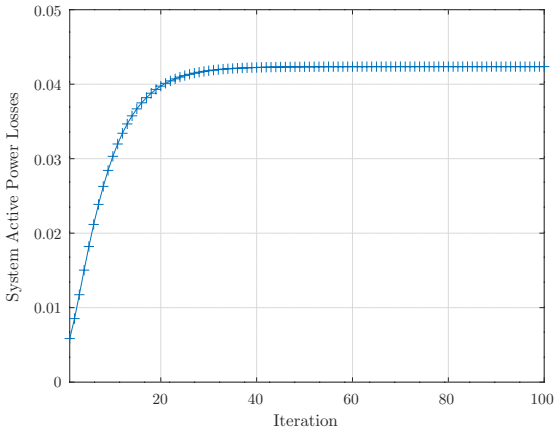

Figure C.29: MinLoss-Flow PF algorithm system losses for 69-bus system in meshed topology with DG.

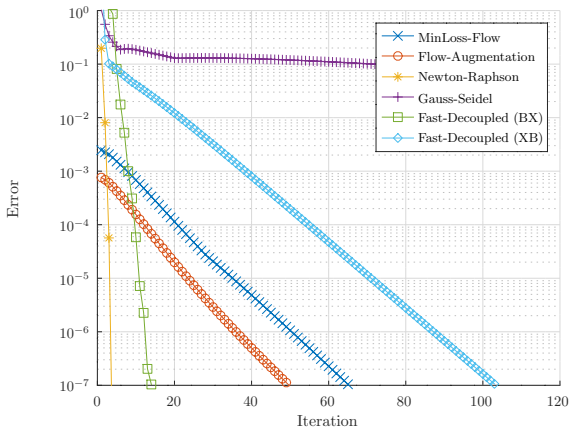

Figure C.30: MinLoss-Flow PF algorithm comparative error convergence for 69-bus system in meshed topology with DG.